Universidade de Lisboa
Faculdade de Ciências
Departamento de Física

Initial Testing of EPID Pre-Treatment Dosimetry for the Varian LINAC

Tatiana Marques Ladeira

Mestrado Integrado em Engenharia Biomédica e Biofísica

Perfil em Radiações em Diagnóstico e Terapia

Dissertação orientada por:

Doutor Joep Stroom e Professor Doutor Luís Peralta

2016

Universidade de Lisboa
Faculdade de Ciências
Departamento de Física

Initial Testing of EPID Pre-Treatment Dosimetry for the Varian LINAC

Tatiana Marques Ladeira

Mestrado Integrado em Engenharia Biomédica e Biofísica

Perfil em Radiações em Diagnóstico e Terapia

Dissertação orientada pelo Doutor Joep Stroom do Departamento de Radioterapia da Fundação Champalimaud e pelo Professor Doutor Luís Peralta do Departamento de Física da Faculdade de Ciências da Universidade de Lisboa

2016

Acknowledgements

The present work was carried out at Department of Radiotherapy of the Champalimaud Foundation. I would like to say that it was a pleasure to spend this year at Radiotherapy Department, surrounded by amazing people and I would like to express my sincere gratitude to those who have supported me and contribute to this work.

First and foremost I would like to express my sincere gratitude to my supervisor **Dr. Joep Stroom**, whose expertise, encouragement and patient have guided my experience in Department of Radiotherapy of the Champalimaud Foundation. A special thank to **Dr. Sandra Vieir**a who was so patient to teach me everything I wanted to know. Even when she was busy with her work, she always found a time for me.

I must also thank to **Dalila Mateus**, **Maria João Cardoso** and **Milton Rodrigues** for being always available to answer all my questions. I would like to thank to all technicians of the Department of Radiotherapy, especially to **Célia** and **Margarida** for being so friendly and for all the concern and help to manage my measurements time.

I would also like to thank very much to **Dr. Peter Keller** and **Dr. Christof Baltes** from Varian Medical Systems, who were always available to respond to my questions about Absolute Pre-Treatment Portal Dosimetry. Their expertise, understanding and patience added considerably to my project.

I would like to show my appreciation to my supervisor **Professor Luís Peralta** for being always available to help me and most of all for all the support that he provided during this year. I must also thank for all the expertise and encouragement that he provided during the time that I have been his student in the Faculty of Sciences of the University of Lisbon, which made me explore the areas of Radiation Physics and Dosimetry. I am also deeply thankful to **Professor Eduardo Ducla Soares**, whose motivation, enthusiasm and passion about Biomedical Engineering were crucial for my achievements during the time I have been student in the Faculty of Sciences of the University of Lisbon.

In addition, thanks to all my friends who have been by my side during the past 5 years, in special to **Sara S.**, who shared with me the experience in Champalimaud Foundation, **Sara F.** and **Felícia**. A very special thanks to **Liliana**, who always supported me in this journey.

Finally, I would like to express my truly and deeply gratitude to my family. There are no words to describe how grateful I am to my wonderful parents **Isabel** and **Serafim**, my sister **Maria** and to the rest of the family who always supported me and were by my side. Anything of this would have been possible without your support and motivation.

Resumo

A Radioterapia Externa assume atualmente uma elevada importância no tratamento oncológico. A utilização controlada de fontes de radiação ionizantes com elevada energia tem como principal objetivo controlar a ação proliferativa e provocar a morte de células tumorais, salvaguardando, no entanto, os tecidos sadios adjacentes.

A necessidade de minimizar o risco de toxicidade e morbidade dos tecidos sadios, otimizando a irradiação do volume tumoral, levou ao desenvolvimento de novas técnicas de entrega de radiação que permitem uma maior conformação geométrica assim como a modulação da intensidade do feixe de radiação, surgindo assim a Radioterapia de Intensidade Modulada (IMRT). Com a introdução da Arco Terapia Volumétrica Modulada (VMAT) que incorpora para além da rotação da *gantry* em torno do paciente, a variação da taxa de dose por grau, tornou-se possível irradiar eficaz e totalmente o volume tumoral. Paralelamente, têm sido exploradas com base em diversas evidências radiobiológicas, novas abordagens nos regimes de fracionamento do tratamento radioterapêutico, surgindo um interesse crescente em regimes hipofracionados. É importante referir que os tratamentos de Radioterapia em regime hipofracionado consideram, comparativamente ao regime de fracionamento convencional, um menor número de frações e consequentemente a entrega de uma dose mais elevada por fração. Para além dos regimes hipofracionados, também os regimes de fração única têm sido considerados no tratamento de diversos tipos de tumor.

A elevada conformação geométrica dos feixes de radiação, inerente às técnicas de IMRT e VMAT, associada à administração de elevadas doses por fração, prescritas nos regimes hipofracionados e de fração única, traduz-se numa maior necessidade de controlo dos tratamentos, reforçando a importância dos procedimentos de Controlo Qualidade (QA). De acordo com a altura no qual são realizados, antes ou durante a sessão de tratamento, é possível distinguir QA de pré-tratamento e in vivo, respetivamente. O principal objetivo da implementação de QA de pré-tratamento é avaliar se a distribuição de dose reproduzida pelo acelerador linear (LINAC) não se desvia significativamente da planeada. A deteção de erros mecânicos ou humanos, antes do início da sessão de tratamento, tem especial significado quando se trata de regimes hipofracionados ou de fração única em que um erro numa primeira fração pode comprometer negativamente a totalidade do tratamento bem como resultar em lesões graves e irreversíveis. Complementarmente, o QA *in vivo* tem como intuito determinar se a dose entregue pelo LINAC é recebida pelo paciente de acordo com o planeado, sendo possível detetar todos os erros que ocorrem durante a sessão de tratamento, entre os quais erros devidos à respiração, alterações anatómicas, posicionamento e movimento do paciente.

Os procedimentos de QA de pré-tratamento são os mais frequentes na prática clínica, sendo que a maioria dos Departamentos de Radioterapia recorrem a um fantoma. Neste sentido, o plano do tratamento do paciente é recalculado no fantoma, a duas ou três dimensões (2D ou 3D), obtendo-se a distribuição de dose planeada no fantoma. Posteriormente o fantoma é irradiado e a distribuição de dose medida pelo fantoma é comparada com a planeada. As medições podem ser realizadas com câmaras de ionização, detetores termoluminescentes ou díodos.

Devido à elevada resolução bem como à aquisição rápida e automatizada de imagens, o potencial dosimétrico dos dispositivos eletrónicos de imagem portal (EPIDs) tem sido amplamente explorado. O facto do EPID se encontrar acoplado ao LINAC, mais precisamente, montado na base da gantry em oposição à cabeça de irradiação do LINAC, representa também uma vantagem na medida em que permite rentabilizar o tempo de realização de procedimentos de QA. Considerando os procedimentos de QA de pré-tratamento é possível distinguir dois métodos de dosimetria com EPID tendo em conta se a radiação passa ou não através de um meio de atenuação (fantoma), dosimetria de transmissão e de não-transmissão respetivamente. Consequentemente, a verificação da distribuição de dose pode ser realizada ao nível do EPID ou dentro do fantoma. Ao nível do EPID, a distribuição de dose determinada a partir da imagem portal adquirida pelo EPID é comparada, através de um *software* específico, com a distribuição de dose calculada ao nível do EPID, tendo em conta as características do mesmo. Por outro lado, a partir da distribuição de dose determinada a partir da imagem portal adquirida pelo EPID é possível reconstruir em 2D ou 3D a distribuição de dose dentro do fantoma, sendo esta posteriormente comparada com a distribuição de dose recalculada no fantoma.

Atualmente, no Departamento de Radioterapia da Fundação Champalimaud, os procedimentos de QA de pré-tratamento são realizados recorrendo a um fantoma cilíndrico que contem uma matriz de 2D composta por 1386 díodos dispostos helicoidalmente, o ArcCHECK$^{\text{circl}}$ (Sun Nuclear Corporation, Melbourne, LA, USA). Tendo em conta que, 24% dos tratamentos totais, realizados nos LINACs da Varian (Varian Medical Systems, Palo Alto, CA, USA) disponíveis no Departamento de Radioterapia, são de regime hipofracionado e 35% de regime de fração única, torna-se fundamental otimizar os procedimentos de QA de pré-tratamento de modo a detetar com maior precisão possíveis erros. Neste sentido, o presente projeto teve como principal objetivo a realização de testes iniciais para a implementação de dosimetria de pré-tratamento com EPID. Os testes realizados recorrem unicamente a dosimetria de não transmissão ao nível do EPID e vão de encontro com as especificidades do EPID acoplado a cada um dos LINACs da Varian, o EPID aS1000 ao TrueBeam$^{\text{TM}}$ e o aS1200 ao EDGE$^{\text{TM}}$. É fundamental referir que para além do EPID, a solução comercial da Varian para realizar dosimetria de pré-tratamento com EPID é composta por um algoritmo que permite calcular a distribuição de dose ao nível do EPID e por um software de Dosimetria Portal que permite comparar e analisar a distribuição de dose determinada a partir da imagem portal adquirida pelo EPID e a calculada pelo algoritmo. Assim, para o Sistema TrueBeam$^{\text{TM}}$ foi testada uma solução de Dosimetria Portal (PDPC) que tem como intuito melhorar e simplificar a configuração do algoritmo

PDIP bem como a calibração dosimétrica do EPID aS1000. Um conjunto de medições foram realizadas a fim de verificar a correta configuração PDPC. Os excelentes resultados obtidos demonstram a eficácia da matriz de correção do perfil do feixe, introduzida aquando da calibração do aS1000 e que incorpora uma correção melhorada para a dispersão causada pelo braço mecânico do EPID, bem como a validação do algoritmo PDIP pré-configurado, que assume que a dispersão do aS1000 pode ser modelado com base no comportamento de dispersão de diferentes EPIDs do mesmo modelo. A validação clínica do novo método de configuração e calibração para a realização de QA de pré-tratamento com EPID foi realizada com recurso a 34 pacientes anónimos, 11 dos quais com planos IMRT para o tratamento do cancro da mama e 23 pacientes de cancro da próstata com planos VMAT. A comparação da distribuição de dose determinada a partir da imagem portal adquirida pelo EPID com a calculada pelo algoritmo foi efetuada no software de Dosimetria Portal através do método de análise gamma com dois critérios distintos, um com 3% de diferença de dose (DD) e 3 mm de distância de concordância (DTA) e um outro com critérios 2% e 2 mm. Para todos os planos analisados, 71 de IMRT e 86 de VMAT, foram obtidas $\%\gamma > 1$ superiores a 95 % e 90% com os critérios (3%, 3mm) e (2%, 2mm) respetivamente. No geral, foram obtidos melhores resultados que os obtidos com o ArcCHECK®. Por outro lado, para o Sistema EDGE™ foi testado uma nova versão do software de Dosimetria Portal, que recorre a um modelo que converte a distribuição de dose determinada a partir da imagem portal adquirida pelo EPID em valores de dose em água, permitindo obter as distribuições de dose em valores absolutos. Para tal recorreu-se a 10 pacientes anónimos com lesões cancerígenas em diferentes localizações, com planos de tratamentos de IMRT ou VMAT com feixes FFF, isto é sem serem filtrados, e com regimes de fracionamento distintos. A comparação das distribuições de dose foi realizada com recorrendo à análise gamma com um critério (3%,3mm). Foram obtidos excelentes resultados para os 40 arcos analisados, sendo que $\%\gamma > 1$ superiores a 98% foram obtidos para todos os planos, menos para um. A fim de estudar a sensibilidade do EPID aS1200 foi desenvolvida uma rotina para introduzir erros nos planos clínicos. Primeiro, os planos foram convertidos XML, através do *software* Veritas. Erros de vários tipos e com magnitudes variando entre 0.5 mm e 1 cm foram introduzidos nas posições das folhas do colimador (MLC) e de seguida os planos XML foram carregados diretamente no LINAC através do *Developer Mode*. As imagens portal adquiridas foram importadas para o *software* de Dosimetria Portal, de modo a compará-las com a distribuição de dose calculada pelo algoritmo clínico. Posteriormente, os erros foram também medidos com ArcCHECK ®. Mais uma vez, os resultados confirmam a elevada sensibilidade do EPID quando comparada com a do ArcCHECK ®. No entanto, mais casos clínicos, considerando diferentes localizações e regimes de fracionamento, devem ser estudados de forma a ter uma maior amostra e consequentemente resultados mais expressivos que suportem a implementação do EPID para a realização dos procedimentos de pré-tratamento.

Palavras-Chave: Controlo de Qualidade, Pré-Tratamento,Dosimetria com EPID; FFF Beams.

Abstract

Nowadays, External Radiotherapy assumes an important role in the treatment of cancer patients. The clinical introduction of more complex radiation delivery techniques, such as Intensity Modulated Radiation Therapy (IMRT) and Volumetric Arc Radiation Therapy (VMAT) as well as with the introduction of hypofractionated and single-shot schemes, patient-specific Quality Assurance (QA) procedures become crucial in order to ensure the accuracy of radiotherapy treatment and to avoid major errors.

Patient-specific QA procedures can be performed priori or during the treatment session and according to that it is possible to differentiate pre-treatment and in vivo patient-specific QA, which are complementary to each other. The pre-treatment patient-specific QA procedures are the most common in clinical practice, and its main goal is to verify whether the dose distribution produced by the linear accelerator (LINAC) does not deviate significantly from the planned, allowing to detect errors before the first or only fraction is given. At Champalimaud Foundation the pre-treatment patient-specific QA is performed using a cylindrical detector array (ArcCHECK®). However, due the cumbersome and low-resolution of ArcCHECK®, Electronic Portal Image Device (EPID) has been studied.

In the present thesis, two different studies to test pre-treatment patient-specific QA with EPID were conducted, according with the specifics of the EPID coupled to each Varian LINACs (Varian Medical Systems, Palo Alto, CA, USA) available in the Radiotherapy Department, the TrueBeam™ and EDGE™ systems. On the first one, a pre-configured method to calibrate the EPID and to configure the portal dose image prediction (PDIP) algorithm, that allow to obtain a portal dose image at the EPID level with which the portal dose image acquired by the EPID is compared, was tested. The positive results, obtained regarding beam profile accuracy, backscatter correction, central axis (CAX) values and modulation of EPID scatter kernels, shown that Pre-Configured Portal Dosimetry (PDPC) solution is better than the commercial Portal Dosimetry. Consequently, pre-treatment patient-specific QAs of IMRT and VMAT plans were evaluated and the results were compared with the ones obtained with ArcCHECK®. A gamma analysis with a dose-difference criterion of 3% and distance-to-agreement (DTA) of 3 mm was used to evaluate the results. In general, better results were obtained for EPID dosimetry than for ArcCHECK®, presenting $\%\gamma < 1$ values higher than 97%. On the EDGE™ System was performed the installation and verification of the Absolute Pre-Treatment Portal Dosimetry that allow to evaluate pre-treatment patient-specific QAs of IMRT and VMAT plans with flattening filter free (FFF) beams, which is a new aspect since usually EPIDs saturate with FFF beams. Considering a gamma criteria of (3%, 3mm), excellent results were ob-

tained since a $\%\gamma$ <1 value higher than 98% was obtained for all patients, with exception of one. An entire routine, including a MATLAB® program to introduce intentional errors XML clinical plans, was developed in order to study the sensitivity of the EPID during pre-treatment patient-specific QA. First, the DICOM-RT plan was converted in XML through Veritas, which is a research software. Then several errors types with magnitudes ranging from 0.5mm to 1 cm were introduced in the leaves positions of multi-leaf collimator (MLC) and therefore the plans were loaded in LINAC through Developer Mode. Acquired portal dose images were imported to the Portal Dosimetry workspace, which allows compare the acquired portal dose image with the dose distribution calculated by clinical algorithm, in Citrix Machine. The errors were also measured with ArcCHECK® and the obtained results were compared. The analysis of the results shown that EPID is more sensitivity than ArcCHECK®. However, more clinical cases, considering several treatment sites and with different fractionation schemes, should be studied with both portal dosimetry and ArcCHECK® in order to verify the obtained results. The obtained first results were very promising and encourages the continuation of the study for implementation of pre-treatment patient-specific QA with EPID, for FFF beams.

Key- words: Quality Assurance; Pre-Treatment Dosimetry; EPID Dosimetry; Pre-Configured Portal Dosimetry; Absolute Pre-Treatment Portal Dosimetry; FFF Beams.

Contents

List of Abbreviations

2D Two-Dimensional

3D Three-Dimensional

3D-CRT Three-Dimensional Conformal Radiotherapy

a-Si EPID amorphous-Silicon EPID

CAX Cental Axis

CCD-based EPID Camera-based EPID

CT Computed Tomography

CTV Clinical Target Volume

DD Dose Difference

DF Dark-Field

DICOM Digital Imaging and Communication in Medicine

DNA Deoxyribonucleic Acid

DRR Digitally Reconstructed Radiograph

DTA Distance-to-Agreement

DVH Dose-Volume Histogram

EPID Electronic Portal Imaging Device

FET Field-Effect Transistor

FF Flood-Field

GTV Gross Tumour Volume

GY Gray

ICRU International Commission on Radiation Units

IMAT Intensity Modulated Arc Therapy

IMRT Intensity Modulated Radiotherapy

ITV Internal Target Volume

Li-Fi-EPID Liquid-Filled EPID

LINAC Linear Acelerator

LQ Linear-Quadratic

MeV Mega Electron Volt

MLC Multi-Leaf Collimator

MRI Magnetic resonance imaging

MU Monitor Units

MV Megavoltage

OAR Organ at Risk Volume

PET Positron Emission Tomography

PRV Planning Organ at Risk Volume

PTV Planning Target Volume

QA Quality Assurance

SAD Source-to Axis Distance

SBRT Stereotactic Body Radiation Therapy

SRS Stereotactic Radiosurgery

SSD Source-to Surface Distance

TPS Treatment Planning System

VMAT Treatment Planning System

WHO World Health Organization

List of Tables

List of Figures

Chapter 1

Introduction

According to the World Health Organization (WHO) cancer is one of the most frequent causes of death worldwide. In 2012, 14 million new cases were registered and about 8.2 million people died from cancer, with correspond to 13% of all deaths worldwide. It is expected that the number of new cases increase 70% over the next two decades which means more than 20 million new cases per year [1]. It is important to realize that more than 30% of cancer could be prevented, mainly by not using tobacco, moderating the use of alcohol, having a healthy diet and being physically active [2].

Currently about 50% of cancer patients require External Radiotherapy as part of their treatment, complementing other cancer treatment modalities such as surgery and chemotherapy. In order to minimize the risk of toxicity and morbidity of healthy tissues as well as to optimize the irradiation of the tumour, new procedures in External Radiation Therapy such as Intensity Modulated Radiation Therapy (IMRT) and Volumetric Arc Radiation Therapy (VMAT) are becoming routine clinical practice. These techniques allow a higher dose in tumour while sparing the surrounding organs. Based on various radiobiological evidences, new approaches in the fractionation schemes of radiotherapeutic treatments have also been explored. Due to the high complexity of IMRT and VMAT techniques and to the high doses per fraction of hypofractionated and single shot schemes, machine and patient-specific Quality Assurance procedures are crucial to avoid major accidents as those that have been reported. For example, in 2000, at the National Institute of Panama an error related with the data introduced into Treatment Plan System (TPS) resulted in prolonged treatment time. As consequence 28 patients were exposed to prolonged irradiation which resulted in 11 deaths due overdose toxicity [3]. In France, between 2004 and 2005, 23 prostate cancer patients received an overdose correspondent to 7-34% of the prescribed dose due to an error in dose intensity calculation in TPS. As result 5 patients died and the remaining developed serious complications. During one year in United Kingdom, 5 patients were exposed to an overdose due to a change in operational procedures resulting in the death of 1 patient [4].

According to the time when QA is performed, it is possible to differentiate pre-treatment and *in vivo* patient-specific QA. The main goal of pre-treatment patient-specific QA is to verify whether the dose distribution produced by the linear accelerator (LINAC) does not deviate significantly from the planned. The detection of mechanical or human

errors, before the treatment session has particular significance in hypofractionated or single shot schemes since an error in the first fraction may compromise the entire treatment and result in serious and irreversible injuries. However, some errors only occur during the treatment session. In this context, the intention of *in vivo* patient-specific QA is to determine if the dose delivered by the LINAC is received by the patient according to the plan, detecting all errors that occur during the treatment session which include errors due to breathing, anatomical changes, positioning and movement of the patient.

Pre-treatment patient-specific QA procedures are most common in clinical practice and are usually performed with a phantom in which the patient treatment plan is recalculated and measured in order to compare the dose distributions against each other. The potential of Electronic Portal Imaging Device (EPID) to perform patient-specific QA has been explored due its high resolution as well as the fast and automated acquisition of portal images. Several methods of EPID dosimetry can be distinguish according to the level where the comparison of the dose distributions are performed, at the EPID level or inside the phantom or patient, and whether the radiation passes or not through an attenuation medium, transit and non-transit dosimetry.

Currently, at the Radiotherapy Department of the Champalimaud Foundation, pre-treatment patient-specific QA are performed using a cylindrical phantom which contain a 2D matrix of diodes, the ArcCHECK® (Sun Nuclear Corporation, Melbourne, LA, USA). However, due to the low resultion of ArcCHECK® and to the fact that this procedure is time-consuming and cumbersome, it becomes essential to optimize the pre-treatment patient-specific QA procedures to detect more accuratly possible errors. Speciallyconsidering that 24% and 35% of total treatments conducted in the Varian LINACs (Varian Medical Systems, Palo Alto, CA, USA) have hypofractionated and single shot schemes respectively. In this sense, the aim of this study is to perform initial tests for the implementation of pre-treatment dosimetry with EPID.

In the present study all the tests were performed with non-transit dosimetry at the EPID level, according to the specifics of the EPID attached to each Varian LINACs (Varian Medical Systems, Palo Alto, CA, USA) in the Radiotherapy Department of the Foundation Champalimaud, the TrueBeam™ and EDGE™ systems. On the TrueBeam™ System was tested an optimized method to calibrate the EPID and to configure the algorithm that allow to obtain a predicted portal dose image at the EPID level, with which the portal dose image acquired by the EPID is compared. Consequently, pre-treatment patient-specific QAs of IMRT and VMAT plans with flattening filter (FF) beams were evaluated. On the other hand, on the EDGE™ System was performed the installation and verification of the Absolute Pre-Treatment Portal Dosimetry that allow to evaluate pre-treatment patient-specific QAs of IMRT and VMAT plans with flattening filter free (FFF) beams. Finally, a MATLAB® program to introduce intentional errors in clinical plans was developed in order to study the sensitivity of the EPID during pre-treatment patient-specific QA and compare it with ArcCHECK®.

This dissertation describes the work developed in the Department of Radiotherapy of the Champalimaud Foundation and is organized in the following way. Chapter 2 provides

background information about Radiotherapy and EPID Dosimetry. Chapter 3 describes the data, materials and methodologies used. Chapter 4 presents relevant results obtained as well as a discussion. Finally, Chapter 5 summarises the conclusions and presents future work.

Chapter 2

Background

In this Chapter, the radiotherapy aim and its radiobiological effects are presented. The production of radiotherapeutic high-energy photons is described as well as the delivery techniques and the clinical procedure in Radiotherapy (Section 2.1). A bibliographic review of the use of EPID in Radiotherapy is reported with reference to dosimetric characteristics, calibration for dosimetric purposes and methods of EPID dosimetry (Section 2.2).

2.1 Radiotherapy

Radiotherapy is a therapeutic technique with curative or palliative intent in which the main objective consists to deliver a homogeneous radiation in order to maximize the dose to a well-defined tumour without compromising healthy tissues and organs at risk (OARs), thereby increasing the probability of cure without serious complications [5].

Depending on the location of the radiation source, Internal and External Radiotherapy can be distinguished. Internal Radiotherapy uses radioactive sources placed on the surface or inside of the patient in a very close location of the tumour while External Radiotherapy uses ionising radiation sources placed at a distance from the patient. The most commons types of ionising radiation used in External Radiotherapy are high-energy photons (X-ray and γ-ray) and electrons, produced by a linear accelerator (LINAC)[6]. To fully understand the effectiveness of External Radiotherapy in cancer treatment it is essential to understand the inherent radiobiological principles.

2.1.1 Radiobiology Concepts

Ionising radiation can interact directly or indirectly with biological tissue. Direct interaction causes immediate structural changes in several specific components of the cells (DNA, proteins and lipids) while indirect interaction occurs through free radicals production by radiolysis of water which is present in the extra and intracellular environments. The presence of the oxygen reinforces the harmful potential of the free radicals which react with the DNA causing irreversible damages. It should be noted that indirect effect accounts for 70% of biological damage caused by radiation and in this context, DNA is considered the critical target of ionizing radiation since breaking the double strands can determine

cell death or loss of proliferative capacity preventing the progression of the pathology [7].

In order to control tumour volume while preserving the integrity of the healthy tissues fractionated radiotherapy schemes have been widely prescribed. Conventional fractionation schemes comprises administering 1.2 to 2.0 Gray (Gy) per fraction, 5 days per week, giving a total dose between 60 and 70 Gy which varies according to the tumour volume and the maximum dose that the adjacent healthy tissues tolerate [8]. The effect of radiation administrated in fractionated schemes is governed by five radiobiological principles, known as the 5R's: (1) Repair of sublethal damage, (2) Repopulation of cells after radiation, (3) Redistribution of cells in the cell cycle, (4) Reoxygenation of the surviving cells and (5) Radiosensitivity of tumour cells [7,10,11].

The first radiobiological effect describe the capacity of the cells to repair sublethal damage induced by radiation, returning to their initial sensitivity values. In contrast to healthy cells, tumour cells exhibit a low capacity to repair sublethal damage which contribute to the accumulation of irreversible damage, fraction to fraction, causing cell death. The rate of the repair damage induced by radiation is directly related to several factors including the dose per fraction, and the nature of the tissues and cells. On the other hand, repopulation is the process by which healthy cells irreversibly damaged or killed are replaced by cell proliferation after a fraction [7,10].

According to the stage of the cell cycle, the sensitivity of the cells varies. In contrast to Interphase, Mitosis is the most sensitive stage to radiation since the DNA compaction makes it more susceptible to the damaging effects of radiation as well as less accessible to the repair enzymes. Tumour cells have a high mitotic rate and therefore are considered more radiosensitive than healthy tissues. Redistribution is the process in which cells progress through the cell cycle reaching the most sensitive stage to radiation. So, as tumour cells exhibit a greater proliferative capacity, an early redistribution is ensured comparing to healthy tissues. As a result, fraction to fraction, there is a higher proportion of the surviving tumour cells in Mitosis stage [6,7].

In turn, reoxygenation is the process by which the hypoxic cells become oxygenated after irradiation. As referred above, the presence of oxygen during irradiation leads to the formation of highly reactive radicals that act at the level of DNA, thus damaging it. Consequently, more oxygenated tumours are considered more radiosensitive and therefore respond better to radiotherapy. It is known that the more oxygenated areas of the tumours are located at the periphery while the less oxygenated areas are in central regions. Upon irradiation corresponding to a fraction the tumour cells at the periphery die more quickly and therefore the oxygen is redirected to neighbouring cells with low oxygen content. Accordingly, in the next fraction there is an increase of oxygenated tumour cells.

The last radiobiological effect, radiosensitivity of tumour cells, is considered an intrinsic factor and it is modelled by the linear-quadratic (LQ) equation. The LQ is used to calculate the effects for different fractionated irradiation schemes comprising dose and fraction number. This model describes the cell survival (S) in terms of the dose prescribed (D) and encompasses two different parameters, α and β which represents lethal and sublethal damage, respectively, such that

$$S = e^{\alpha D + \beta D^2} \tag{2.1}$$

where the ratio of α and β indicates the sensitivity of tissues to different irradiation schemes since this ratio represents the dose at which the lethal and sublethal damage are equal, so $\alpha \setminus \beta \sim 3$ Gy for late responding tissues and $\alpha \setminus \beta \sim 10$ Gy for early responding tissues as shown in Figure 2.1[8,10].

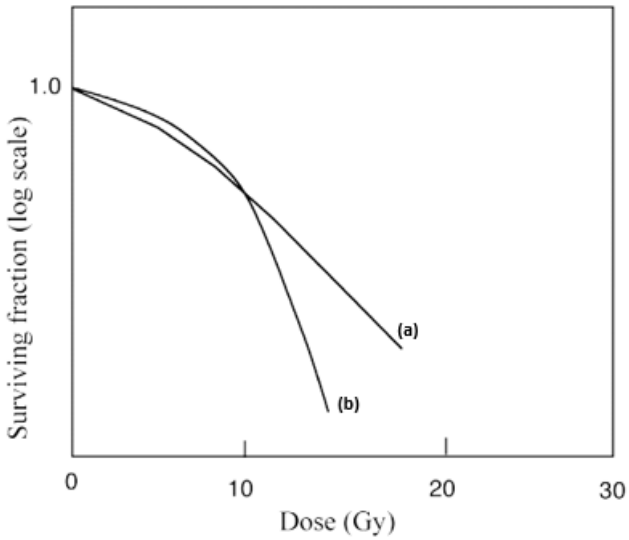

Figure 2.1: The dose-response relationship for late-responding tissue shown in (b) is more curved than for early-responding tissues in (a). In the LQ formulation this translates into a larger $\alpha \setminus \beta$ for early effects than for late effects. Adapted from [10]

In recent years, a significant interest in hypofractionated schemes, higher than 2.5 Gy per fraction, has been observed mainly influenced by the clinical results obtained by Stereotactic Radiosurgery (SRS). Developed between 1950 and 1960, SRS was usually limited to brain tumours in that the entire dose, between 15 and 25 Gy, is delivered in a single fraction [10]. The technique of SRS has then been adapted to irradiate extracranial tumours and from there the Stereotactic Body Radiation Therapy (SBRT) has emerged in which the total dose is delivered in 1 to 5 fractions. Several studies have shown that SBRT with total doses higher than those prescribed in conventional fractionated schemes is effective in the treatment of malignant tumours of the lung, breast, liver, prostate and spine.

The possibility to clinically implement such innovative techniques is the result of technologic advances in image guidance and treatment delivery techniques which together enable the delivery of high doses to the tumour without compromising the surrounding healthy tissues. However, as the biological considerations made previously were based in fractionated schemes is important to understand the role of 5 R's in the response of tumours to SRS or SBRT [8]. Some studies conducted with high-dose fractionated schemes concluded that the capacity of healthy cells to repair sublethal damage is significant during

the treatment session, which is more prolonged in hypofractionated or single shot schemes than in conventional schemes, enabling to healthy cells to return to the initial sensitivity values.

Tumour irradiation in a single fraction prevents cell cycle redistribution and tumour cells death in the cell cycle phases where they are irradiated. The repopulation of tumour cells during the course of treatment is also negligible since SRS or SBRT treatment is completed within 1 or 2 weeks [8,10].

Blood vessels directly control the survival and proliferation of tumour cells. So, damage in tumour blood vessels by irradiation, which is more considerable with high-doses fraction schemes, causes indirect death in the tumour. A consequence of vascular damage is that the reoxygenation of hypoxic tumour cells is compromised. This implies that reoxygenation of tumour cells may not occur when the tumours are treated with high-doses fraction schemes, higher than 10 Gy per fraction. However, for tumours treated with a single fraction or extremely high-dose fraction, vascular damage is so extensive that the intra-tumour environment is drastically changed leading to indirect cell death [10]. Consequently, the LQ model is inapplicable when tumours are treated with doses higher than 10 Gy in a single fraction due to the vascular damage that causes indirect tumour cells death. However, the LQ model should be considered when tumours are treated with hypofractionated schemes with doses smaller than 10 Gy per fraction [8,11].

2.1.2 Production of High-Energy Photons

Medical LINACs used in External Radiotherapy generate directed beams of electrons or photons in megaelectron-volt (MeV) range through an acceleration and collimation mechanism [6]. The present study was conducted only with MV photon beams whose production process is described below.

As shown in Figure 2.2 the main components of a modern medical LINAC generally consists of: (1) injection system, (2) radiofrequency power generation system, (3) accelerating tube, (4) auxiliary system, (5) beam transport system and (6) beam collimation and monitoring system [6,12,13]. The electrons are produced and injected in LINAC system by a triode gun which basically consists in a cathode-anode system with a grid. The electrons are produced by thermionic emission from a heated tungsten filament, serving as cathode which is maintained at a static negative voltage (-20 kV). In turn, the grid placed between the cathode and the anode is held sufficiently negative with respect to the cathode [6]. A pulsed modulator unit is responsible to apply voltages pulses to the grid and as consequence the electrons are accelerated in vacuum towards a perforated grounded anode through which the low energy electrons (50 keV) are injected into an accelerated tube, located in the LINAC gantry. At the same time, pulsed microwave radiation produced by a radiofrequency generation system (Magnetron or Klystron) are injected into the accelerated tube via a waveguide system. The radiofrequency system uses as input high voltage pulses from the pulsed modulator unit. In the accelerated tube, which can be either a standing or travelling waveguide type, low energy electrons interact with the electromagnetic field of the microwaves and are accelerated to kinetic energies in the MeV

range.

The beam of MeV energy electrons that exists the accelerated tube is directed down through the treatment head by a 90° or 270° bending magnet [6]. At this point, the electrons strike a high atomic number X-ray target, usually tungsten, generating a continuous spectrum of photons predominantly by bremsstrahlung emission which is a result of Coulomb interaction between the incident electrons and the nuclei of the target. The resulting photon beam is shaped by different collimation devices, flattened and monitored in order to achieve the final treatment beam.

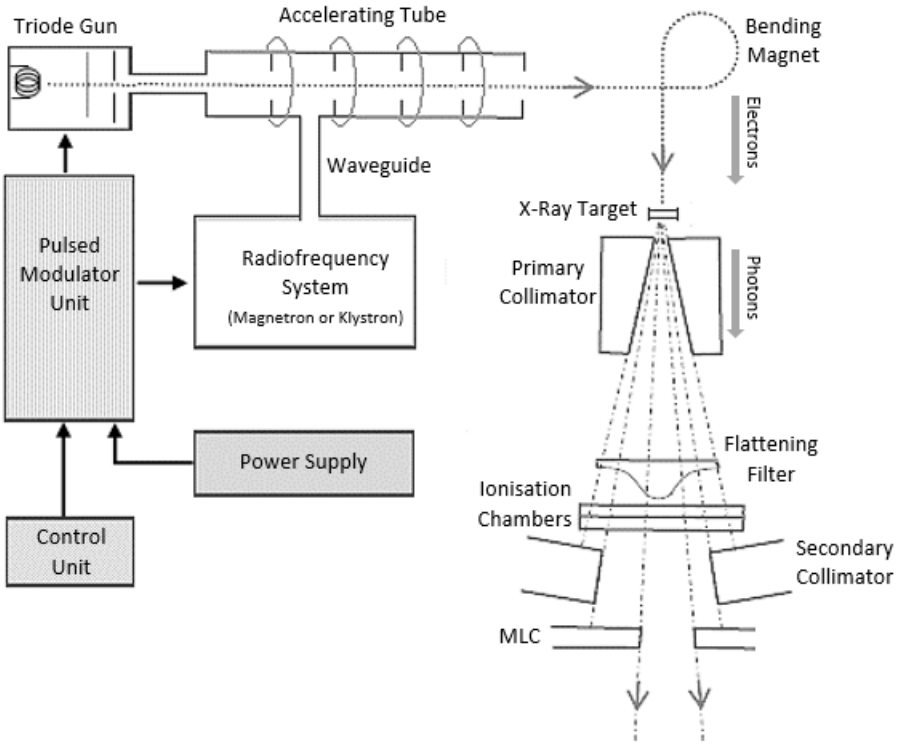

Figure 2.2: Main components composing a modern medical LINAC: (1) injection system, specifically a triode gun (2) radiofrequency power generation system which can be a magnetron or a klystron (3) accelerating tube, (4) auxiliary system, (5) beam transport system and (6) beam collimation and monitoring system constituted by all the collimators and ionisation chambers. Adapted from [14]

The primary collimator is fixed and consists of a conical hole through a tungsten block defining beam aperture that correspond to the maximum circular field [6]. It attenuates the beam less than 0.1%. Due to the use of MeV energy electrons to produce photon beams, these are forward-peaked as is shown in Figure 2.3 (b). Therefore, after the primary collimation the photon beam passes through a flattening filter whose main functions are to obtain a uniform photon beam dose distribution at the reference depth, by differentially absorbing more photons in the centre and less in the periphery, and filter the low-energy photons [6, 12].

Located directly under the flattening filter are two parallel ionisation chambers to monitor the LINAC output which is measured in terms of monitor units (MU). Thus, the

LINAC output is inspected for deviations from the calibration. This is usually performed using a 10x10 cm^2 field and 100 MU are delivered when the dose is 1 Gy at the depth of the maximum dose in water at a source-surface distance (SSD) equal to 100 cm. The ionization chambers are completely independent and sealed to avoid changes in room temperature and pressure. The first ionisation chamber measures the MU and stops the beam when it is completely delivered, while the second ionisation chamber provides a backup in case of the failure of the first chamber.

The secondary collimator consists of two adjustable jaws in X and Y directions that can move independently and provide symmetrical or asymmetrical rectangular and square fields at the LINAC isocenter. Lastly, the multi-leaf collimator (MLC), which is the most recent collimation device, consists of two banks of computer-controlled leaf pairs that provide mechanical variable collimation in order to modulate the intensity and to conform asymmetric shapes to shield the OARs [14]. The maximum displacement distance of the leaves, the transmission factor and the maximum speed of displacement are some other inherent characteristics of the MLC.

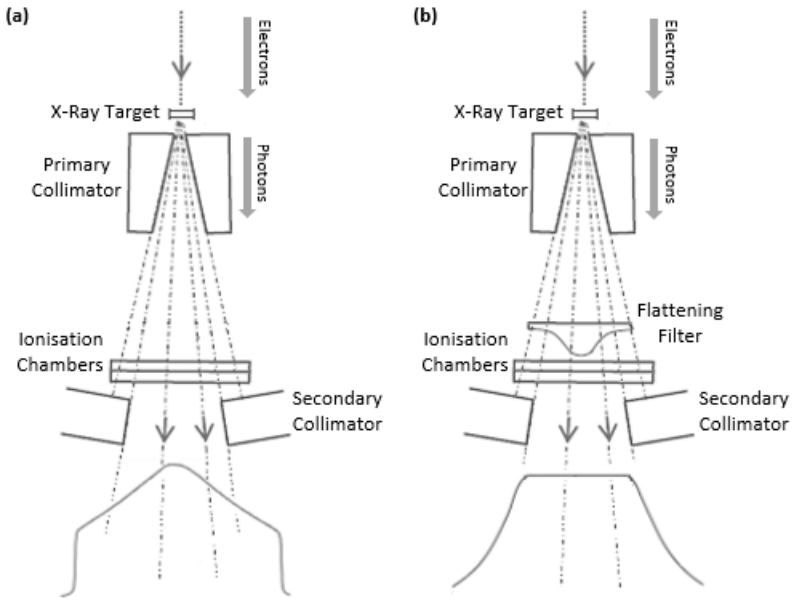

Figure 2.3: A schematic representation of the beam profile of a conventional (with flattening filter) photon beam in (a) is compared to the beam profile of an unflattened photon beam of an equivalent energy in (b). In this scheme the MLC is not represented. Adapted from [14]

2.1.3 Radiotherapy Delivery Thechniques

In the past few decades the advances in the delivery of Radiotherapy have been constant, mainly motivated by the need to reduce the dose delivered to healthy tissues minimizing the risk of toxicity and morbidity [15].

After the implementation of Conventional Radiotherapy, in which the planning treatment was based on two-dimensional (2D) X-ray images, and with the development of Computed Tomography (CT) the Three-dimensional Conformal Radiotherapy (3D-CRT) emerged in the late 1980s [16]. The 3D-CRT allows three-dimensional (3D) reconstruction

of the target volume, through the identification and delineation of the tumour in each image of the various CT cross-sections [15,17]. The main advantage of this technique lies in the geometrical conformation capacity of the radiation beam allowing the delivery of higher doses to the volume target. The geometric conformation of the beam is achieved using mainly wedge filters, blocks, compensators and more recently the MLC as referred in Section 2.1.2.

In the early 1990s the fixed angle Intensity Modulated Radiotherapy (IMRT) was introduced. Besides greater precision in the geometrical conformation of the radiation beam, it also modulates the intensity making it more effective in tumour control. In order to overcome some of the limitations of fixed angle IMRT and to improve the radiation delivery, arc-based therapies that implemented the continuous rotation of the gantry around the patient during irradiation have emerged, such as Tomotherapy and Intensity Modulated Arc Therapy (IMAT). Tomotherapy, which first emerged in 1993, uses a LINAC with a specific design, similar to a CT scanner with a radiation source that continuously rotates and is provided with a MLC that only admits two positions of the leafs, open or closed. It is possible to distinguish between axial and helical Tomotherapy. Although the patient is moved through the LINAC in both, in the first one the radiation is delivered slice-by-slice and in the latter the radiation is delivered in continuous spiral. In turn the IMAT which was first introduced by Yu *et al.* in 1995, relies on the use of dynamic MLC along with the rotation of the gantry [15,16]. In Figure 2.4 is possible to see the diferences of 3D-CRT, IMRT and VMAT techniques for a prostate plan[18].

2.1.3.1 Intensity Modulated Radiotherapy

The IMRT technique modulates the intensity across each radiation beam allowing to obtain highly conformal dose distributions adapted to the anatomical and physiological characteristics of the tumour, particularly important in target volumes with concave or more complex shape with close proximity to OARs [15,17].

The geometrical conformation and intensity modulation of the beam are currently obtained by MLC and based on the delivery mode it is possible to distinguish two methods: static (SMLC) and dynamic (DMLC). In the SMLC mode, each radiation beam is subdivided into smaller beams, called segments, each one defined by a different MLC setting and associated to specific number of MU serving as a control point [15]. Each time that a control point is reached the beam is interrupted and the MLC acquires a different configuration from the previous segment. The intensity of each segment is individually modulated, resulting in discrete levels of intensity which provides modulation of the field with the desired pattern of fluence. Thus, modulation of the beam fluence is obtained by controlling the number of segments as well as the intensity of each one. On the other hand in DMLC mode each radiation beam is modulated by continuously moving the MLC without interrupting the radiation beam. The variation of the position and the speed of each leaf of the MLC allow to obtain a modulated intensity matrix yielding the desired fluence profile. Despite the advantages in the conformation of the dose distributions, the angle fixed IMRT treatment plan uses a larger number of MU when compared with the

3D-CRT, leading to an increase of the amount of low dose radiation on the rest of the body.

In contrast, the IMAT technique allows the irradiation from all angles in one or more rotations of 360° around the patient. The shape of the field are defined by the MLC in dynamic mode while the intensity modulated is obtained through multiple rotational arcs. The major advantage of IMAT over IMRT fixed angle is the improvement in treatment delivery efficiency due to more efficient use of time and to the reduction of MU on the rest of the body. The reduction in treatment delivery time is an extremely important factor since it reduces the occurrence of potential motion of the target volume as well as the discomfort of the patient, minimizing set-up variations.

Until recently, the major drawback of the IMAT technique was the impossibility to vary angular dose rates (MU/°) and therefore multiple full arcs were necessary to achieve IMAT dose distributions. Presented by Karl Otto in 2008, VMAT is the technique that combines the modulation of the temporal and spatial intensity through the simultaneous variation of different parameters: gantry rotation speed, dose rate and the shape of the irradiation field controlled through the coordinated movement of the MLC [15]. By changing these parameters it is possible to control the dose per degree of gantry angle improving the modulation of the treatment field. This way the dose distributions can be achieve by combining full or partials arcs with sectors where there is no debit of dose, named the avoiding sectors.

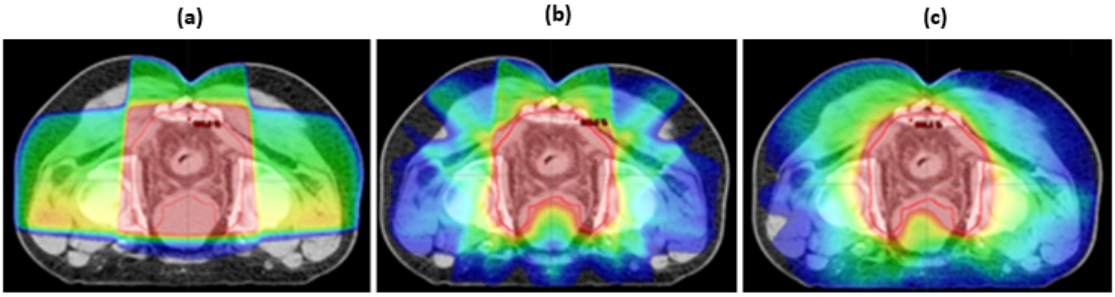

Figure 2.4: Prostate Plan comparison between (a) 3D-CRT, (b) IMRT and (c) VMAT Techniques. From [19]

2.1.4 FFF Beams

The improvement of IMRT and VMAT as well as the development of new radiotherapy schemes such as SRS and SBRT, where large MUs are often required, have stimulated the interest in operating the LINAC in a flattening filter free (FFF) mode, see Figure 2.3 (a).

The main benefit of FFF beams is the possibility of deliver higher dose rates and therefore a shorter delivery time is required. Reducing the delivery time, keeps the patient on the treatment couch for a shorter period, improving patient comfort and decreasing the possibility of inaccuracies due patient movement [20]. For example for prostate and nasopharynx treatments the time can be reduced by 43% with FFF beams.

2.1.5 Clinical Procedure in Radiotherapy

The main tasks of the External Radiotherapy procedure consists of: clinical evaluation of the patient, definition of the patient immobilization system, image acquisition, definition and delineation of volumes of interest, treatment planning, pre-treatment patient-specific quality assurance, radiotherapeutic treatment and clinical follow-up [6].

The first step consist at collecting the patient's clinical history and evaluation of the extent of pathology, defining accordingly the objective of treatment, curative or palliative. After the initial assessment the immobilisation system of the patient is determined, according to the location of the tumour. The main function of the immobilisation system is the reproducibility of the position of the patient over the treatment sessions. Subsequently anatomical images of the patient are acquired to plan the radiotherapy treatment. CT is the primary image modality used to acquire anatomical images, however it can be supplemented with MRI and/or PET. Consequently, from the acquired anatomical images the medical oncologist geometrically defines the volumes of interest, using a specific nomenclature formalized by the International Commission on Radiation Units and Measurements (ICRU), and sets the total dose to administer as well as the dose per fraction. According to the location of the tumour are defined the following volumes: (1) GTV (Gross Tumour Volume), (2) CTV (Clinical Target Volume), (3) ITV (Internal Target Volume), (4) PTV (Planning Target Volume), (5) OAR (Organ at Risk) and (6) PRV (Planning Organ at Risk Volume). The delineation of the corresponding volumes to GTV, CTV and OARs must be independent of the radiotherapy delivery technique, taking into account only oncological and anatomical considerations. Conversely, ITV, PTV and PRV concepts are introduced to ensure that the dose absorbed by the CTV and OARs coincides with the prescribed doses, satisfying the defined constraints [9].

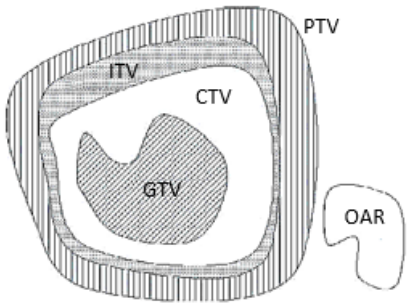

Figure 2.5: Schematic representation of the volumes of interest in Radiotherapy treatment, as defined by the ICRU report. Adapted from [9]

The GTV corresponds to the palpable or visible tumour extension, where the location of tumour cells is considerably higher. In turn, the CTV corresponds to a volume of tissue that contains the GTV and an additional margin associated with sub-clinical tumour extent, which includes microscopic tumour spread in the GTV limit, the potential emergence of metastases in organs seemingly healthy in clinical and radiological examinations and the possible infiltration in lymph nodes. Thus, it is considered that the therapeutic

success depends on the control and elimination of this volume. In order to ensure that the prescribed dose is distributed to all parts of the CTV with clinically acceptable probability, despite the uncertainties associated geometric, PTV is set. This volume considers, in addition to internal variations driven by mobility and anatomical changes of internal organs, the external variations that specifically correspond to uncertainties related to patient positioning, location of the tumour and alignment of the radiation beam. The OARs are healthy organs, which generally show a high radiosensitivity and are located near the CTV [9].

Using the Treatment Planning Systems (TPS) the physicist determines the most suitable treatment technique as well as the configuration of the beams that best reproduce the desired dose distribution. The need to determine the most effective way to modulate the beam intensity introduced a new concept of TPS, the Inverse Treatment Planning. This method, based on the inverse calculation, allows obtaining the dose distribution from the definition of beam parameters, volumes of interest and prescribed dose. Initially, the clinical objective of the treatment is specified by a mathematical function, called objective function. Then the dose limits required by PTV, dose-volume constraints and priority factors relating to the OARs are set. After introducing all of these data, starts the optimization process of the fluence in all irradiations beams, in which the goal is to minimize the objective function. If the calculated dose distribution is not satisfactory, the optimization is repeated changing the clinical parameters in order to achieve an optimal solution. The dose calculation algorithms are the main components of the TPS software since they are responsible for the correct representation of the dose to the patient.

Finally, it is the responsibility of the medical oncologist to give the final approval of the treatment plan. It is a fundamental step that implies, sometimes the decision to admit more dose in a particular OAR to protect others or to better irradiate the target volume. All risks are considered taking into account the radiosensitivity of different tissues. Usually the evaluation is carried out using isodose curves and dose-volume histograms (DVH).

2.1.5.1 Quality Assurance

With the increasing complexity of Radiotherapy techniques, it becomes more important to ensure the delivery of the prescribed doses within accepted criteria since an incorrect delivery of megavoltage energy beams may lead to serious damage to healthy tissues. Therefore, dedicated Quality Assurance (QA) programs are required to ensure the quality of the treatments and the safety of the patients.

In general two types of QA programs are employed in Radiotherapy Departments: (1) machine-specific QA and (2) patient-specific QA. The first allows checking whether the machine characteristic do not deviate significantly from their base line values at the time of commissioning. Depending on each specific machine functionality (such as output, MLC position, couch, gantry rotation, jaws motion and beam quality) these QA programs are performed at different frequencies (daily, weekly, monthly and annually). On the other hand, the patient-specific QA ensure the quality of each individual patient plan, specifically for advanced treatment techniques such as IMRT, VMAT and SBRT. These

QA programs can be performed *priori* or during the treatment session and according to that it is possible to differentiate pre-treatment and *in vivo* patient-specific QA, which are complementary to each other.

The main purpose of pre-treatment patient-specific QA is to verify whether the delivered dose distribution does not deviate significantly from the planned dose distribution due to the overall performance of the LINAC, incorrect transference of the plan to the LINAC or human factors, before the beginning of the first treatment session. If the difference between the planned and the measured dose distributions is beyond the defined acceptance criteria, the recalculation of the patient treatment plan needs to be considered. In turn, *in vivo* patient-specific QA allows comparison between the planned and the delivered dose distributions based on measurements acquired during the irradiation of the patient.

In Radiotherapy Departments, pre-treatment patient-specific QA is more common than *in vivo* and it is usually performed by applying the plan to a 2D or 3D phantom and comparing the planned and measured phantom dose distributions. These measurements may be performed using ionization chambers, thermoluminescent detectors or diodes at a single or multiple points. Although the 2D devices such as diode or ionization chamber arrays contain more measurement points, a resolution higher than 1 cm is rarely achieved. In turn, film measurements provide high resolution but require digitization of the measured data which is time consuming. In addition to high resolution of the digital data, the electronic portal imaging device (EPID) allow a faster acquisition of the data, reason why their potential to perform pre-treatment dosimetric verification has been explored.

2.2 Electronic Portal Imaging Device

EPIDs are two-dimensional X-ray detectors, mounted at the base of the gantries in opposition to the treatment heads of the LINAC, as shown in Figure 2.6. They were clinically introduced in Radiotherapy Departments to verify patient set-up priori to or during treatment session by acquiring portal images which are taken using the treatment radiation beam. The accuracy of radiotherapy relies largely on the correct positioning of the patient on the day of the treatment session and portal images have become an effective method to verify if the patient was positioned according to the reference position from CT used in treatment planning [13, 14, 21].

Traditionally the most commonly method used to acquire portal images for patient set-up verification was a radiographic film which was placed between metal plates and/or phosphor screens. However, the demanding processing that the acquired portal images require before to being able to be used, led to the development of an electronic method for acquiring portal images in order to confirm the patient position in real time. EPIDs allow acquiring digitally portal images which are immediately comparable with the digitally reconstructed radiographs (DRRs) from the TPS that record the intended patient position [14]. The resulting information can be used to make clinical decisions and if necessary to perform appropriate positional adjustments. Therefore EPIDs were developed and surpassed film as the portal image standard.

In addition to the patient set-up verification, it was realised that the portal images

acquired by EPIDs contain dose information and their capacity as a dosimeter to perform patient-specific QA has been investigated.

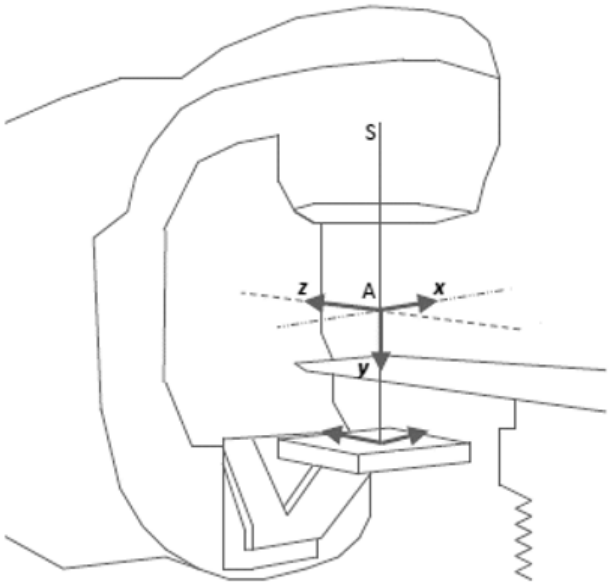

Figure 2.6: Scheme of LINAC geometry showing the patient coordinate system and coordinate system of EPID. The patient coordinated system is set with respect to the isocentre, denoted with A. Considering a patient head-first with respect to the gantry in the supine position the xy, xz and yz planes correspond to axial, coronal and sagittal imaging planes. The beam central axis is representing by the S-A line which also correspond to the source-to axis distance (SAD). The EPID coordinated system is fixed with respect to the plane defined by the EPID surface. As the linear accelerator gantry and EPID rotate about the isocenter the EPID z axis is parallel to the patient z axis, however the x axis is only parallel to the patient x axis at gantry angle zero. The vertical distance from the gantry head to the EPID surface is denoted as source-to-surface distance (SSD). Adapted from [14].

2.2.1 EPIDs Used for Dosimetry

Over the past three decades various types of EPIDs have been developed but only three of them have become commercially available [22]. One of the first EPID to be developed was the Liquid-Filled EPID (Li-Fi EPID) which are classified as a directly detector since the high-energy photons are directly converted into electrons. At the same time, were introduced the indirect detectors starting with the camera-based EPID (CCD-based EPID), which convert high-energy photons in visible light which in turn is converted into electrical charge. Currently the most common detector is the amorphous-Silicon EPID (a-Si EPID) which have also an indirect configuration.

Between 1980 and 1990, Meertens and van Herk in the Antoni van Leeuwenhoek Hospital in Amsterdam developed the Li-Fi EPID, described in one of the first publications which reports the use of EPIDs for dosimetry [23]. The Li-Fi EPID consist of a matrix of two sets of electrodes immersed in an ionization medium, the 2,2,4-trimethylpentane, forming ionization chambers. The electrodes arranged in row are connected to a high-voltage controller and the electrodes in column are associated to an electrometer. Each ionization chamber is read out row by row applying a polarizing voltage to the row electrodes and

measuring the current in each column electrometer [24,25]. The current measured in each ionization chamber is mapped to a grayscale value corresponding to the pixel value [23]. Thus, this device was not suitable for direct dose measurements providing only dose rate measurements.

The CCD-based EPID consists of an X-ray converter, a camera, mirrors and lens. A metal plate and a phosphor screen converting the high-energy photons into visible light constitute the X-ray converter. The light emitted is reflected by a mirror oriented at 45° in direction of a lens and the signal is recorded by a camera. Lastly, the signal is digitized and displayed by an imaging unit.

Firstly described in 1998 by Antonuk *et al.* from the University of Michigan Medical Center in USA, the a-Si EPID consists of an X-ray converter, an active matrix light detector and an electronic acquisition system that receive and process the resulting digital image [22,26]. A metal plate, usually copper, and a scintillating phosphor screen which are placed directly above the active-matrix acts as an X-ray converter, transforming the incident photon beam in light. The copper plate converts the high-energy photons into high-energy electrons and filters the low-energy photons, reducing the scatter and improving the signal-to-noise ratio. The generated electrons interact with the phosphor screen causing the release of visible light by phosphorescence.

Each pixel of the active-matrix consists of a photodiode and a field-effect transistor (FET), both of them composed of hydrogenated amorphous silicon as shown in Figure 2.7. The photodiode is responsible for the detection of the visible light emitted by the phosphor screen while the FET acts as a switch to control the readout of the generated charge [27].

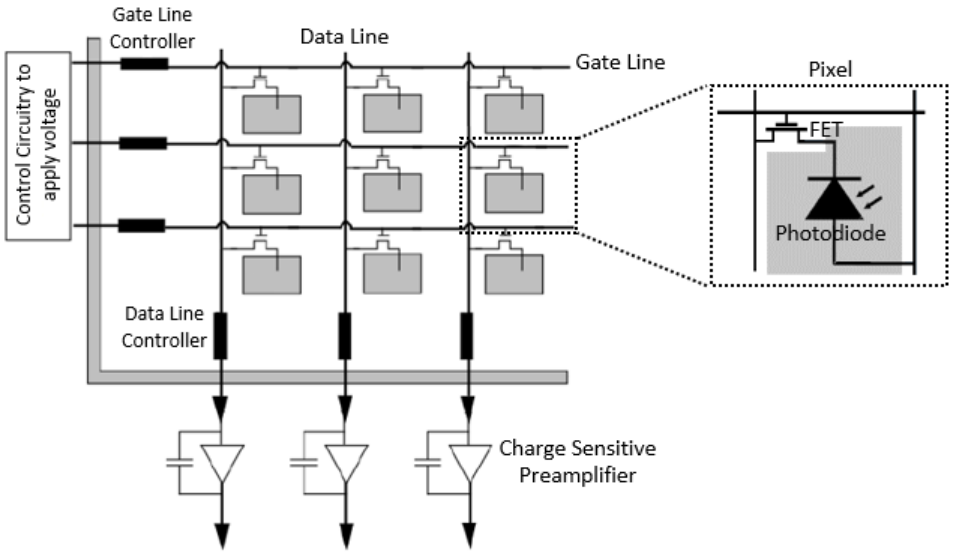

Figure 2.7: Schematic arrangement of the active-matrix of a modern a-Si EPID. Each pixel consists of a photodiode which detect the visible light emitted by the phosphor screen, and a FET that acts as a switch to read the generated charge. The conductivity of each FET along a row is controlled by the voltage applied to the gate line. In turn, the readout of the charge of each FET along a column is controlled by the voltage applied to the respective data line. Each data line is connected to an external charge sensitive preamplifier.

The conductivity of the FETs, conducting or non-conducting, is controlled by the voltage applied to the gate line which have a common controller connected to the gate of each FETs along a row of the active-matrix. On the other hand, the drain of each FET along a column is connected to a data line that in turn is connected to an external charge sensitive preamplifier. So, the voltage applied to the data line controls the readout of the stored charges.

During imaging, the visible light emitted is detected and absorbed by the photodiode creating electron-hole pairs. In turn, due reverse-bias voltage applied to the photodiode, the created holes moves towards the anode and the electrons are drawn to the cathode generating a current proportional to the light detected. This current is integrated and the charge is recorded in the photodiodes by keeping the FETs non-conducting through the application of a negative voltage to all the gate lines. In order to provide maximum spatial resolution the readout of the active-matrix is performed one row at a time by applying to the correspondent gate line a positive voltage which allow the FETs conducting the charge. At the same time, a positive voltage is applied to the data line and the pixel charge is integrated in the preamplifier where the signal is multiplexed and digitized, obtaining for each pixel a grayscale value proportional to incoming radiation. When all pixels of one row have been reading, a positive voltage is applied to the next gate line and so on. The image from reading out the entire matrix once is called a frame.

2.2.1.1 Dosimetric Calibration of a-Si EPID

The standard calibration of the EPID requires the acquisition of a dark-field image, a flood-field image and a defective pixel map to achieve a more uniform EPID response.

First, in order to correct individual pixel background signals, the dark-field image is obtained which is the average of several frames acquired without radiation and for this reason it is the same for all treatment energies. In turn, for each treatment energy, is obtained a flood-field image which is the average of several frames acquired by irradiating the EPID with an open uniform field, large enough to cover the entire active matrix. This flood-field image is used to correct differences in pixel sensitivities by normalizing each individual pixel response [28]. Consequently, the off-axis differential energy response, which is explained in Section 2.2.1.2, is also corrected.

To enhance the image quality, a defective pixel map, which identifies all the non-responding pixels to assign them the mean value of the neighbouring pixels, is acquired. Before to be stored and displayed each frame acquired by EPID is automatically dark-field and flood-field corrected by the Image Acquisition System [29]. So, each portal image (PI_{Raw}) is subtracted by the dark-field (DF) image and divided by the normalized flood-field (FF) image, which is also dark-field corrected, and multiplied by a mean value of the normalized flood-field image (FF_{Mean}) according with

$$PI_{Corrected}(x,y) = \frac{PI_{Corrected}(x,y) - DF(x,y)}{FF(x,y)} FF_{Mean}\,. \tag{2.2}$$

Ideally, for dosimetry purposes the FF image should be perfectly flat. However, since the FF image is generated from an open photon beam, it exhibits the characteristics horns caused by the flattening filter. Therefore, the FF image not only corrects pixel-to-pixel sensitivity variation or off-axis differential energy response but also removes the beam profile present in the acquired portal image, causing spatial distortions in the fluence distribution [30]. For this reason, a previously calculated or measured (with film or ionization chamber in water) beam profile (BP) is used to restore the initial beam profile of the acquired portal image, so

$$PI_{Corrected}(x,y) = \frac{PI_{Corrected}(x,y) - DF(x,y)}{FF(x,y)} FF_{Mean} BP\,. \tag{2.3}$$

To perform dosimetric calibration of the EPID, two different approaches have been adopted: prediction of the grayscale pixel value or conversion of grayscale pixel value to dose or fluence value. The first one models the EPID response by Monte Carlo simulation or empirical models. For this reason, an accurate and detailed knowledge regarding EPID composition is required. Parent *et al.* and Siebers *et al.* developed an effective method, based on Monte Carlo simulation, to modulate the EPID response for IMRT fields [31,32]. In turn, the second approach converts the portal image acquired by EPID into a portal dose image applying empirical models based on measurements in water with a calibrated detector, usually an ionisation chamber. The portal dose image can be described by a primary (D_P) and a scatter (D_S) dose component, such that

$$PDI = D_P + D_S \tag{2.4}$$

where the scatter dose component can be described by a convolution of the primary dose with the EPID scatter kernel. Consequently, assuming that the primary energy fluence, is proportional to the primary dose component, the incident energy fluence at the EPID level can be determining by the deconvolution of the portal dose image with the EPID scatter kernel [33].

In general, converting grayscale values to dose or fluence is simpler and faster than a modulation of the EPID response and therefore more suited for clinical implementation [34]. However, an accurate knowledge of dosimetric characteristics of the EPID is fundamental in order to implement a reliable model to convert the grayscale pixel value.

2.2.1.2 Dosimetric Characteristics of a-Si EPID

The dosimetric characteristics of the EPIDs such as sensitivity, reproducibility, dose-response, dose rate dependence, and energy response have been investigated for several groups.

The availability of EPID as a dosimeter is dependent on the ability to provide reproducible results, over a certain period of time. The reproducibility is verified by the variation in the pixels response to the same field and in the same conditions. Several

studies have demonstrated that the reproducibility of different a-Si EPIDs is within 2%, either over short or long periods of time [28].

As for the relation between the dose rate and EPID response, the studies concluded that the response is independent of the dose rate, in other words the measured dose of each pixel is independent of the rate that the dose was accumulated, which is a fundamental characteristic for a dosimetry purposes. However, with large dose rates the EPID saturation is observed. In addition, in most studies the response of a-Si EPIDs has proved to be linearly related to the dose [27,29,32,35,36].

The major drawback for the use of a-Si EPID for dosimetry is its over-response to low-energy photons relative to water, due to the phosphor layer which has a high atomic number and therefore increases the probability of photoelectric effect [28]. For that reason, the EPID response is sensitive to factors that may change the incident photon beam spectrum such field size, off-axis distance or the presence of an attenuating medium [35,38,39]. With increasing distance from the central axis is verified a softening of the incident photon beam or in other words a decrease in the beam mean energy which causes an over-response of the EPID with respect to ionization chambers in water. On the other hand, the presence of an attenuating medium (phantom or patient) causes a hardening of the incident photon beam by filtering the low-energy photons which results in a marked decrease in the response of the EPID.

The components of the EPID support arm also increase the amount of backscattered radiation.

2.2.2 Methods of EPID Dosimetry

Recently, Van Elmpt *et al.* published a comprehensive review of EPID dosimetry methods in which the capabilities and limitations of each one are explored [22].

Independent of the type of detector used it is possible distinguish two different dosimetry methods based whether the radiation beams pass or not through an attenuation medium (phantom or patient), respectively transit and non-transit dosimetry. Non-transit images are a valuable tool for performing quality control of treatment parameters related to dosimetric and geometric characteristics of the LINAC, such as symmetry of the beam, the absolute output of LINAC or MLC leaf positions or trajectory. As mentioned in Section 2.1.5.1 the dosimetry verifications can be performed *priori* or during treatment and according to that is also possible to differentiate pre-treatment and *in vivo* dosimetry [22].

Considering the previous definitions and according to the different configurations of the EPID is possible to define different methods to perform EPID dosimetry, as described in Figure 2.8. In each method the dosimetric verification can be performed at the EPID level or inside the patient or phantom [22]. At the EPID level the acquired portal image, which can be in grayscale values or converted to fluence or dose values depending the used approach for the dosimetric calibration, is compared with the predicted EPID response or dose distribution calculated at the EPID by a specific algorithm. The alternative is to reconstruct, from the portal image acquired by EPID, the dose inside the patient or phantom CT and compare with the treatment plan calculated with patient or phantom,

respectively, by the TPS.

The present study focuses on pre-treatment dosimetry, specifically in non-transit configuration, in which an image is acquired for each IMRT field or VMAT arc without a phantom in the beam in order to verify whether the intended fluence is delivery correctly by the LINAC. Therefore, in the next Section an overview of pre-treatment dosimetry to perform patient-specific QA is presented and several approaches are described.

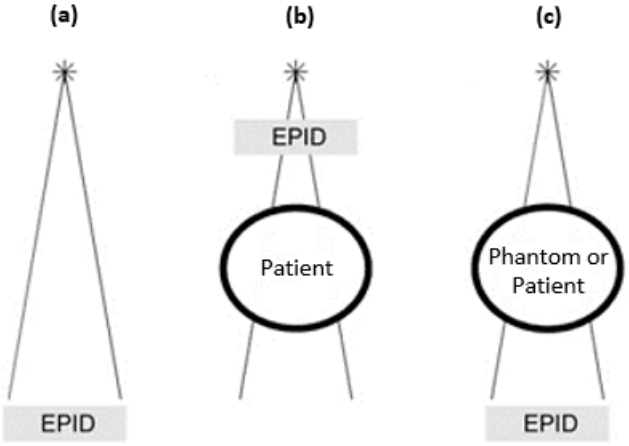

Figure 2.8: Three arrangements for EPID dosimetry, each with the possibility to verify a dose distribution at the EPID level or inside the phantom or patient: (a) non-transit configuration for pre-treatment dosimetry, (b) non-transit configuration for in vivo dosimetry and (c) transit configuration for pre-treatment or in vivo dosimetry. From [22].

2.2.2.1 Overview of EPID Pre-Treatment Dosimetry

With the introduction of advanced radiotherapy techniques and higher dose prescriptions the complexity of the treatment plans increase and pre-treatment patient-specific QA routines are mandatory. Consequently, different methods to perform EPID pre-treatment dosimetry using a non-transit configuration have been investigated by several groups including 2D fluence or dose comparison at the EPID level or 2D and 3D dose reconstruction in phantom or patient CT.

Van Esch *et al.* developed a method to perform a 2D dose verification at EPID level. Thus was developed an algorithm to predict the dose distribution at the EPID level and to compare that with the dose distribution measured by the EPID for different clinical IMRT fields [28,40]. Where comparing the acquired to the predicted portal dose image, the percentage of points that are in agreement according to gamma criteria of (3%, 3mm), see Section 2.3, is more than 95% for all tested IMRT fields.

Nijsten *et al.* reported a method to verify the absolute dose at the centre of the field at the level of the EPID, developing an algorithm to calculate the dose at the centre. To determine the accuracy of the central dose values measured with the EPID as well as the one calculated by the algorithm, ionization chamber measurements were performed. The mean difference between ionization chamber and EPID was $0.8 \pm 1.2\%$ [41].

Warkentin *et al.* proposed an EPID pre-treatment dosimetry method in which the measured energy fluence is converted to a 2D dose distribution inside a phantom at a

specific depth. This method involves a deconvolution of EPID scatter kernel generated by Monte Carlo simulation from the EPID portal image in order to obtain the incident photon's energy fluence. The dose distribution in phantom is then reconstructed from the primary energy fluence and consequently compared with the planned dose distribution at the same depth. EPID pre-treatment verifications of IMRT fields delivered with SMLC have shown a good agreement with the verifications performed with film for 3 IMRT plans, corresponding to 24 fields [42].

van Elmpt *et al.* describe an alternative method that use the primary energy fluence extracted from a measured portal dose image as input for a Monte Carlo algorithm that calculates 3D dose distribution in a phantom or patient CT. An agreement within 3% was achieved for dose measurements using ionization chamber. A similar approach was used by Steciw *et al.* but to calculate 3D dose distribution, the same TPS as used to calculate the treatment plan was applied instead a Monte Carlo algorithm [43]. So, the 3D dose distribution calculated by the TPS from the portal dose image acquired by the EPID was compared with the dose distribution of the treatment plan also calculated by the TPS.

At Erasmus Medical Centre – Daniel den Hoed Cancer Center in Rotterdam, EPID dosimetry to preform pre-treatment patient-specific QA is already clinically implemented. van Zijtveld *et al.* used the algorithm developed by the Rotterdam group to predict the dose distribution at the EPID level for 270 patients treated with IMRT fields. The dose distribution measured with the EPID was compared with the predicted dose distribution for each field of each patient. Four clinically relevant errors were revealed, in one a wrong treatment plan was transferred to the LINAC and for three times one of the leaves were malfunctioning. Also at MAASTRO Clinic in Maastricht pre-treatment dosimetry using EPIDs has been performed for all patients. Several errors such as wrong manual entering of treatment parameters and errors in the machine output [22].

2.3 Dose Distributions Comparison

The efficient and accurate comparison between the calculated and the measured dose distribution are essential in the pre-treatment patient-specific QA of IMRT and VMAT plans to avoid the underdose of the target volume or the overdose of the normal tissues, as referred in Section 2.1.5.1. Therefore in clinical practice a number of different evaluation methods can be used to compare the dose distributions.

2.3.1 Profile Comparison

The dose distributions profiles in the X, Y or diagonal directions can be plotted against each other and be visually compared. This method is very useful when evaluating local deviations between distributions found with other comparison methods.

2.3.2 Absolute and Relative Dose Difference

The Dose Difference (DD) is the most intuitive and straightforward quantitative evaluation method in which the absolute or relative difference between two dose distributions is calculated point-by-point in a dose domain [44]. In this way, considering a point in the reference dose distribution ($\vec{r}_r$) and the corresponding point in the evaluated dose distribution ($\vec{r}_e$) the DD is given by

$$\delta(\vec{r}_e, \vec{r}_r) = D_e(\vec{r}_e) - D_r(\vec{r}_r) \tag{2.5}$$

where $D_e(\vec{r}_e)$ represents the evaluated dose at position $\vec{r}_e$ and $D_r(\vec{r}_r)$ the reference dose at position $\vec{r}_r$ [45]. A DD criterion (ΔD) is set such that the points with a dose difference value higher than Δ fail the criterion and the points with a dose difference value lower than Δ pass the criterion. In clinical practice normally ΔD=3% of the maximum dose.

Although this method is considered clinical significant for low-dose gradient regions, it is inadequate to evaluate high-dose gradient regions since a small spatial shift in the alignment can translate into a large dose difference.

2.3.3 Distance to Agreement

The Distance-to-Agreement (DTA) is the spatial difference between a point in the reference dose distribution ($\vec{r}_r$) and the closest point with the same dose value in the evaluated dose distribution ($\vec{r}_e$) which can be given by

$$r(\vec{r}_e, \vec{r}_r) = min|\vec{r}_e - \vec{r}_r| \,. \tag{2.6}$$

A DTA criterion (Δd) is also set, typically Δd=3mm, and the points with a DTA value at higher than Δd fail the criterion and the points with a DTA value lower than Δd pass the criterion.

Unlike the DD, the DTA method is sensitive in high-dose gradient regions. However, for low-dose gradient regions the DTA method can display regions of disagreement greater than the DTA criterion, defined as clinically acceptable criterion, for relatively small dose differences [45].

2.3.4 Gamma Evaluation

Nowadays, the most accepted evaluation method in clinical practice is the gamma analysis. It was introduced by Low et al. and combines the DD and DTA methods, which are complementary with respect to high and low-dose gradient regions [45,46,47].

Considering the points $\vec{r}_r$ and $\vec{r}_e$ and the correspondent dose value $D_r(\vec{r}_r)$ and $D_e(\vec{e}_r)$ of two 2D dose distributions. The gamma evaluation is based on an ellipsoid surface with centre in $\vec{r}_r$ corresponding to the acceptance criterion which combines the ΔD and Δd, usually (3%, 3mm). The ellipsoid, geometrically represented in Figure 2.9, is defined in

the 3D space with two special dimensions and one dose dimension according to

$$\Gamma(\vec{r}_r, \vec{r}_e) = \sqrt{\frac{r^2(\vec{r}_r, \vec{r}_e)}{\Delta d^2} + \frac{\delta^2(\vec{r}_r, \vec{r}_e)}{\Delta D^2}}\,. \tag{2.7}$$

In turn the gamma index at point $\vec{r}_r$ is calculated by finding the minimum value of $\Gamma(\vec{r}_r, \vec{r}_e)$ varying $\vec{r}_r$ and it is expressed by

$$\gamma(\vec{r}_r) = min\{\Gamma(\vec{r}_r, \vec{r}_e)\}\forall\{\vec{r}_e\} \tag{2.8}$$

where, according to the acceptance criterion defined, the points with $\gamma(\vec{r}_r)$ <1 passes and on the other hand the points with $\gamma(\vec{r}_r)$ >1 fails the criterion. Another parameter clinically used to compare two dose distributions is the gamma passing rate ($\%\gamma < 1$).

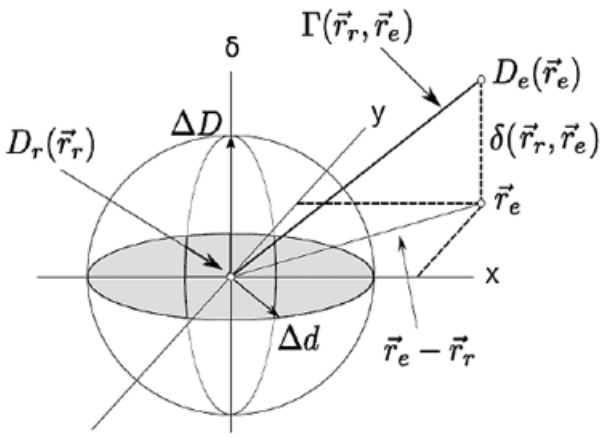

Figure 2.9: Geometric representation of the theoretical concept of the gamma evaluation method for 2D dose distributions. The x and y axes represent the spatial location of the point in the evaluated distribution ($\vec{r}_e$) relative to the point in the reference distribution ($\vec{r}_r$). The δ represents the dose difference between the evaluated dose ($D_e(\vec{r}_e)$) and the reference dose ($D_r(\vec{r}_r)$). The ellipsoid that correspond to the criteria acceptance is defining by the dose difference tolerance (ΔD) and the maximal distance to agreement (Δd). In this example point r_e fails the criterion. From [46].

Chapter 3

Materials and Methods

In the Department of Radiotherapy of the Champalimaud Foundation there are two Varian LINACs, TrueBeam™ and EDGE™ System (Varian Medical Systems, Palo Alto, CA, USA). The LINACs have attached by a retractable robotic arm different versions of a-Si EPIDs, the PortalVision aS1000 and aS1200, respectively. Apart from the EPID, the current Portal Dosimetry solution commercially available by Varian is composed of a Portal Dose Image Prediction algorithm and a Portal Dosimetry software to analyse and evaluate the dosimetric results. The Portal Dosimetry solution only allows to perform pre-treatment dosimetry, for both IMRT and VMAT plans.

As mentioned before, the main purpose of this work is to perform initial testing to implement pre-treatment dosimetry for the Varian LINAC. For this reason, to evaluate the Portal Dosimetry solution and the performance of both EPIDs for dosimetric proposes two different studies were conducted:

1. On the TrueBeam™ System was tested the Portal Dosimetry Pre-Configuration Package, which is a research approach to improve and simplify the configuration of the Portal Dosimetry solution. Consequently the performance of the Portal Dosimetry solution for pre-treatment patient-specific QA of IMRT and VMAT plans with FF beams was evaluated.

2. On the EDGE™ System was performed the installation and verification of the Absolute Pre-Treatment Portal Dosimetry to evaluate pre-treatment patient-specific QA of IMRT and VMAT plans with FFF beams. This research software allows to perform absolute dosimetry for pre-treatment verifications once it uses a model that convert the EPID grayscale values to dose in water. A MATLAB® program was developed in order to study the sensitivity of the EPID during pre-treatment patient-specific QA.

In this Chapter the data sets and the EPIDs characteristics used for each study are presented. The calibration models as well as the workflows for dosimetric calibrations are also described.

Figure 3.1: EDGE^{TM} Radiosurgery System by Varian. All the acquired portal dose images are acquired at SSD equal to 100 cm and such that the couch is not in the beam.

3.1 Data Sets

The first study includes data from 11 anonymized breast cancer patients treated with IMRT on the TrueBeam ^{TM} System and 22 anonymized prostate cancer patients treated with VMAT also on the TrueBeam^{TM}. Only patients treated with 6MV energy and FF beams were selected since the EPID attached to TrueBeam System, the aS1000, saturates for FFF beams due to the high dose rates.

For the second study data from 10 anonymized cancer patients treated in EDGE^{TM} System were included. In Table 3.1 is shown the treatment site, fractionation scheme, prescription dose and the dose per fraction for each patient. Contrary to the first study, all the selected patients were treated with 6MV and FFF beams, and were selected in order to provide a variety of complexity of the plans.

Table 3.1: Table describing treatment site, number of fractions and prescribed dose per fraction for each patient plan included in the evaluation of the Absolute Pre-treatment Portal Dosimetry.

Patient	**Treatment Site**	**# of Fractions**	**Dose (Gy)**
H&N	Maxilla	5	6
B1	Frontal	3	9
B2	WBRT	5	4
P	Paravertebral	1	24
M	Femur	1	24
T1	Oropharynx	5	6
T2	Sternum	1	24
T3	Clavicle	3	9
G	Testicles	9	2
A	Inguinal	1	24

3.1.1 DICOM Format

DICOM (Digital Imaging and Communication in Medicine) is the standard format for management of medical imaging and related data and for the communication between different types of medical imaging devices and computers.

DICOM-RT is an extension of the DICOM that is specified for radiotherapy modality and it includes different type of information: (1) DICOM-RT Structure describes all the different structures delineated from the planning CT, (2) DICOM-RT Plan includes information related to the treatment beams configuration, collimator geometric configuration and dose prescription, (3) DICOM-RT Dose describes the dose distributions calculated and (4) DICOM-RT Image includes the images acquired during the treatment and their related information.

3.2 Varian Portal Dosimetry Solution

The Varian Portal Dosimetry solution is composed by three main components: (1) EPID (PortalVision aS500, aS1000 or aS1200), (2) Portal Dose Image Prediction algorithm to obtain a reference image with which the EPID acquired images are compared for dosimetric verification and (3) Portal Dosimetry software to evaluate the agreement between predicted and EPID acquired images.

3.2.1 Varian Portal Dosimetry Configuration

The configuration of Varian Portal Dosimetry solution consists mainly of two parts: (1) dosimetric calibration of the EPID, in this specific case PortalVision aS1000 or aS1200 and (2) configuration of the Portal Dose Image Prediction (PDIP) algorithm in Eclipse workstation. Eclipse^{TM} is a Varian software that provides an interface for treatment planning including contouring of the structures, beam planning, dose calculation and plan evaluation.

Each configuration procedure will be briefly describe in the next Sections 3.2.1.1 and 3.2.1.2.

3.2.1.1 EPID Dosimetric Calibration

The calibration of the EPID, PortalVision aS1000 or aS1200, is performed on a Vision Workstation and requires the acquisition of a dark-field image, a flood-field image, a defective pixel map and a beam profile as referred in Section 2.2.1.1. The first step for standard calibration is accomplished by taking a dark-field image and then a flood-field is acquired by delivering a 40x32 cm^2 uniform field, Figure 3.2. The defective pixel map is also acquired in order to achieve a more uniform EPID response. Finally, a diagonal profile of a 40x40 cm^2 field measured in water is used to recover the beam profile.

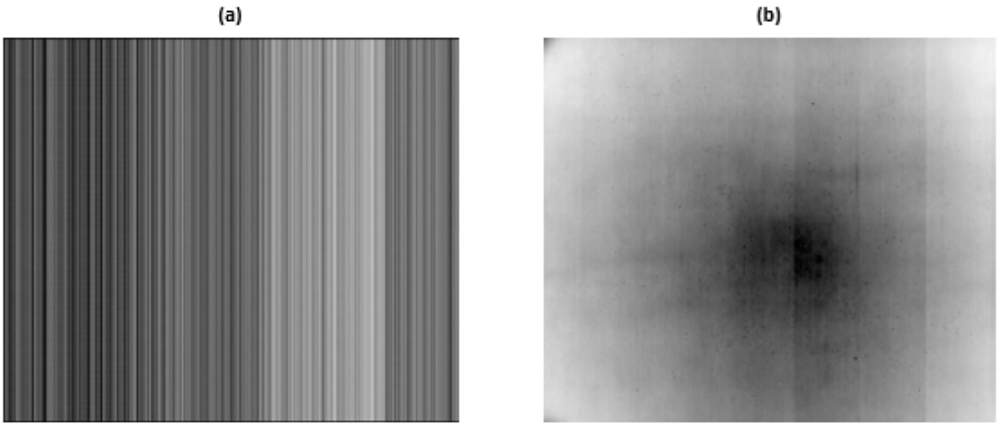

Figure 3.2: Images acquired during a dosimetric calibration of PortalVision aS1000:(a) Dark-Field Image and (b) Flood-Field Image

The dosimetric calibration of the EPID is performed in terms of Calibrate Units (CU) in which the portal dose images are displayed, so that usually 1 CU is defined as corresponding to the CAX value of a 10x10 cm^2 field at a SSD equal to 100 cm when 100 MU delivered. However, in the Department of Radiotherapy of the Champalimaud Foundation the calibration is preformed such that 100 CU correspond to the CAX value at the centre of a 10x10 cm^2 field at a SSD equal to 100 cm when 100 MU are delivered. This normalization makes 1 CU correspond to 1 cGy in reference condition. It is important to state that CU is a unit specific to Varian and does not properly represent a physical unit.

3.2.1.1.1 Portal Vision aS1000 and aS1200

The focus of the first study was the PortalVision aS1000 (Varian Medical Systems, Palo Alto, CA, USA) which consists of: (1) a 1.6mm protective cover plate (2) a 9mm of a rohacell foam and circuitry, (3) a 1mm copper plate, (4) scintillating phosphor screen made of Terbium-activated Gadolinium Oxysulfide (Gd_2O_2S: Tb) with 0.4 mm of thickness, (5) an active matrix with 30 cm x 40 cm of area which consists of 1024 x 768 pixels, each one with size of 0.39 x 0.39 mm^2 and (6) electronics to translate the charge into an image as is represented in Figure 3.3 (a). PortalVision aS1000 has the ability to acquire 10 frames per second and a dose rate maximum of 1000 MU/min.

The as1000 is part of a large system, the Image Acquisition System, schematically represented in Figure 3.3 (b), which includes electronics necessary for the acquisition, display and storing of the images. The image information acquired by the aS1000 is sent as an analog signal to the digitization unit where it is transformed into a digital signal. Therefore, the signal is transferred to the Vision Workstation, which is responsible to manage images and related information. The universal control board in the Vision Workstation is responsible for the synchronization of the aS1000, the digitization unit and the LINAC. Then the frame processing board processes and corrects the portal image according to the procedure described in Section 2.2.1.1.Finally the corrected image is stored on a Vision server and can be displayed posteriorly [48].

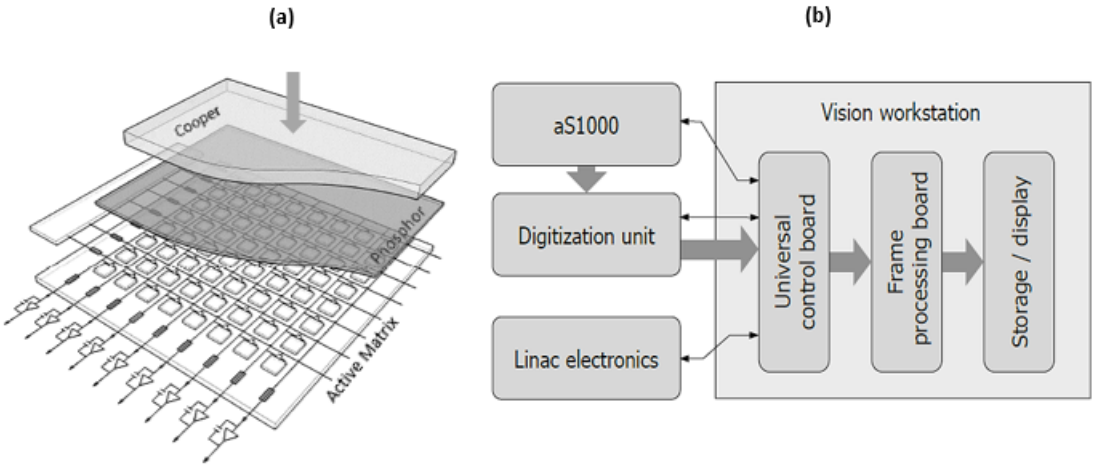

Figure 3.3: (a) Schematic PortalVision aS1000 showing the main components. The photon's energy fluence from the LINAC focuses on EPID. The cooper plate converts the high-energy photons into high-energy electrons which in turn interact with the phosphor screen causing the release of visible light. The active matrix is responsible for detecting the visible light emitted by the phosphor screen and to record the generated charge which is reading by the electronics. Figure is not to scale. Adapted from. (b) Schematic overview of the main components of the Image Acquisition System. The grey arrows represent the flow of the acquired portal image information and the black arrows represent the synchronization system. From [48].

For the second study carried in EDGE was used the PortalVision aS1200 (Varian Medical Systems, Palo Alto, CA, USA) which is an improved version of aS1000. First, the PortalVision aS1200 is constituted by an active matrix with 43 cm x 43 cm of area which consists of 1280 x 1280 pixels, each one with size of 0.34 x 0.34 mm^2. Besides that, the maximum frame rate is 25 frames per second, the maximum dose rate is 5 times higher than the aS1000 as well as the lifetime radiation exposure which is 1000 Gy. This recent version also incorporates a backscatter shielding to reduce the backscatter from the retractable robotic arm, the ExactArm (E-arm).

3.2.1.2 Portal Dose Image Prediction Configuration

The predicted portal dose image, with which the acquired portal dose image is compared, is calculated in the Eclipse workstation with an algorithm specifically for this purpose, the Portal Dose Image Prediction (PDIP) algorithm. This algorithm can only be used for pretreatment dosimetry verification since it does not consider the patient and the treatment couch and it is based on Pencil Beam Convolution algorithm, originally developed by Storchi *et al.*[28,49].

As with the Pencil Beam Convolution algorithm, in PDIP the radiation beam is modelled as being composed of a set of infinitesimally small beams and the total dose is therefore the sum of the dose contributed by each small beam. In the first step the theoretical energy fluence (Ψ_P) at the isocenter distance is multiplied by a radial symmetric beam profile correction ($P_{correction}$), which describes the off-axis variation of the beam depending only on the distance in millimetres from the beam centre. The portal dose image ($PDI_{Predicted}$) in function of EPID position (x,y) at a SDD distance is then calculated by

convolving ($\otimes$) the obtained theoretical energy fluence at the EPID level with the EPID scatter kernel (k_{EPID}), which is radially symmetrical, such that

$$PDI_{Predicted}(x,y) = \frac{1}{N}\Psi_P(x,y).P_{Correction}(r) \otimes k_{EPID}(r).CFS \tag{3.1}$$

where N is a normalization factor and CSF is the collimator scatter factor, which only depends on the opening of the jaws or in other words on the field size.

Considering the PDIP algorithm its configuration in Eclipse workstation requires three different measurements: (1) a specific test field, the AIDA, (2) the output factors, which are both measured with the EPID and (3) a beam profile. The beam profile can be a diagonal profile measured in water with ionisation chamber. However, to avoid performing extra measures the beam profile used in PDIP algorithm is taken from an existing intensity profile in the Treatment Planning System, at the shallowest depth.

The AIDA test plan has an ideal modulation where the MLC limitations have not been taken into account, representing a field with optimal fluence. From the measured portal dose images of this field is determined the EPID scatter kernel, required for the PDIP algorithm. EPID scatter kernel is assumed to be a sum of Gaussians whose parameters are adjusted iteratively until the difference between the predicted portal dose image (see 3.1) and the measured portal dose image of the AIDA field is minimised. The output factor of a particular field corresponds to the value measured at the CAX, normalized to the dose point at CAX for the 10x10 cm^2 field. The output factors are measure from the portal dose image acquired with EPID for field sizes from 3 cm x 3 cm to 28 cm x 38 cm and the missing values are interpolated by the PDIP algorithm in order to determine the CSF. The largest field size that can be measured at SSD equal to 105 cm is 28 cm x 38 cm since a larger field would irradiate the sensitive electronics of the EPID.

3.2.1.3 Portal Dosimetry Review Workspace

The Portal Dosimetry Review Workspace in Figure 3.4 allows the comparison between the predicted portal dose image with the portal dose image acquired.This software has tools for comparison and evaluation of dosimetric portal dose images such as gamma analysis and dose differences, see Section 2.3.

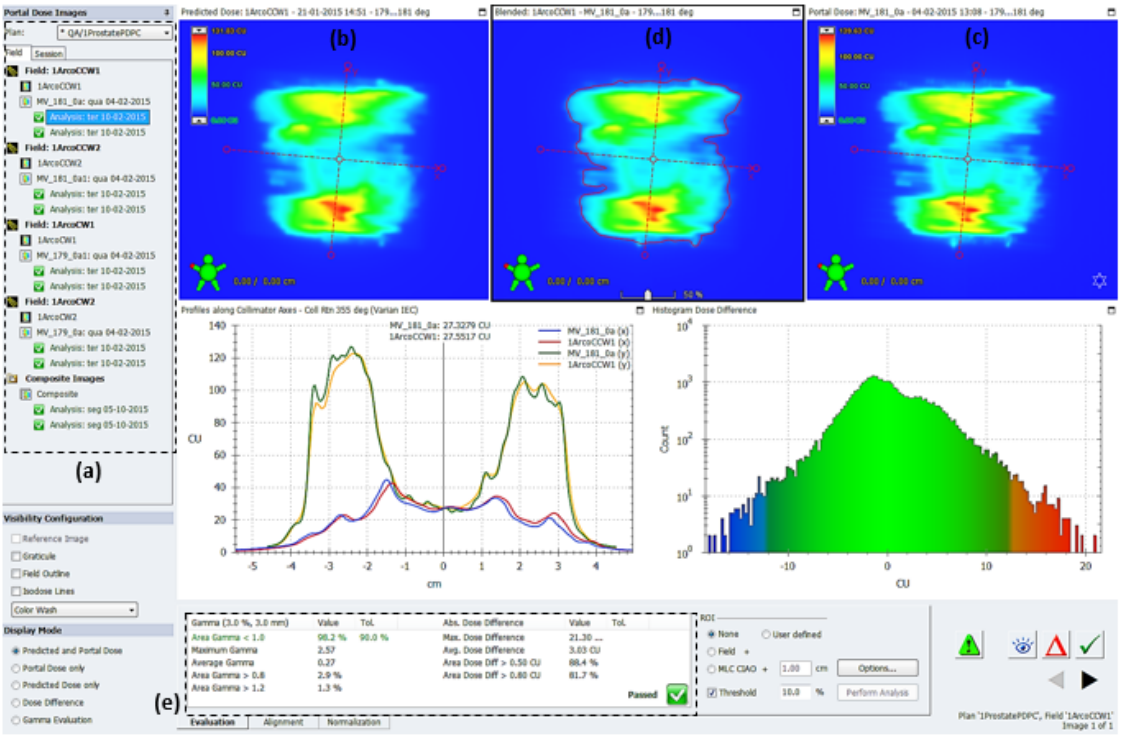

Figure 3.4: Varian Portal Dosimetry Review Workspace:(a) navigation panel where we can select each field to perform a gamma or dose difference analysis. For the selected field is presented in the upper left side (b) the predicted portal dose image calculated by the configured PDIP algorithm and in the upper right side (c) the portal dose image acquired with the EPID. The predicted portal dose image and acquired portal dose image are automatically blended and the resulting image is presented in the centre as is shown in (d). The results of each preformed analysis are display in the evaluation box as is shown in (e). A profile along collimator x and y axis are displayed for both images as well as a dose difference histogram.

3.3 Portal Dosimetry on TrueBeam^{TM} System

TrueBeam^{TM} is a fully-integrated system for image guided radiotherapy and it is used to treat tumours in any localization in the body where radiation is indicated.

Despite the commercial version of Portal Dosimetry being available and installed in the Department of Radiotherapy of Champalimaud Foundation this solution is only used to perform some machine specific QA. A research approach to simplify the configuration of the Portal Dosimetry solution was installed and clinically evaluated in TrueBeam^{TM} which are equipped with aS1000.

3.3.1 Configuration of PDPC Package on TrueBeam^{TM}

The configuration of PDPC package consists of two parts: (1) configuration of the PDIP algorithm on Eclipse Workstation and (2) calibration of the EPID in Vision Workstation. A backup of the existing Portal Dosimetry was performed in order to be restored at a later point in time.

The pre-configured PDIP algorithm which assumes that the scatter behaviour of different EPIDs of the same type can be modelled by identical scatter kernels, is easily imported

into Beam Configuration in Eclipse. The 2D beam profile correction matrix is imported on the treatment console during the dosimetric calibration of the PortalVision aS1000 and is used to recover the beam profile that is removed from the EPID images by the flood field correction. Remember that during the standard calibration of aS1000, a diagonal profile of a 40x40 cm^2 is used to recover the beam profile, see Section 3.2.1.1, and in the standard configuration of PDIP algorithm the EPID scatter kernels are determined from the portal dose image of AIDA field, see Section 3.2.1.2.

As the PDPC package is under research and is not yet a commercial solution details about its content and configuration are not exhaustively discussed. In Figure 3.5a genereal scheme describing the Portal Dosimetry study in TrueBeam^{TM} System is shown.

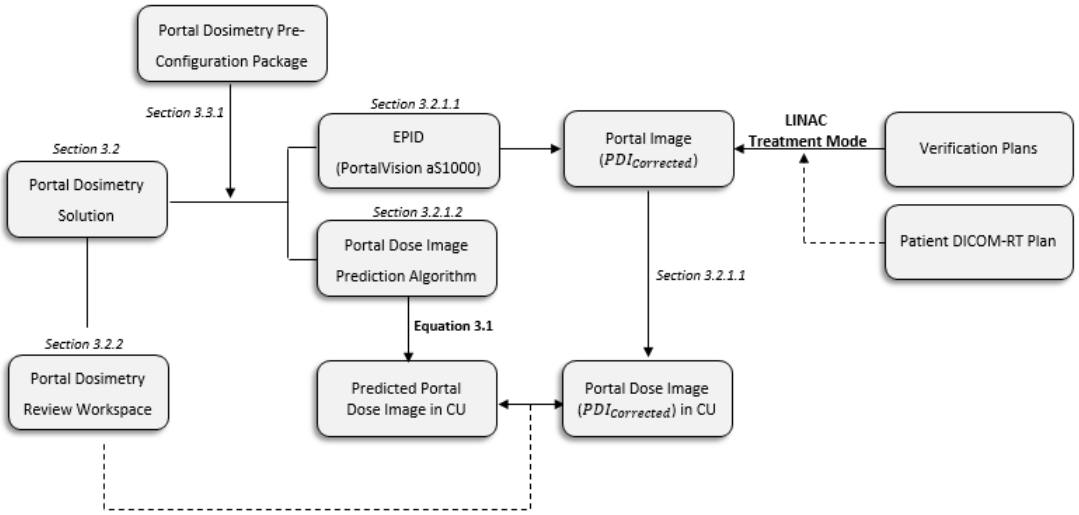

Figure 3.5: General flowchart describing the Portal Dosimetry study in TrueBeam^{TM} System. The calibration of the PDIP algorithm on Eclipse Workstation and the calibration of the EPID in Vision Workstation were done with the PDPC package. A set of verification plans were delivered in Treatment Mode and then the acquired portal dose image was compared with the predicted portal dose image through the Portal Dosimetry Review Workspace, in order to verify the correct configuration of the Portal Dosimetry with the PDPC package. Also some clinical plans of breast and prostate cancer patient were analysed. The section and equation describing the operations required to progress to the next step are shown.

3.3.1.1 Verification Plans

In order to verify the correct installation of the PDPC a set of plans were analysed. These verification plans allows to evaluate MLC parameters settings, output factor, beam profile and backscatter correction. All verification plans were evaluated in accordance with Varian specification as described in the next Sections 3.3.1.1.1 to 3.3.1.1.4.

3.3.1.1.1 Multi-Leaf Collimator Parameters

The accuracy and performance of the Portal Dosimetry solution strongly depends on a proper setting of the MLC parameters: Transmission Factor and Dosimetric Leaf Gap since the fluence is influenced by both, thus affecting the predicted portal dose image.

Two different verification plans are evaluated to verify whether the current MLC pa-

rameters are compatible with the PDPC package. Described by van Esch *et al.* the Dynamic Chair test plan in Figure 3.6 (b) is used to separate the impact of Transmission Factor and Dosimetric Leaf Gap. In turn, AIDA test plan (see Section 3.2.1.1) presented in Figure 3.6 (a) was developed to commission the PDIP algorithm and it is irradiated to verify the proper calculation of the EPID scatter kernel used in the algorithm.

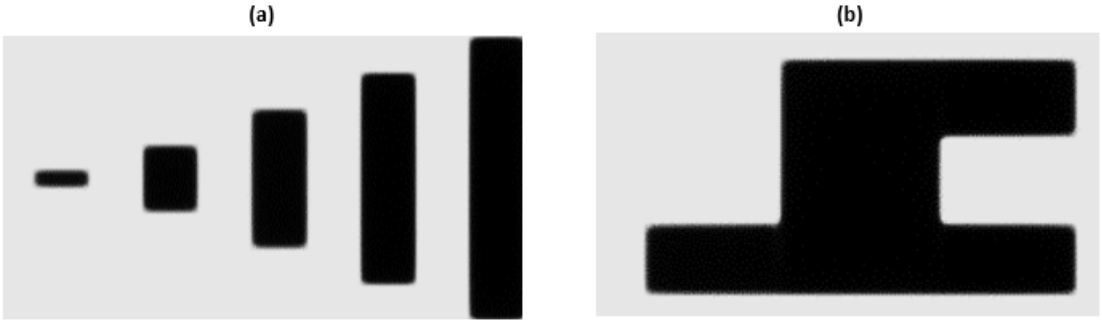

Figure 3.6: MLC Parameters verification plans: (a) AIDA test plan represents a field with optimal fluence and it is developed to verify the calculations of EPID scatter kernel used in PDIP algorithm, and (b) Dynamic Chair test plan is used to evaluate of the impact of MLC parameters: Transmission Factor and Dosimetric Leaf Gap, which are requested in TPS configuration in order to calculate the fluence with accuracy. The right part of the pattern is used to estimate the proper setting of the transmission factor, where the null dose area in grey corresponds to the transmission through the leaves. On the other hand, in the left part of the pattern the leaves are moving at maximum speed in the null dose area between the legs of the chair which are influenced by both MLC parameters.

The portal dose images of both verification plans were acquired at SSD equal to 100 cm with the gantry angle set at 0° gantry angle and collimator angle set at 90°. The evaluation was performed in the Portal Dosimetry Review Workspace with a (3.0 %, 3.0 mm) gamma analysis as shown in Figure 3.7, comparing the acquired portal dose image with the predicted portal dose image. An adaptation of the MLC parameters can be considered in case deviations are observed.

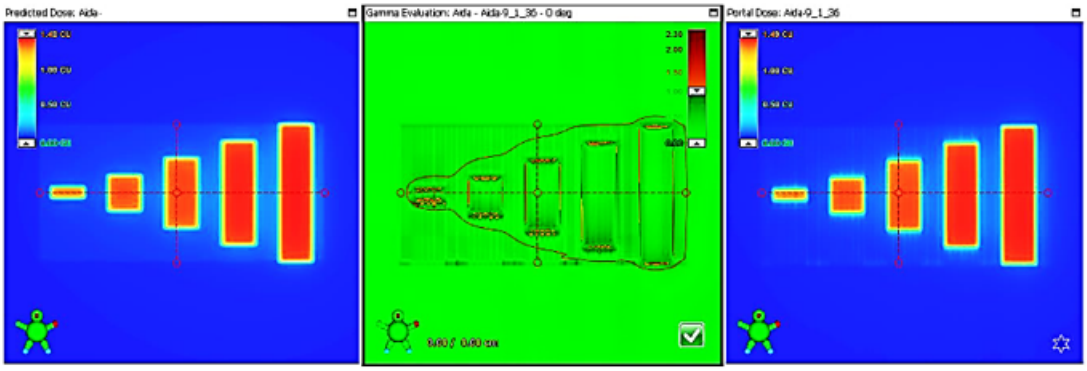

Figure 3.7: Gamma analysis of AIDA test plan verifying proper commissioning of the PDIP algorithm.

3.3.1.1.2 Output Factors

As referred previously in Section 3.2.1.2, the output factor is the point dose measured at the CAX, normalized to the point dose at CAX for the 10x10 cm^2 field. In order to verify whether the output factors used in the PDIP algorithm match with the actual output factors of the EPID, the CAX value of the predicted as well as the acquired EPID image were compared for different square field sizes (3x3 cm^2, 5x5 cm^2, 10x10 cm^2, 15x15 cm^2, 20x20 cm^2, 30x20 cm^2, 30x30 cm^2).

The CAX value was extracted using the Point Dose tool of the Portal Dosimetry Review Workspace, Figure 3.8 and to evaluate the results the relative difference between the CAX of the predicted image and the acquired image was calculated using output factor values of the predicted image as reference. For field sizes ranging from 5x5 cm^2 to 30x30 cm^2 the relative difference should be within ±1.0%.

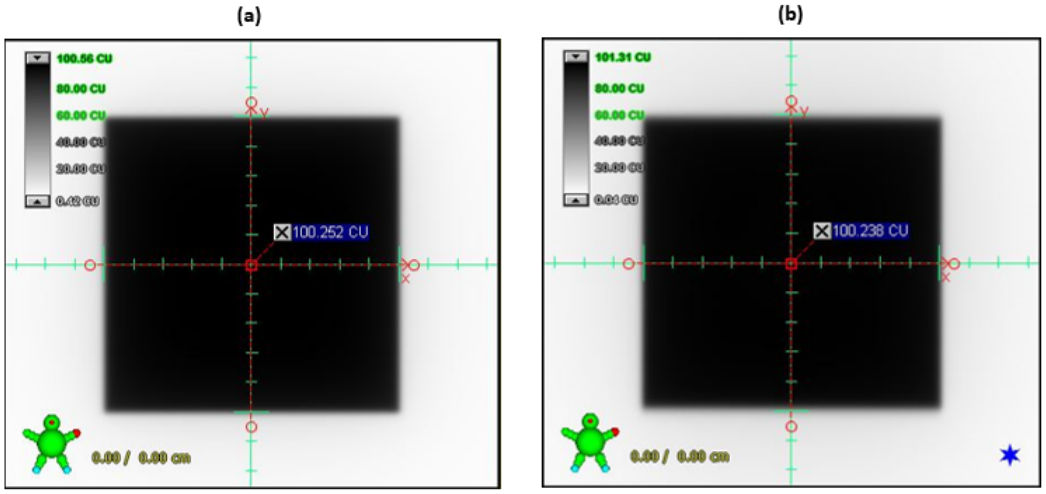

Figure 3.8: Evaluation of the central axis value of the (a) predicted and (b) acquired portal dose images for a 10x10 cm^2 with the Point Dose tool. The images are in grayscale in order to select with precision the point dose at CAX.

3.3.1.1.3 Beam Profile and Backscatter Correction

The PDPC package provides a 2D beam profile which incorporate an improved backscatter correction in vertical direction. The accuracy of the beam profile can be observed in the crossline direction, Figure 3.9 and the backscatter effect in inline direction, Figure 3.10 of the EPID. The crossline and inline profile within the flat field region of the predicted as well as the acquired EPID image were compared for different square field sizes (3x3 cm^2, 5x5 cm^2, 10x10 cm^2, 15x15 cm^2, 20x20 cm^2, 30x20 cm^2, 30x30 cm^2). The flat field region is defined as 80% of the area within the 50% field limit.

For each field the dose difference was normalized relative to the dose at the isocenter. The profiles were selected using the Profile Tool of the Portal Dosimetry Review Workspace and to evaluate the results for the accuracy of beam profile, the mean relative difference between the crossline profile of the predicted portal dose image and the acquired portal dose image was calculated. For field sizes ranging from 5x5 cm^2 to 30x30 cm^2 the mean relative difference should be within ±1.0%.

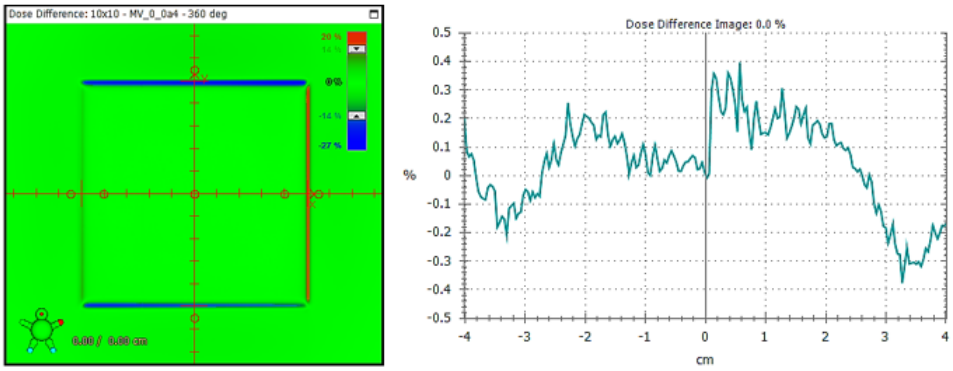

Figure 3.9: Dose difference normalized relative to the dose at the isocenter. The Profile Tool was used to select a crossline profile covering the central flat field region.

On the other hand, to evaluate the results for backscatter correction the maximum difference between half inline profile of the predicted portal dose image and the acquired portal dose image was calculated. For field sizes ranging from 5x5 cm^2 to 15x15 cm^2 the maximum relative difference should be within $\pm 1.5\%$.

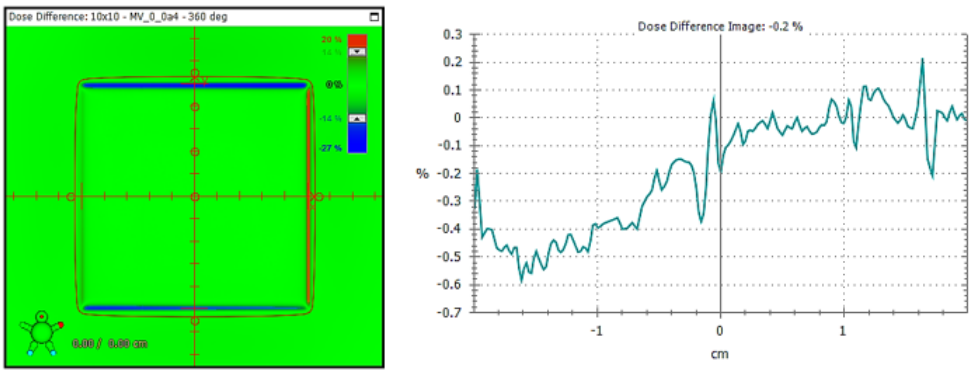

Figure 3.10: Dose difference normalized relative to the dose at the isocenter. The Profile Tool was used to select a half inline profile covering the central flat field region.

3.3.1.1.4 IMRT and VMAT Plans

Four exemplary of IMRT and VMAT plans were added to the set of verification plans in order to investigate the performance of the PDPC package under clinical conditions. The portal dose images of both plans were acquired at SSD equal a 100 cm. The evaluation was performed in the Portal Dosimetry Review Workspace with a (3.0%, 3.0 mm) gamma analysis and a dose threshold of 5%, comparing the acquired portal dose image with the predicted portal dose image. The threshold of gamma passing rate was set at 97%.

Beside the verification plans provided with the PDPC package the plans of 12 Breast cancer patients treated with IMRT and 20 Prostate cancer patients treated with VMAT in TrueBeam System were also analysed. The evaluation was performed in Portal Dosimetry Review Workspace with a (3.0%, 3.0 mm) and (2.0%, 2.0 mm) gamma analysis.

3.4 Portal Dosimetry in EDGE^{TM} System

The EDGE^{TM} Radiosurgery System is a solution for delivering full body, intracranial and extracranial, radiosurgery treatments with extremely accuracy. The EDGE^{TM} System can track the tumour in real time, precisely calculate the patient movement and monitors the respiratory motion. Therefore, it is possible to deliver highly focused treatments, in less sessions and at a fast dose rate, minimizing the dose received by the surrounding healthy tissues.

Considering the growing clinical evidences of the benefits of delivering high doses in a small number of fractions and the innovative characteristics of the EDGE^{TM} System, most of the treatments are performed with FFF beams. However, the version of ARIA® installed in the Department does not support the Portal Dosimetry solution for FFF beams so it is not possible to automatically generate a plan to acquire portal dose images. ARIA® is the information and image management solution which combines radiation, medical and surgical oncology information. The Absolute Pre-treatment Portal dosimetry is the only solution that allows to preform EPID pre-treatment dosimetry regardless of the ARIA® version.In Figure 3.11 a flowchat describing the mainly processes of the Absolute Pre-Treatment Portal Dosimetry study in EDGE^{TM} System is shown.

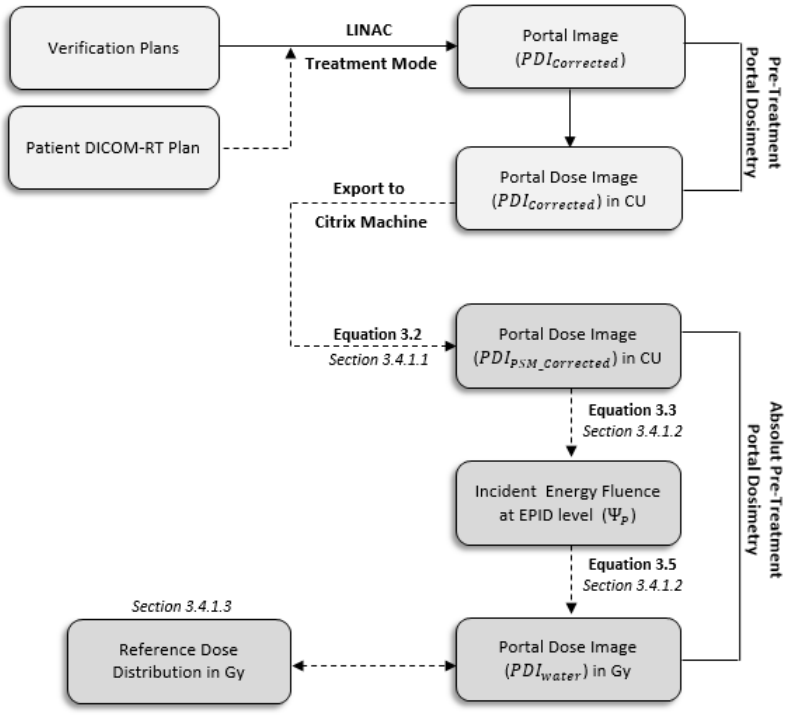

Figure 3.11: General flowchart describing the Absolute Pre-Treatment Portal Dosimetry study in EDGE^{TM} System, mainly the process to obtain a water equivalent portal dose image in Gy from a portal dose image in CU. In order to verify the correct configuration of the Absolute Pre-Treatment Portal Dosimetry a set of verification plans were delivered in Treatment Mode and then the acquired portal dose images were exported to the Citrix Machine, where they are compared with the predicted portal dose image. Also some patient clinical plans were analysed. The section and equation describing the operations required to progress to the next step are shown.

3.4.1 Absolute Pre-Treatment Portal Dosimetry

As mentioned in Section 2.2.1.2, the main disadvantage to using EPIDs for dosimetry is their lack of a water equivalent response. The Absolute Pre-Treatment Portal Dosimetry solution allows converting a portal dose image in CU to a portal dose image in water. However, the installation of the Absolute Pre-Treatment Portal Dosimetry requires the configuration of the commercial Portal Dosimetry solution for the EDGE^{TM} System, specifically the dosimetric calibration of the PortalVision aS1200. So, the configuration of the Portal Dosimetry solution was performed in the EDGE^{TM} System, according the procedure described in Section 3.2.1.

The Absolute Pre-Treatment Portal Dosimetry is implemented as a research add-on to the Portal Dosimetry Review Workspace and is only accessible through remote Citrix Machine. After the configuration of the Absolute Pre-Treatment Portal Dosimetry a set of verification plans identical to those described in Section 3.3.1.1 were analysed.

3.4.1.1 EPID Calibration for Absolute Portal Dosimetry

As described in Section 2.2.1.1 the beam profile is present in both flood-field and EPID images. For this reason, EPID images can only be acquired in the same position in which the flood-field image was acquired since any displacement of the EPID will result in misalignment between these two images.

Greer developed a new method, instead of the usual flood-field correction, to correct the portal image for pixel sensitivities regardless of the position of the EPID at the calibration time [30]. The pixel sensitivity map (PSM) is the pixel response to a beam with uniform intensity and the same energy spectrum at all pixel locations in the EPID matrix. As result the PSM contains only the differences in pixel sensitivities, specified with respect to the central pixel and ensures that the beam profile is conserved.

To measure the PSM, different calibration images in open field conditions for a set of different field sizesand EPIS shifts are acquired. The EPID is irradiated for each field size and then the EPID is displaced laterally in the cross-plane between each irradiation. Therefore, the PSM is formed from the combination of the central region of each raw portal image, since this region of the field aproximates to a uniform intensity beam without any variation in the energy spectrum [30].

In order to correct portal images for the pixel sensitivity variation using the PSM, it is first necessary to remove the flood-field correction that is automatically applied by the EPID software (see Section 3.2.1.1), so the flood-field corrected portal image ($\mathrm{PDI}_{Corrected}$) is multiplied by the normalized flood-field image (FF) and divided by the mean value of the normalized flood-field image (FF_{Mean}) as well as to the diagonal beam profile (BP) to obtain portal image only corrected for individual pixel background signals, such that

$$PDI_{PSM_Corrected}(x,y) = \frac{PDI_{Corrected}(x,y)FF(x,y)}{FF_{Mean} * BP} \frac{1}{PSM(x,y)}\,. \tag{3.2}$$

Finally it is required to correct defect pixels again since they were reintroduced by undoing the flood-field calibration.

The configuration of the Absolute Pre-Treatment Portal Dosimetry implies that the acquired portal images are corrected using the PSM. For these reasons to configure this Portal Dosimetry solution it was necessary to retrieve for each energy (6MV–FF and 6MV-FFF) the calibration data from EDGE^{TM} System in order to undo the flood-field calibration, such as (1) flood-field image, (2) beam profile, (3) pixel defect map. The PSM matrix was acquired together with Varian Medical Systems service engineer. The resultant portal dose image corrected by PSM ($PDI_{PSM_Corrected}$), see Equation 3.2 is also presented in terms of CU.

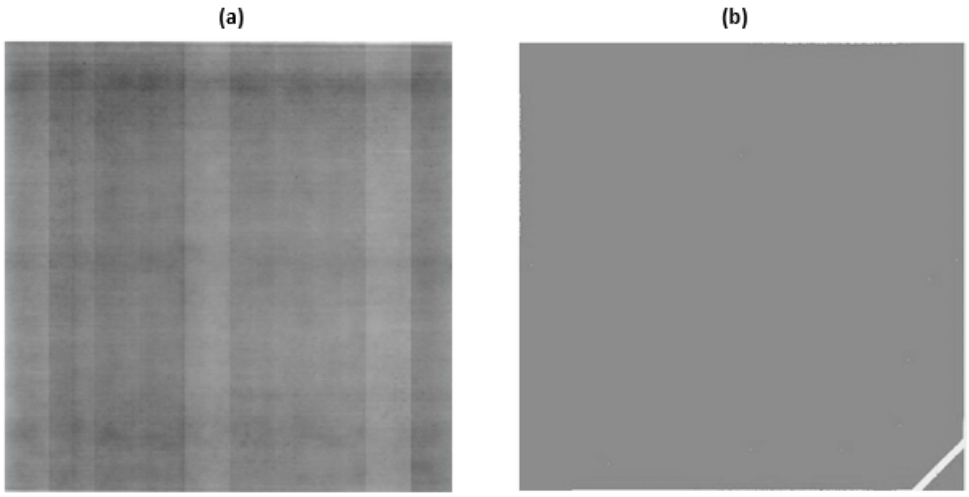

Figure 3.12: Portal images retrieved from EDGE^{TM} System to configure the Absolute Pre-Treatment Portal Dosimetry(a) Pixel Sensitivity Matrix and (b) Defect Pixels Map.

3.4.1.2 Mathematical Model for Absolute Portal Dosimetry

A model has been developed to convert EPID grayscale values to dose in a water phantom. This model uses the EPID scatter kernels to obtain the incident photon's energy fluence at the EPID level (see Section 2.2.1.1) and then uses the water dose kernels to convert that energy fluence to the dose that would be deposited in water at a given depth [50]. As referred in Section 2.2.1 in order to increase the signal-to-noise ratio the EPID consists of high atomic number materials causing photon scattering within the EPID. In this sense, to obtain the incident photon's energy fluence (Ψ_P) at the EPID level in function of its position (x,y) is performed a desconvolution ($\otimes^{-1}$) of the the portal dose image ($PDI_{PSM_Corrected}$)with the EPID scatter kernel (k_{EPID}), such that

$$\Psi_P(x,y) = [BP_{Correction}(r) PDI_{PSM_Corrected}(x,y)] \otimes^{-1} k_{EPID}(r) \tag{3.3}$$

where the beam profile correction ($BP_{correction}$), which depends only on the distance in millimetres from the beam centre (r), is determined from the ratio between a EPID image

corrected for pixel sensitivity with a PSM and a diagonal profile measured in water, Figure 3.13.

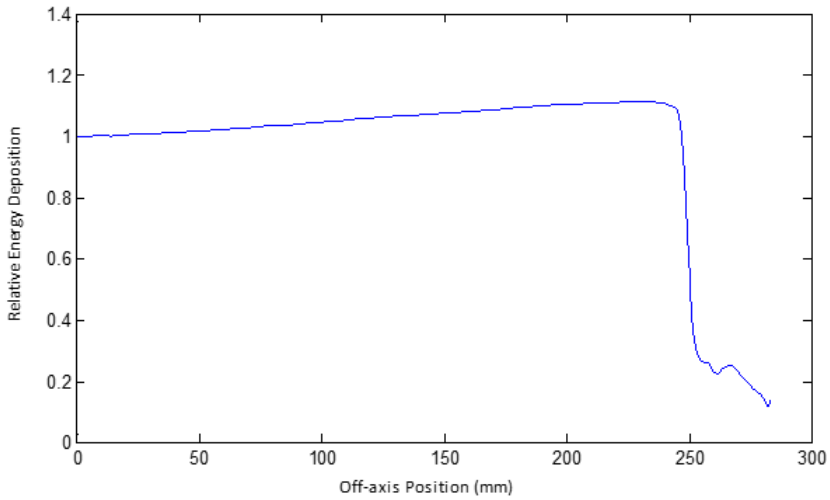

Figure 3.13: The beam profile correction used in Absolute Pre-Treatment Portal Dosimetry only depends on off-axis distance and it is determined from the ratio between EPID image corrected with a PSM and a diagonal profile measured in water.

In this model, the EPID scatter kernel is assumed to be a triple exponential function and the parameters (a_i) are based on empirical measurements which are optimized by comparing the fluence obtained by Equation 3.3 with the fluence calculated by the TPS algorithm. Regarding the form, the scatter kernel used in this model is similar to that used by Kirkby and Sloboda,

$$k_{EPID}(r) = exp(-a_1 r) + a_2 exp(-a_3 * r) + a_4 exp(-a_5 r) \tag{3.4}$$

where the scatter kernel depends on the radial distance in millimetres from the beam centre (r) which corresponds to the centre of the acquired portal dose image [51].

As mentioned in Section 2.2.1.2 as result of the photoelectric interactions of low-energy photons in the phosphor layer an over-response of the EPID for off-axis positions is observed. As the increased response of the EPID due the low-energy photons varies with the distance to the centre, a radially symmetric termal factor ($T(r)=1+b_1*r$) is applied to the fluence obtained in Equation 3.3. A radially symmetric attenuation factor ($A(r)=exp(-b_2*r^2)$) is also applied to the fluence in order to take into account the longer path lengths that would be experienced by off-axis beam. Having determined the incident photon's energy fluence, a convolution ($\otimes$) with the water dose kernels (k_{water}) is applied to determinate the dose that would be deposited in water at a given depth

$$PDI_{Water}(x,y) = D_{Conversion} \cdot [T(r)\Psi_P(x,y)A(r)] \otimes k_{Water}(r) \tag{3.5}$$

where $D_{conversion}$ is an absolute conversion factor that converts the CU on the EPID image into Gy. This it is determined by comparing the central axis dose in water calculated by

this model with the dose measured in water. The water dose kernel parameters are based on empirical measurements which are optimized by comparing the dose in water obtained by Equation 3.4 with the dose measured in water tank phantom.

In the present study all the absolute doses were determined to a depth of 5 cm and the factors used in the conversion model to perform absolute portal dosimetry are presented below in Table 3.2 and Figure 3.14.

Table 3.2: Table with the values of the factors used in the conversion model to perform Absolut Pre-Treatment Portal Dosimetry for 6-FFF energy. The dose conversion factor was adjusted in order to eliminate the discrepancy between the reference and the measured dose in the reference field (10 cm x 10 cm). For Pre-Treatment Portal Dosimetry, the optimizer process found that a Terma factor of (very close to) 1 provides the best conversion results since the Beam Profile correction used in Equation 3.3 also does a radially symmetric correction.

Factor	Value
Atenuation	1.30 x 10^{-6}
Terma	1
Dose Conversion	0.99

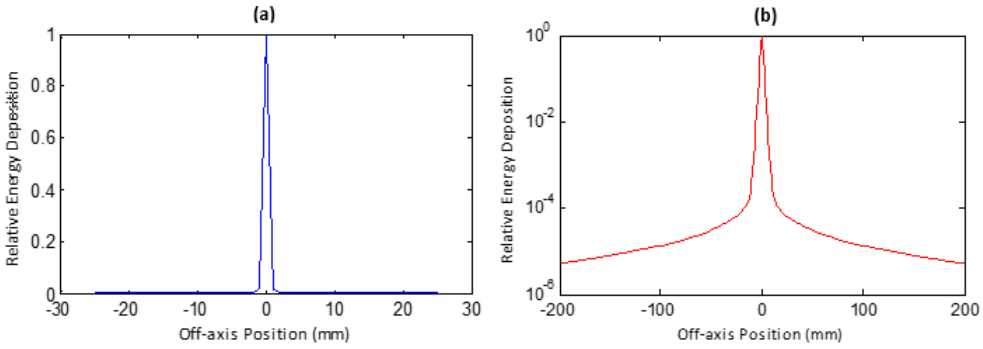

Figure 3.14: The EPID scatter kernel and Water dose kernel used in Absolute Pre-Treatment Portal Dosimetry are based on empirical measurements comparing the fluence calculated by the TPS algorithm and the dose measured in water tank, respectively. The off-axis relative energy deposition of EPID scatter kernel is shown on linear scale in (a) while the water dose kernel is shown on logarithmic scale in (b).

3.4.1.3 Absolute Pre-Treatment Portal Dosimetry for FFF Beams

As referred previously, with the version of ARIA® installed in the Department of Radiotherapy it is not possible to create a verification plan to acquire portal dose images for FFF beams through the commercial Portal Dosimetry solution. The workaround is to acquire the portal dose images on a different plan. So, in the Eclipse™ workstation the patient plan is calculated in a phantom like the one shown in Figure 3.15(a). It is mandatory to

ensure that the images are acquired at SSD equal to 100 cm and that the couch is not in the beam, see Figure 3.1.

As the point is to convert the acquired portal image to a portal dose image in water, the patient treatment plan is recalculated in a water phantom in order to obtain a reference dose distribution. In Eclipse^{TM} workstation, the calculations were performed in a water tank phantom of volume 40x40x20 cm^3 cm3 with water Hounsfield Unit (HU), which is a quantity obtained from a linear transformation of the measured attenuation coefficients in CT. It is important make sure that the calculation is performed taking into consideration that the water surface is at SSD equal to 100 cm, once the portal images are acquired with the EPID placed in this position. The gantry is also reset to 0 degrees so the beam axis is normal to the water surface.

The reference dose distribution in Gy, correspondent to the predicted portal dose image, was extracted at a depth of 5 cm since it is larger than D_{max} for any clinical beam and thus ensures that the charge particle equilibrium is achieved.

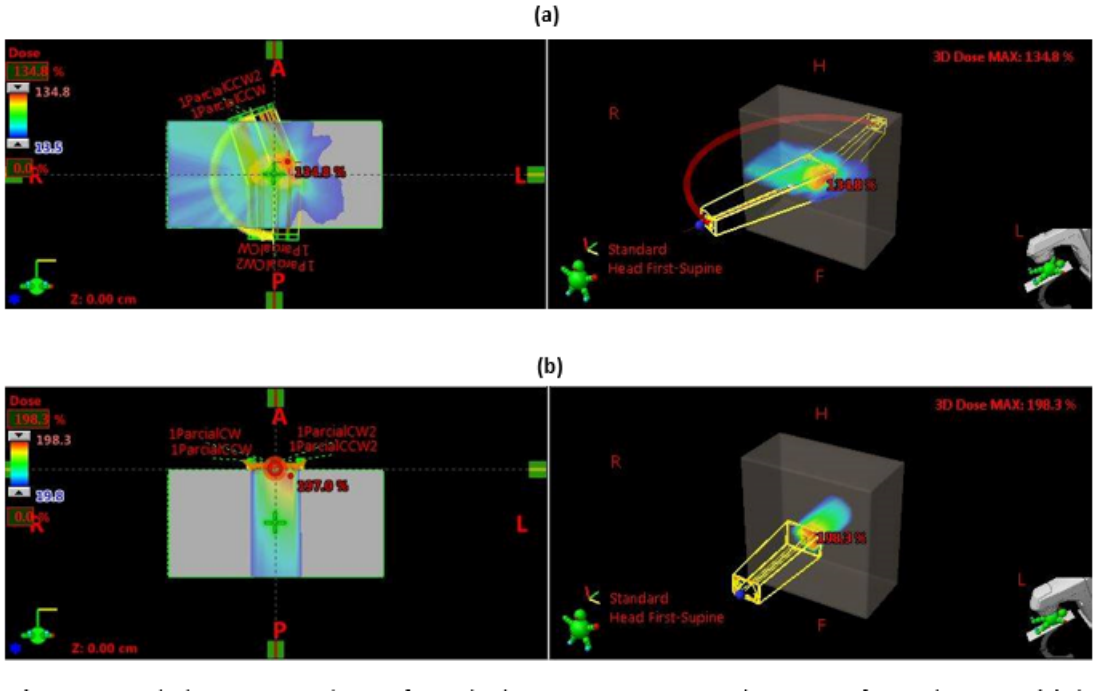

Figure 3.15: Calculations required to perform Absolute Pre-Treatment Portal Dosimetry for FFF beams. In (a) the patient plan is recalculated in a phantom in order to acquire portal dose images with FFF beams and in (b) the EPID is modelled as water tank phantom of volume 40x40x20 cm^3 with water HU to obtain the reference dose distribution which is extracted at a depth of 5 cm.

After acquiring all the portal images, some data were exported from Eclipse^{TM} in ARIA® environment, where the calculation were performed, and imported to Eclipse^{TM} in a remote Citrix machine: (1) DICOM-RT Plan corresponding to the verification plan used to acquire the portal dose images and plan calculated in the water tank phantom to determine the predicted portal dose image, (2) DICOM-RT Structure of both plans, (3) DICOM-RT Dose of the plan that contains dose to water and (4) DICOM-RT Images acquired with EPID.

3.5 Sensitivity of EPID for Pre-Treatment Dosimetry

In order to evaluate the sensitivity of the aS1200 EPID during pre-treatment patient-specific QA a complete workflow was developed to introduce some intentional errors in 2 different DICOM-RT plans totalling 8 fields.

The primary goal consisted of developing a viable and effective method which does not require to recalculate the patient plan in Eclipse™ workstation since it is time consuming. The solution is introduce the errors in the patient plan in XML format which is then directly loaded on the Vision Workstation of EDGE™ System. The entire process is as follows:

1. As the native language of EDGE™ System is XML, the DICOM-RT Plan was converted to a XML-file, through Veritas (Varian Medical Systems, Palo Alto, CA, USA). This software is an open tool that lets users generate XML-files from DICOM-RT Plan without any prior knowledge about XML-Schema rules;

2. An in-house MATLAB® (v.2013a MathWorks Inc., Natick, MA, USA) code was written in order to add some attributes which are mandatory to load the XML-file in Developer Mode nd to correct some parameters which are not correctly converted by Veritas. Developer Mode is a research user interface in which the features that could affect machine performance in the Clinical Mode have been disabled. The mentioned code also separates each field or arc in different XML-files in order to introduce in each one an Image Point through Veritas, which makes possible acquire a portal dose image for each arc;

3. Systematic or random errors are introduced in each XML-file through an in-house program written in MATLAB®(v.2013a MathWorks Inc., Natick, MA, USA);

4. The modified XML-file is transferred to Varian network and loaded directly in LINAC operated in Developer Mode which is a research environment. Unlike the Treatment Mode the Developer Mode is driven by XML-Files loaded on the Vision Workstation of EDGE™ System;

5. DICOM-RT Images acquired with aS1200 EPID are edited in DICOM Editor software in order to change the Image Type to ORIGINAL\PRIMARY\PORTAL\ ACQUIRED_DOSE and the Image Description to 6xFFF;

6. The modified DICOM-RT Images are then imported to the Eclipse™ in the Citrix Machine and connected to the correspondent field in order to perform Absolute Pre-Treatment Portal Dosimetry.

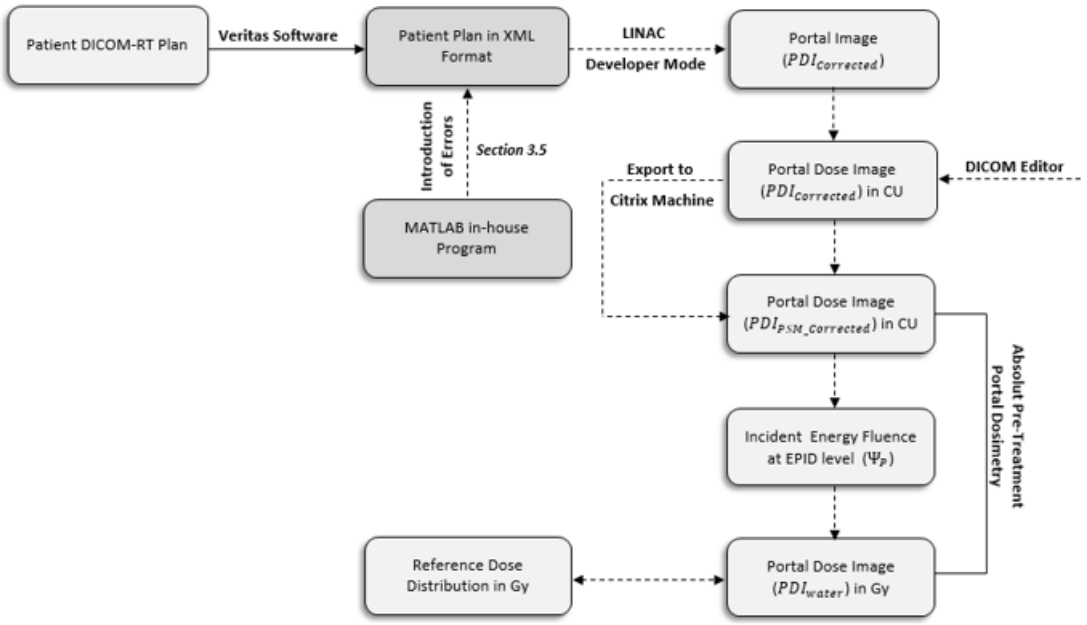

Figure 3.16: General flowchart describing the routine to introduce errors in XML-file in order to evaluate the sensitivity of Absolute Pre-Treatment Portal Dosimetry in EDGE^{TM} System. The patient DICOM-RT Plan is converted in XML-File through Veritas and systematic or random errors are introduced by an in-house program written in MATLAB®. The modified XML-File is then delivered by LINAC operated in Developer Mode and the acquired portal dose image in CU is edited in DICOM Editor in order to import the acquired portal dose image to the Eclipse^{TM} in Citrix Machine to perform Absolute Pre-Treatment Portal Dosimetry. Before testing the described method in clinical plans it is advisable to test it with the simplest plan.

3.5.1 MATLAB® Program to Introduce Errors

An in-house program written in MATLAB® (v.2013a MathWorks Inc., Natick, MA, USA) was developed to introduce errors in XML-files modifying the gantry position, monitor units values, collimator rotation, collimator jaws and MLC leaf positions for all the control points.

To introduce errors in the parameters previously mentioned, it is crucial to study each one in order to take into account all the limitations. In gantry rotation is necessary to consider the direction, clockwise and counter clockwise, in order to ensure that the direction of a particular arc does not change between clockwise and counter clockwise with the introduction of a random error. A verification code was added to guarantee that the values with errors do not exceeded the mechanical limitations of the gantry, getting between 1 and 359 degrees. This code was also used for the introduction of errors in collimator rotation. The values of MU are cumulative in each control point, so to modify the total MU of a plan we determined the value of Mu corresponding to each control point by calculating the difference between two consecutive control points and then the average of MU was determined. The error introduced was applied to the achieved average MU. For the modification of collimator jaws, it was necessary to ensure that the values with errors do not exceeded the mechanical limitations of the jaws which corresponds to an aperture of 20 cm from centre for X and Y directions (a square field of 40x 40 cm^2). Regarding to the MLC, the errors in leaves positions were only introduced in the active leave, in other words

in the leaves that are involved in the arc delivery. It was also considered the mechanical limitation of the MLC which correspond to an aperture of 19 cm and a code was created to verify if the gap between to opposite leaves was lower than 0.051 cm. To avoid an error or warning during the delivery, it was ensured that the distance between the most open leaf and the correspondent jaw was the same before and after the introduction of the error. For the graphic representation of the leaves position of the MLC, the thickness of each leaf was considered so the central 32 leaves pairs was represented with a thickness of 2.5 mm and the remaining 28 pairs with a thickness of 5 mm.

Although the developed program allows the introduction of errors in all the parameters mentioned above, for the present the errors were only introduced into MU and leaves positions of MLC.

A user-friendly Graphical User Interface (GUI) of the program was also developed in MATLAB®, see Figure 3.17. Is important to mention that this program only works on a computer with licensed MATLAB® software.

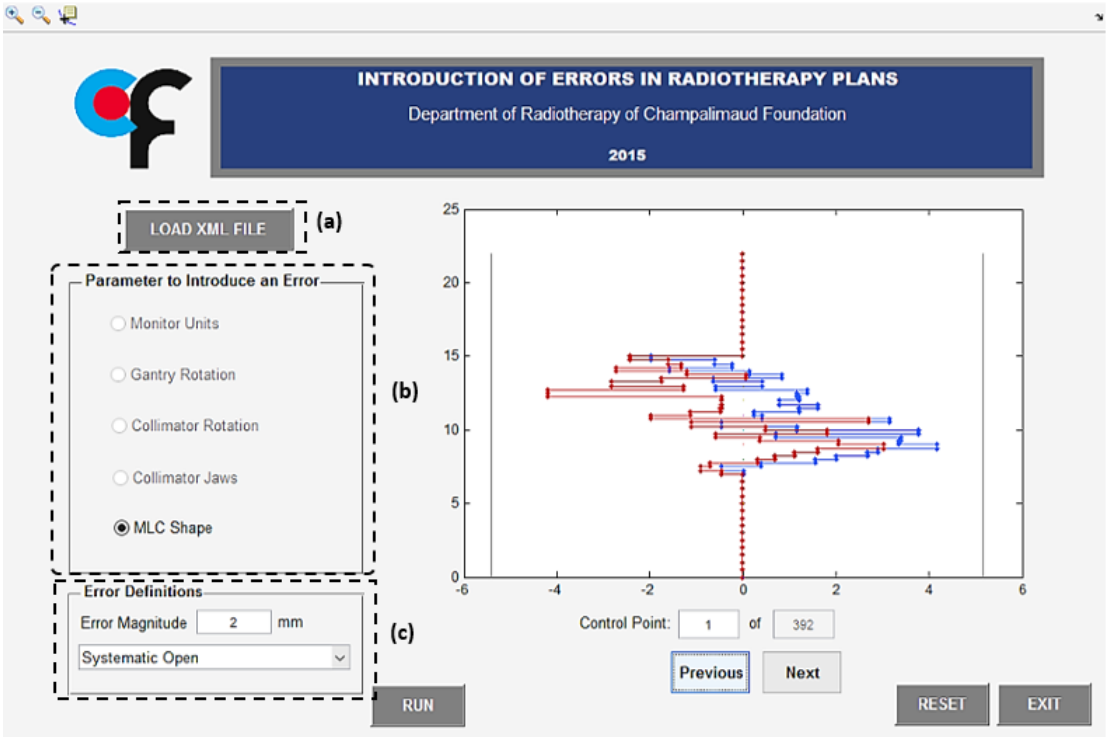

Figure 3.17: Graphical User Interface to introduce errors in XML-file. The first step is to load the XML- file corresponding only to a field or arc. Next is selected the plan parameter in which an error will be introduced. In error definitions the magnitude as well as the type of the error is defined and then the program is run. In this case, in the graphical area is shown the position of each MLC leaf after the introduction of the defined error in order to verify if some overlap occurs

3.5.1.1 MLC Position Errors

Three types of systematic errors were introduced in MLC positions: (1) Systematic Shift that involves move both MLC banks in the same direction, left (SL) or right (SR), by adding the error magnitude to each leaf position, (2) Systematic Open (SO) where MLC banks are moved in opposite directions by adding the error magnitude to each leaf position so that the MLC leaf gap is increased and (3) Systematic Close (SC) where MLC banks are moved in opposite directions by subtracting the error magnitude to each leaf position so that the MLC leaf gap is reduced. On the other hand, random errors were introduced by adding or subtracting random errors determined by sampling a Gaussian distribution with a standard deviation equal to the error magnitude. Systematic and random MU errors were introduced for mag-nitudes of 0.5 mm, 1 mm, 2 mm and 3 mm or 5 mm.

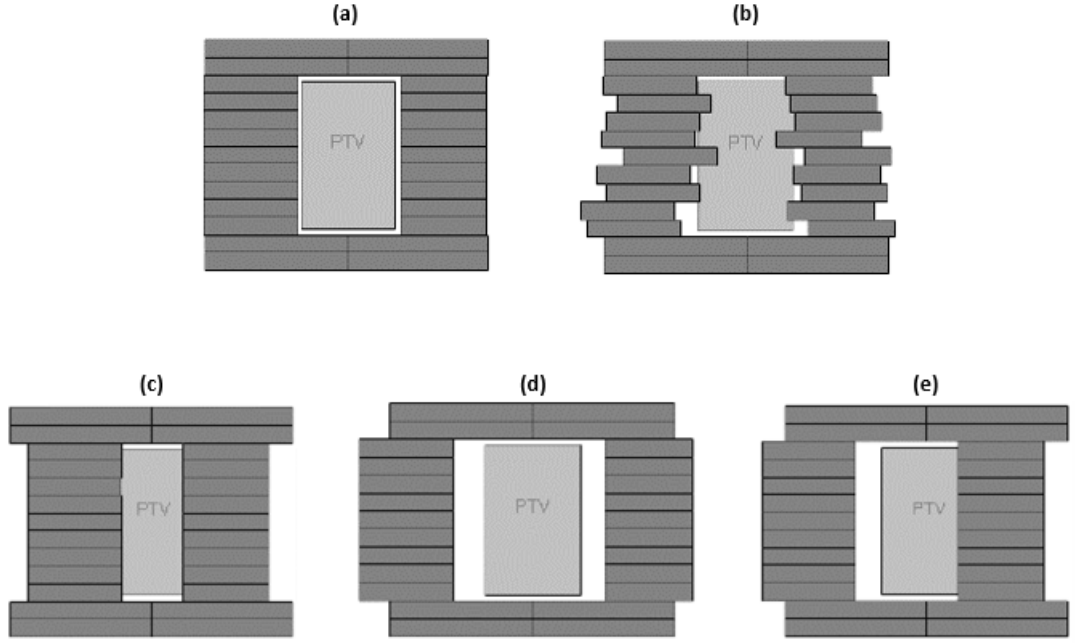

Figure 3.18: Scheme of the MLC errors introduced for one control point. In (a) is presented a MLC shape which conforms to the PTV. The PTV is then modified with (b) random, (c) systematic closing, (d) systematic opening or (e) systematic shift errors introduced in the MLC positions.

3.5.2 EPID versus ArcCHECK

The goal of this study is to implement the EPID to preform pre-treatment patient-specific QA instead of the ArcCHECK® (Sun Nuclear Corporation, Melbourne, LA, USA), which is the device currently used in the Radiotherapy Department of the Champalimaud Foundation. Thus, the patient plans in XML format, which were previously modified with intentional errors, were also measured with ArcCHECK®.

ArcCHECK® is a cylindrical poly-methacrylate (PMMA) phantom containing a three-dimensional array of 1386 diodes (SunPoint™) arranged helically with size of 0.8 x 0.8 mm^2 and spaced 10 mm. Each SunPoint™ (Sun Nuclear Corporation, Melbourne, LA, USA) diode presents a negligible deterioration when exposed to radiation with a response

stability within 0.15% and 0.2% over short and long periods of time respectively.

Figure 3.19: Montage Pre-treatment patient-specific QA with ArcCHECK®. The ArcCHECK® is placed at SDD of 100 cm

Chapter 4

Results and Discussion

The present Chapter summarizes the results obtained from the data analysis and their discussion. Due to the large amount of data analysed, only some results obtained were selected to be shown. This Chapter is divided in three main parts:

1. Analysis of the simplified configuration of Portal Dosimetry solution;
2. Analysis of Absolute Pre-Treatment Portal Dosimetry for FFF beams;
3. Results of the developed system to measure the sensitivity of as1200 EPID for Pre-treatment Dosimetry.

4.1 Analysis of PDPC package

4.1.1 Verification Plans

The verification plans used to verify the correct installation of the PDPC were analysed according to explained in Section 3.3.1.1.

In Figures 4.1 and 4.2 are presented the gamma analysis results regarding MLC parameters settings. For each test field (AIDA and Dynamic Chair) the gamma analysis was performed according with Varian specifications. So, a (3%, 3mm) criteria and a dose threshold of 5% were set once for the MLC parameters analysis only the points with at least 5% of the maximum dose are considered relevant. A gamma passing rate value of 99.8% and 99.7% was obtained for the AIDA and Dynamic Chair test fields respectively. A gamma mean lower than 0.5%, which is defined as maximum acceptable value, was also achieved for the both plans, 0.31 for Aida and 0.29 for Dynamic Chair.

The excellent result obtained for AIDA field indicates the accuracy of the EPID scatter kernel used in PDIP algorithm to predict a portal dose image.

In Figure 4.2 is possible to verify that the points that fail the gamma analysis are in the upper part of the pattern, which is used to estimate the proper settings of the Transmission Factor. However, as the deviations observed are not relevant, gamma analysis 99.7%, an adaptation of the MLC parameter is not advisable since changing the MLC parameters impacts clinical treatments.

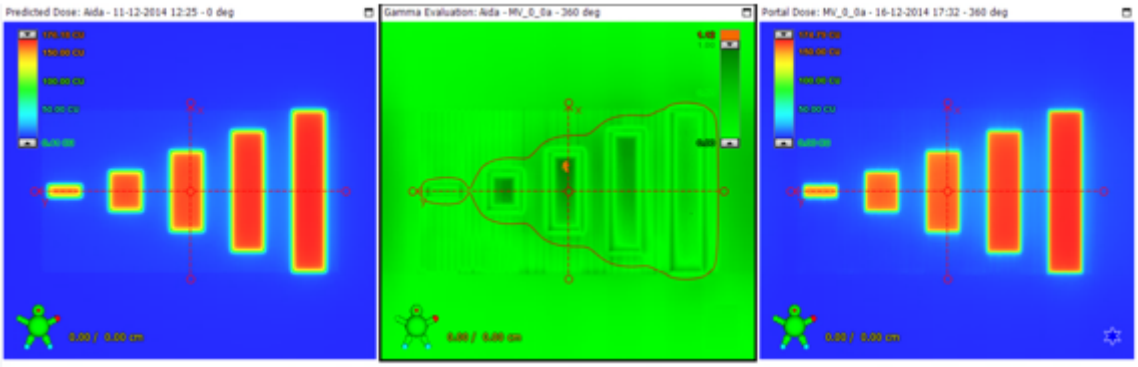

Figure 4.1: Gamma analysis of AIDA test plan with a (3%, 3mm) criteria and a dose threshold of 5%. The predicted and acquired portal dose images, left and right images respectively, are displayed on colour scale (CU), blue represents the lowest dose and red the highest. The comparison between the two portal dose images is done through gamma evaluation, which corresponds to the centre image. As is possible to see, only a few points, in red, have a gamma value higher than 1, being the gamma maximum value equal to 1.12.

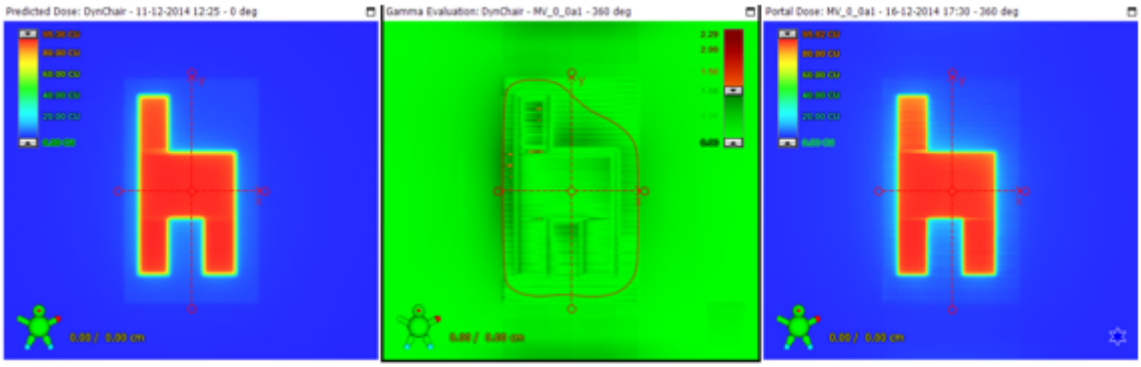

Figure 4.2: Gamma analysis of Dynamic Chair test plan with a (3%, 3mm) criteria and a dose threshold of 5%. The predicted and acquired portal dose images, left and right images respectively, are displayed on colour scale (CU), blue represents the lowest dose and red the highest. The comparison between the two portal dose images is done through gamma evaluation, which corresponds to the centre image. As is possible to see, only a few points, in red, have a gamma value higher than 1, being the gamma maximum value equal to 2.29.

To verify if the output factors used in the PDIP algorithm match with the actual output factors of the EPID, the CAX value of the predicted and acquired portal dose image were compared, Table 4.1 As shown all the absolute values obtained for the relative difference between the predicted and acquired portal dose image are lower than 1%, which means that the output factors used in PDIP algorithm are in accordance which the ones used to perform EPID dosimetry. The worst result is the one obtained for the 3x3 cm^2 field. However, according to Varian specifications a relative difference between -1% and 1% is only expected for field sizes ranging from 5x5 cm^2.

As referred before in Section 3.3.1.1.3 the crossline and inline profiles within the flat field region of the predicted portal dose image and acquired EPID image were compared for different square fields. For each square field the dose difference map comparing predicted and acquired portal dose image was normalize relative to the dose at isocentre in order to isolate potential deviations due to output factor differences from deviations in beam profile, for crossline profile analysis, or from backscatter effects, for inline profile analysis.

Table 4.1: Table with CAX values of predicted and acquired portal dose image and with the relative difference between both portal dose images. Since the output factor correspond to point dose measured at the CAX normalized to the point dose at CAX for the 10x10 cm^2 field, measured at the time of PDIP configuration, the relative difference between the CAX values of predicted and acquired portal dose image corresponds to the relative difference between the output factors . The CAX value is presented in CU.

	Predicted Portal Dose Image (CU)	**Acquired Portal Dose Image (CU)**	**Relative Difference (%)**
3x3 cm^2	86.819	85.989	-0.96
5x5 cm^2	90.804	90.935	0.14
10x10 cm^2	100.252	100.228	-0.02
15x15 cm^2	106.338	106.450	0.11
20x20 cm^2	110.501	110.333	-0.15
22x15 cm^2	107.973	107.984	0.01
22x22 cm^2	111.461	111.496	0.03

As shown Table 4.2, the mean relative difference between the predicted and acquired central crossline profiles is within ±1% for all tested square field. Even when the standard deviation value is considered, the absolute values are still lower than 1% which indicates the accuracy between the beam profile calculated by the pre-configured PDIP algorithm and the 2D beam profile correction matrix used during the dosimetric calibration of the Portal Vision aS1000. The higher values of mean relative difference, 0.593%±0.374% and 0.473%±0.374%, were obtained for the smallest square fields, 3x3 cm^2 and 5x5 cm^2 respectively, which was expected since the smallest plans are the most demanding. For the square fields from 10x10 cm^2, all the absolute values achieved are lower than 0.038%±0.163% which is a very positive result.

Table 4.2: Table with beam profile accuracy and backscatter correction results, corresponding to mean relative difference and maximum relative difference respectively. The standard deviation (SD) is also presented and all the results are in percentage (%).

	Mean Relative Difference (%)	**SD(%)**	**Maximum Relative Difference (%)**	**SD(%)**
3x3 cm^2	0.593	0.374	-4.352	0.797
5x5 cm^2	0.473	0.358	-0.785	0.108
10x10 cm^2	0.038	0.163	-0.576	0.208
15x15 cm^2	-0.112	0.181	0.485	0.158
20x20 cm^2	-0.116	0.158	1.272	0.379
22x15 cm^2	0.012	0.108	0.580	0.155
22x22 cm^2	-0.092	0.160	1.647	0.487

On the other hand, the maximum relative difference between the predicted and acquired central inline profiles are within ±1% only for square fields from 5x5 cm^2 to 15x15 cm^2 and for the 22x15 cm^2 field. These results were expected since the 2D beam profile correction matrix contains a backscatter effect correction for clinically more relevant field sizes. As is possible to see through analysis of Table 4.2, the 15x15 cm^2 and 22x15 cm^2 fields have similar absolute values for the maximum relative difference, 0.576%±0.208% and 0.580%±0.155% respectively. The reason why we found so similar values is because

the accuracy of backscatter correction is only possible to be analysed in the inline direction. Considering, that the inline direction corresponds to the conventional y axis and that in this case the width of the fields is the same (15 cm) in this direction, it is expected that the applied backscatter correction has the same behaviour for the two referred fields. Consequently the maximum relative difference values between the predicted and acquired inline profile are the very close to one another.

For 20x20 cm^2 field size, a maximum relative difference of 1.272%±0.379% between the predicted and acquired inline profile was achieved, since the solution used to reducing the backscatter effect from beam profile only cover field until 15 cm in y direction, which are considered clinically more relevant. In Champalimaud Foundation several plans consider fields with 20x20 cm^2 of size. So, for that reason and considering that major fields are now commonly considered it would be important try to correct the backscatter effect of support arm also for field sizes between 15x15 cm^2 and 20x20 cm^2. In the table below, Table 4.3, are the gamma analysis results, with criteria (3%, 3 mm), obtained for IMRT and VMAT plans. All the tested plans present a gamma passing rate higher than 97%, very close to 100%, and a mean gamma lower than 0.5%, which are very positive results. Despite what was expected, the VMAT plans have better gamma analysis results than IMRT plans, which can be related with the complexity of the MLC leaves positions of IMRT plans. On the other hand, these results suggest the accuracy of the algorithm to calculate the predicted portal dose images for VMAT plans, which require a lot of considerations and variables.

Table 4.3: Table with IMRT and VMAT verification plans results. The presented results correspond to a gamma analysis with criteria (3%, 3mm) and a dose threshold of 5%, so only the points with at least 5% of the maximum dose are considered clinically relevant. The main purpose of defining a threshold is to not consider the background. The gamma passing rate ($\%gamma < 1$), gamma mean value ($gamma_{\text{mean}}$) and gamma maximum value ($gamma_{\text{maximum}}$) are presented.

	$\%\gamma < \mathbf{1}$	$\gamma_{\mathbf{maximum}}$	$\gamma_{\mathbf{mean}}$
IMRT_1	98.6	4.68	0.28
IMRT_2	99.2	3.22	0.27
IMRT_3	97.4	4.36	0.31
IMRT_4	98.0	3.06	0.31
VMAT_1	99.6	2.52	0.21
VMAT_2	99.7	1.61	0.23
VMAT_3	99.7	4.33	0.24
VMAT_4	99.7	3.60	0.26

All the results obtained with the verification plans suggest the correct configuration of PDPD package. The 2D beam profile which incorporates an improved backscatter correction leads to positive and reliable results, so the portal dose images acquired with EPID are in accordance with the ones predicted by the pre-configured PDIP algorithm. Consequently, the assumption that the scatter behaviour of different EPIDs of the same type, in this case PortalVision aS1000, can be modelled by identical scatter kernels was confirmed. In this way, it is possible conclude that the PDPC package is valuable approach to simplify the configuration of Portal Dosimetry solution. However, it is important to

test clinically the performance of the Portal Dosimetry configured with the PDPC package.

4.1.1.1 Clinical Evaluation

In order to clinically evaluate the performance of the Portal Dosimetry configured with the PDPC package, three breast IMRT plans were analysed.

A portal dose image was acquired by the EPID for each individual field of each IMRT plan and a gamma analysis with criteria (2%, 2mm) and (3%, 3mm) was performed through the Portal Dosimetry Review workspace. A dose threshold of 10% was defined to perform the gamma analysis in order to exclude the background which can lead to a false positive in gamma analysis and moreover guarantee that all the areas with a considerable dose are considered.

Each field was individually analysed and then a composite portal dose image, which take into account the contributions of all fields of the clinical plan, was created. The obtained results for the worst and best field as well as for composite portal dose image were then compared with the results achieved with the standard configuration of Portal Dosimetry, in which a diagonal profile of a 40x40 cm^2 field is used to recover the beam profile that is removed by flood-field calibration, see Table 4.4.

Table 4.4: Evaluation of PDPC package clinically performance. Three breast patients plans treated with IMRT, two of them with 5 fields and one with 7 fields, were measured with standard configuration and PDPC package. In the table are presented the values obtained through gamma analysis with (3%, 3mm) criteria for the worst and better field of each patient as well as the composite result, which consider all the fields of the plan.

Patient	STANDARD CONFIGURATION						PDPC PACKAGE					
	Worst Field		Best Field		Composite		Worst Field		Best Field		Composite	
	% γ <1	γ_{mean}	% γ <1	γ_{mean}	% γ <1	γ_{mean}	% γ <1	γ_{mean}	% γ <1	γ_{mean}	% γ <1	γ_{mean}
B1	96.6	0.29	100	0.16	98.2	0.24	99.5	0.26	100	0.24	99.8	0.25
B2	92.9	0.38	99.1	0.29	96.9	0.29	99.5	0.24	100	0.24	99.8	0.26
B3	91.5	0.41	100	0.16	97.8	0.26	99.8	0.26	100	0.17	99.9	0.22

Analysing the Table 4.4 it is possible to see that in general and for all tested patients (B1, B2 and B3) the results obtained with the PDPC package are better than the results obtained with the standard configuration procedure. Considering the standard configuration results for the composite portal dose image, a gamma passing rate ranging from 96.9% to 98.2% were obtained with a (3%, 3mm) criteria. On the other hand, with the PDPC package we were able to obtain gamma passing rate of between 99.8% and 99.9% for the three patients. In fact, observing the results obtained for the worst and better fields is possible to see that with the PDCP package the worst plans had a gamma passing rate equal or higher than 99.5% which are excellent results. In contrast, with the standard configuration values between 91.5% and 96.6% were obtained for gamma passing rate, which are poor results comparatively with the results obtained for the PDPC pack-

age. Also a significant difference between the gamma mean values was achieved since for PDPC package the values were around 0.20 and for standard configuration a range from 0.29 and 0.41 was obtained in respect to gamma mean values. It is important to refer that the worst and best results were not obtained for any specific IMRT treatment field.

The discrepancies obtained between the standard and PDPC configuration can be explained by the profile used to recover the beam profile that is removed by the flood-field correction. As was previously mentioned, in the standard configuration procedure a diagonal profile of a 40x40 cm^2 field is used to recover the beam profile. However, the acquisition of the flood-field is performed using an open field of size 40x32 cm^2. As consequence the penumbra region in the acquired portal dose image is overestimated resulting in discrepancies between predicted and acquired portal dose images which can explain the previous results. In contrast, the PDPC package uses a 2D beam profile correction matrix instead of a diagonal beam profile and consequently the penumbra region of the 40x32 cm^2 field is correctly take into account which allows obtaining better results when both portal dose images are compared. Besides that, the excellent results obtained with the PDPC package can also be explained by the improved backscatter correction included in the 2D beam profile which allows reducing the backscatter effect of the EPID support arm for clinically more relevant field. In order to evaluate the accuracy of the PDPC package, 11 IMRT plans from breast cancer patients and 22 VMAT plans from prostate cancer patients , a total of 71 and 86 fields respectively, were analysed. As is possible to see in Figure 4.3 (a) all the plans except one have a gamma passing rate higher than 96% when a gamma analysis with a (3%, 3 mm) criteria are performed. In general, the gamma passing rate value is higher for IMRT fields which are expected since the VMAT fields are usually more demanding. For a gamma criteria of (2%, 2mm) all the fields have a gamma passing rate higher than 90% as is shown in Figure 4.3 (b).

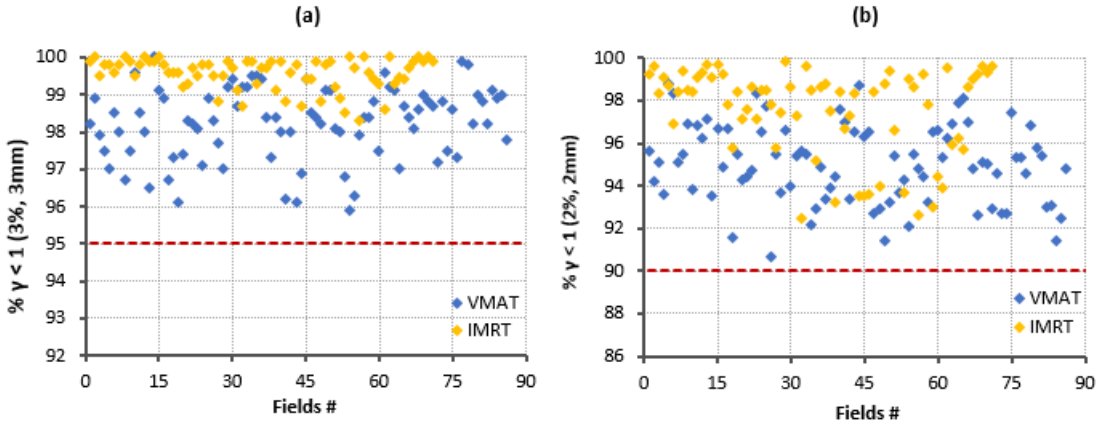

Figure 4.3: Gamma passing rate results obtained for 71 IMRT fields from breast cancer patients (yellow dots) and 92 VMAT fields from prostate cancer patients (blue dots) considering: (a) (3%, 3mm) as gamma criteria and (b) (3%, 3mm) as gamma criteria

As is possible to see in Figure 4.3, the gamma passing rate of VMAT and IMRT plans come closer with a gamma criteria of (2%, 2mm) since with a narrow criteria the IMRT worst fields are most expressive than the VMAT worst fields. So, for IMRT fields a bigger

difference between a gamma analysis with (3%, 3mm) criteria and (2%, 2mm) criteria is achieved when comparing with VMAT fields. Currently, at the Radiotherapy Department of the Champalimaud Foundation, pre-treatment patient-specific QA is performed using ArcCHECK®. With this device and considering a gamma analysis with a (3%, 3mm) criteria, an acceptance level for gamma passing rate value equal to 90% is defined in order to accept and proceed with a radiotherapy plan. However, considering the results obtained with Portal Dosimetry maybe would be necessary adjust the threshold for gamma passing rate when pre-treatment patient-specific QA is performed with EPID in order to evaluate correctly the plans. Based on the results previously presented, an acceptance level of 95% is a reasonable value to take into account when a (3%, 3mm) gamma analysis. The composite portal dose image for each plan was created, considering each portal dose image measured for each field, and the results obtained were compare with the ones obtained with ArcCHECK®, see Figure 4.4.

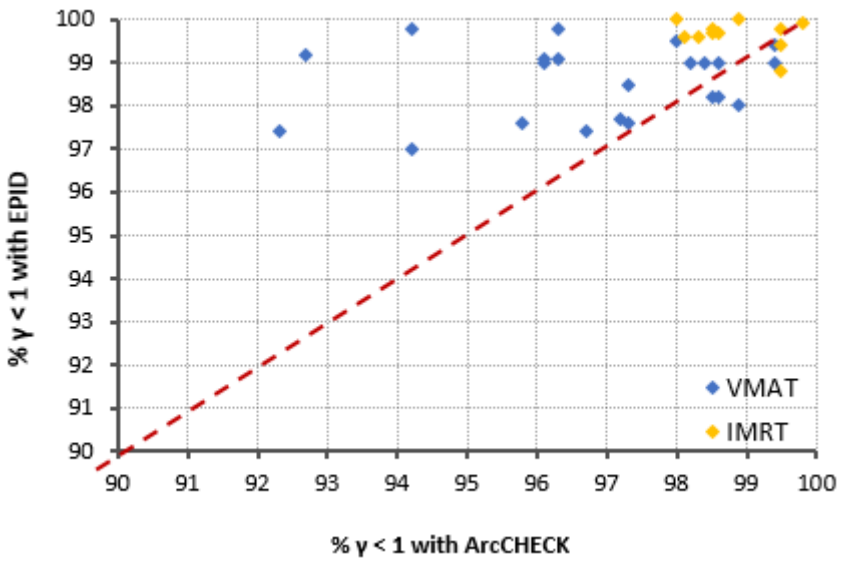

Figure 4.4: Comparison of gamma passing rate results, with a (3%, 3mm) criteria, between IMRT (yellow dots) and VMAT (blue dots) plans measured with ArcCHECK® and EPID. The majority of the plans were better when measured with EPID than ArcCHECK®.

The gamma analysis show that in general the results obtained with EPID are better that the ones obtained with ArcCHECK ®, 16 plans were better results when measured with EPID, 6 were better with ArcCHECK ® and 1 had the same result for both devices. These results can be explained by the EPID resolution, since the PortalVision aS1000 is constituted by a matrix of 1024x780 pixels, each one with size of 0.39x0.39 mm^2 while ArcCHECK® consists of 1386 pixels, each one with 0.8x0.8 mm^2 of area, placed helically. Furthermore, pixels of ArcCHECK® are spaced 10 mm so, in these places the dose could not be measured correctly. The geometry of each system can also be related with obtained results, while EPID is attached to the LINAC and located at the opposite side to LINAC's head following its movement, the ArcCHECK® is placed in treatment couch. However it is important to refer that the results obtained with EPID and ArcCHECK® are not directly

comparable since they are different systems with different sensitivities. Although EPID and ArcCHECK® results are not directly comparable, the results obtained confirm that a new threshold should be defined when pre-treatment patient-specific QA is performed with EPID in order to maintain a similar quality level in the radiotherapy plans that the one used with ArcCHECK®.

4.2 Absolut Pre-Treatment Portal Dosimetry

4.2.1 Verification Plans

The verification plans used to verify the correct configuration of the Absolut Pre-Treatment Portal Dosimetry Solution were also analysed according to Varian specifications. Although the verification plans have been measured for 6 MV and 6MV with FFF beams only the results for the last one will be presented since the clinical study focus on patient plans with FFF beams and because EPID dosimetry with FFF beams is a new aspect. Unlike the previous Chapter only the most relevant verification results will be presented and discussed.

It is important to remember that here the main point was to compare the portal dose image acquired with EPID and converted to water dose, through the model explained in Section 3.4.1.2, with the dose distribution calculated by Eclipse™. Therefore, the dosimetric results obtained with AIDA field were not considered, since this field was designed to verify the accuracy of the EPID scatter kernel used in PDIP algorithm to predict a portal dose image.

Similar to what happened in the previous Chapter the results obtained with the Dynamic Chair and square fields suggest the correct configuration of Absolute Pre-Treatment Portal Dosimetry.

Table 4.5: Table with verification plans results for MLC parameters and relevant square fields. The presented results correspond to a gamma analysis with criteria (3%, 3mm) and a threshold of 5%. The gamma passing rate ($\%\gamma < 1$), gamma mean value (γ_{mean}) and gamma maximum value (γ_{maximum}) are presented.

	$\%\gamma < 1$	$\gamma_{\mathbf{maximum}}$	$\gamma_{\mathbf{mean}}$
5x5 cm^2	100	0.61	0.16
10x10 cm^2	100	0.75	0.32
20x20 cm^2	100	0.99	0.40
AIDA	100	0.50	0.16
DynChair	100	0.52	0.13

As shown in Table 4.5 , for all the relevant square fields, from 5x5 cm^2 to 20x20 cm^2, the gamma passing rate obtained with (3%, 3 mm) criteria was 100% and the gamma mean under 0.5. As expected the higher value for gamma maximum was obtained with the 20x20 cm^2 field. The gamma passing rate achieved for MLC parameters was also 100% and gamma mean values are lower than 0.20. These results were suggest that MLC parameters are correctly defined for EDGE™ system.

The CAX value of the dose distribution calculated by the Eclipse^{TM} and acquired portal dose image for a 10x10 cm^2 field were compared, Figure 4.5. A CAX of 0.84 was obtained for the dose distribution calculated by the Eclipse^{TM} while the CAX value achieved for the acquired portal dose image was 0.86, which means that exists a difference of 2% between the two dose images. Since all calibration is based on the results obtained for the 10x10 cm^2 field it is mandatory to correct this difference. So, the dose conversion factor was adjusted to 0.99 in order to match the CAX values of both dose distributions. After that the CAX value obtained for the acquired portal dose image was 0.84.

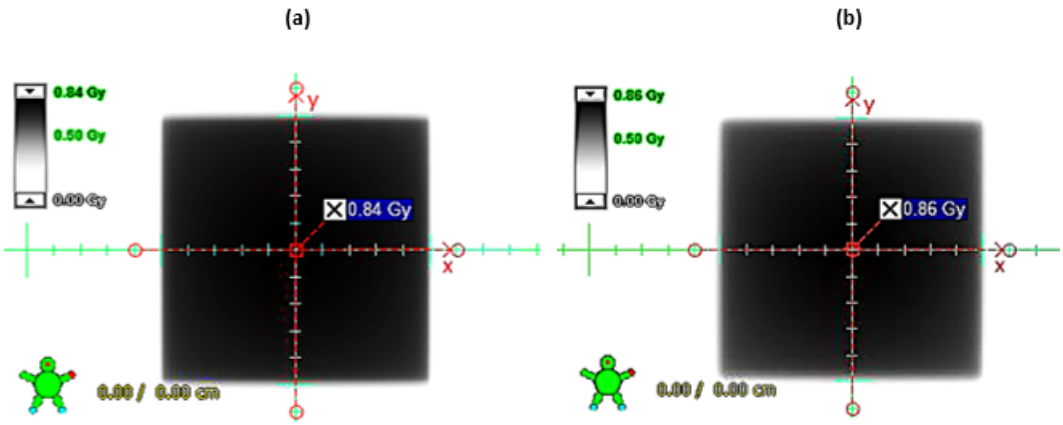

Figure 4.5: Evaluation of the central axis value, CAX value, of the (a) dose distribution calculated by the Eclipse^{TM} and (b) acquired portal dose images for a 10x10 cm^2 with the Point Dose tool. As shown a difference of 2% was achieved. The images are in grayscale in order to select with precision the point dose at CAX.

As mentioned in Section 3.4.1.2 the dose conversion factor converts the CU on the EPID image into Gy, and it is determined comparing the CAX value of a portal dose image converted to dose in water by the presented model, Equation 3.4, with the dose measured directly in water. The obtained value for dose conversion factor is a reference value and can suffer some adjusts depending on EPID model, output of the LINAC and other clinical variants. Since, the reference value was calculated for PortalVision aS1200 and considering an energy of 6 MV as well as FFF beams, the difference previously obtained for CAX value seems to be only related with the output of the LINAC.

In Table 4.6 is possible to see that the gamma passing rate, obtained with (3%, 3 mm) gamma analysis, for IMRT and VMAT plans is 100% and a mean gamma lower than 0.20%, which are excellent results. For gamma maximum the value obtained is under 1 in both cases which together with the other gamma results suggest the validation of the PMS to correct portal dose image instead the usual flood-field correction.

Comparing the results obtained with square fields and clinical fields, it is possible to see that the clinical fields are better. Although the gamma passing rate is 100% in both cases, the gamma mean is considerable lower for IMRT and VMAT fields. Considering that the calculated dose distribution, with which the acquired portal dose image is compared, is determined through Eclipse^{TM} by the clinical algorithm, it is expected that the

clinical plans are better results since they are better modelled by this algorithm than the square fields.

Table 4.6: Table with IMRT and VMAT verification plans results. The presented results correspond to a gamma analysis with criteria (3%, 3mm) and a threshold of 5%. The gamma passing rate ($\%\gamma < 1$), gamma mean value (γ_{mean}) and gamma maximum value (γ_{maximum}) are presented.

	$\%\gamma < 1$	γ_{maximum}	γ_{mean}
IMRT	100	0.84	0.18
VMAT	100	0.55	0.15

Besides the IMRT and VMAT verification plans provided by Varian, it is important to test clinically the performance of the Absolute Pre-Treatment Portal Dosimetry.

4.2.2 Clinical Evaluation

To evaluate the clinically performance of the Absolute Portal Dosimetry for 6 MV energy with FFF beams, 10 VMAT plans with hypofractionated or single shot schemes were measured. For each arc of each VMAT plan, the dose distribution calculated by the Eclipse^{TM} considering a water phantom was compared with the acquired portal dose image, converted to Gy through the algorithm explained in Section 3.4.1.2.

The obtained results for the worst and best arc as well as for composite portal dose image, which is the sum of each field, using a (3%, 3mm) gamma analysis and a dose threshold of 10%, are presented in Table 4.7 Dose difference maps were also displayed and dose profiles at isocentre were compared too in order to analyse and understand the results obtained.

Table 4.7: Evaluation of the clinically performance of Absolute Pre-Treatment Portal Dosimetry. Ten cancer patient plans treated with VMAT, a total of 40 arcs, were analysed. In the table are presented the values obtained through gamma analysis with (3%, 3mm) criteria for the worst and best field of each patient as well as the composite result, which consider all the arcs of the plan.

Patient	**Worst Field**		**Best Field**		**Composite**	
	$\%\gamma < 1$	γ_{mean}	$\%\gamma < 1$	γ_{mean}	$\%\gamma < 1$	γ_{mean}
H&N	100	0.16	100	0.14	100	0.15
B1	100	0.17	100	0.13	100	0.18
B2	100	0.27	100	0.12	100	0.38
P	100	0.22	100	0.12	99.6	0.34
M	100	0.13	100	0.12	100	0.22
T1	100	0.21	100	0.14	99.7	0.23
T2	99.9	0.20	100	0.16	99.5	0.25
T3	99.4	0.28	100	0.18	98.3	0.36
G	71.7	0.73	80.2	0.59	62.7	0.89
A	100	0.13	100	0.17	99.9	0.19

Analysing the results of Table 4.7, all patients with exception of one, patient G1,

present a gamma passing rate higher than 98% and a mean gamma lower than 0.4 for composite portal dose image, which consider the entire treatment. Although generally excellent results are obtained, some of these plans had a gamma passing rate lower than the gamma passing rate obtained for the worst arc of the corresponding plan, including patients P, T1 or T2. These results can be easily explained by an underdose or overdose in a particular region of the treatment field, resulting of the arcs contribution.

Taking T2 as example, a gamma passing rate of 99.9% was obtained for one field and 100% for the other ones, with a (3%, 3mm) gamma criteria. However a slight dose difference corresponding to an underdose was achieved in each individual arc. When all the arcs are compose in a unique portal dose image, these slight dose differences come more expressive and as result a significant dose difference is obtained which is also revealed in gamma analysis. As shown Figure 4.6, the maximum dose difference obtained between the dose distribution calculated by Eclipse^{TM} and composite portal dose image acquired by EPID is around 4.59 Gy, corresponding to an underdose.

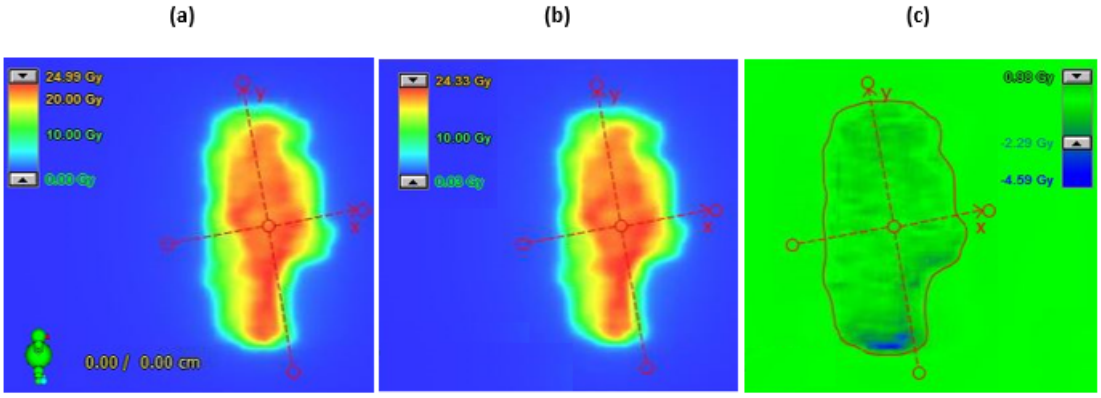

Figure 4.6: Dosimetric results obtained for patient plan T2: (a) dose distribution, calculated through Eclipse^{TM}, (b) composite portal dose acquired by EPID and (c) dose difference map, where a dose threshold of 10% was defined, is shown.

Analysing the profiles through the isocentre obtained for patient plan T2, Figure 4.7, it can be seen that for both axes (x and y) the calculated dose distribution and acquired portal dose profile has the same shape and a very close dose magnitude. As expected, after the previous analysis, the dose magnitude of acquired portal dose image profile is lower than the dose magnitude of calculated dose distribution profile in both axes.

Regarding patient G that correspond to a gynaecologic cancer patient, a gamma passing rate of 62.7% was achieved. This result was not expected since the plan is not the most demanding one. The fractionated scheme, 9 fractions with 2 Gy of dose, can also not justify the poor result obtained for this plan since the dose prescribed is very lower. One possible justification is related with the calculation of the reference dose distribution. As mentioned before in Section 3.4.1.3 the reference dose distribution in Gy, calculated in a water phantom through Eclipse^{TM} is extracted at a depth of 5 cm in order to guarantee that the charge particle equilibrium is achieved for any clinical beam. For this particular plan, the calculation volume of water phantom was reduced to the limit and the plane at

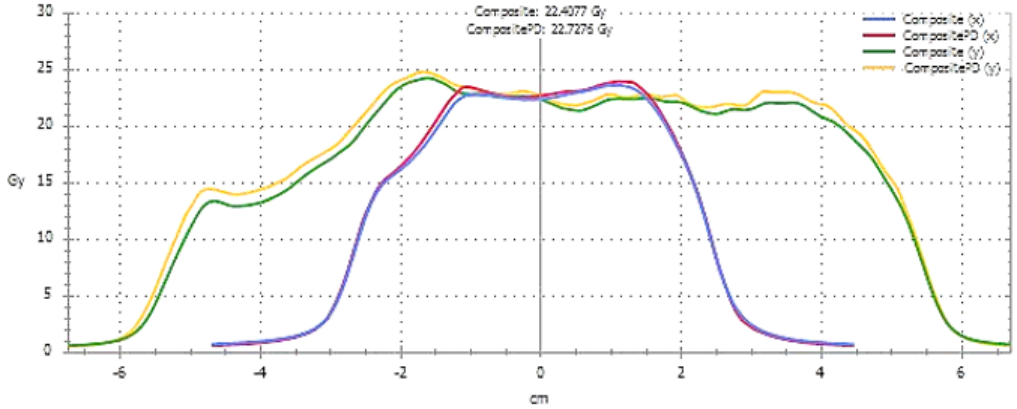

Figure 4.7: Comparison between the profiles at isocentre of the dose distribution, calculated through Eclipse^{TM}, and composite portal dose image acquired by EPID for patient plan T2. The x profile is represented with blue colour for the acquired portal dose image and with red colour for the calculated dose distribution. In turn, the y profile with the green colour corresponds to the acquired portal dose image and the one in yellow corresponds to the one calculated.

5 cm water depth may not have been properly calculated.

Consequently when the dose distribution at a depth of 5 cm is compared with the portal dose image acquired by the EPID significant differences could be seen. Another possible explanation is that the dose calculated by Eclipse^{TM} may not have been properly exported to Absolute Portal Pre-Treatment Portal Dosimetry.

Although promising results were obtained for VMAT treatments delivered with FFF beams and planed with hypofractionated and single shot schemes, it is important to measure more patient plans to evaluate more efficiently the clinical performance of Absolute Pre-Treatment Portal Dosimetry and to implement the EPID dosimetry to perform pre-treatment patient-specific QA in the future. However, it is important to guarantee that the dose distribution is calculated at 5 cm of deep, as well as that the dose, DICOM file, is correctly imported to Eclipse^{TM} in Citrix Machine in order to perform Absolute Pre-Treatment Portal Dosimetry. The main advantage associate to EPID implementation is the reducing QA time and the high sensitivity. Similar to what was obtained in Section 4.1, the results obtained with EPID are better than the ones obtained with ArcCHECK®. A particular advantage associated to Absolute Pre-Treatment Portal Dosimetry is the fact that the dose distribution, with which the portal dose dosimetry acquired by EPID, be calculated by the same algorithm used to calculate the clinical plans. In that way, it is possible to present the analysis in Gy, which is much more intuitive that analysing the results in CU.

Before to considering the adoption of the Absolute Portal Dosimetry, it is important to ensure that this solution allows detecting all significant errors that may arise during the pre-treatment patient-specific QA. So, the sensitivity of the aS1200 EPID during pre-treatment patient-specific QA was studied in order to understand whether this solution is able to detect some particular and common errors.

4.2.3 Developed Method to measure Sensitivity of aS1200 EPID

4.2.3.1 Developer Mode Validation

Before testing the MATLAB® program which was developed to introduce errors in the patient plan in XML format and considering that the present study was carried out in Developer Mode, it is important to check if there are significant differences between portal dose images acquired in Developer Mode at different times of the day as well as the relation between the portal dose images acquired with Developer Mode and Treatment Mode. For that, several portal dose images of a square field with 10x10 cm^2 size were acquired.

Firstly, the 10x10 cm^2 plan was acquired in Treatment Mode and then in Developer Mode, obtaining the TM_1 and DM_1 portal dose images respectively. The process was immediately repeated, acquiring the TM_2 and DM_2 portal dose images.

The portal dose images acquired with Treatment Mode (TM_1 and TM_2) were compared through a gamma analysis, as well as the portal dose images acquired with Developer Mode (DM_1 and DM_2) in order to verify if there are significant differences between portal dose images acquired in the same mode but at different times of the day. Gamma analyses were performed and dose difference maps were displayed to analyse and understand the results obtained. A dose threshold of 20% was defined to perform the gamma analysis as well as to analyse the dose difference maps.

Considering the portal dose images acquired with Treatment Mode (TM_1 and TM_2), it is possible to see in Figure 4.8 (a) that 100% of the points pass the (3%, 3mm) criteria in gamma analysis which is also verified with the (2%, 2mm) criteria.

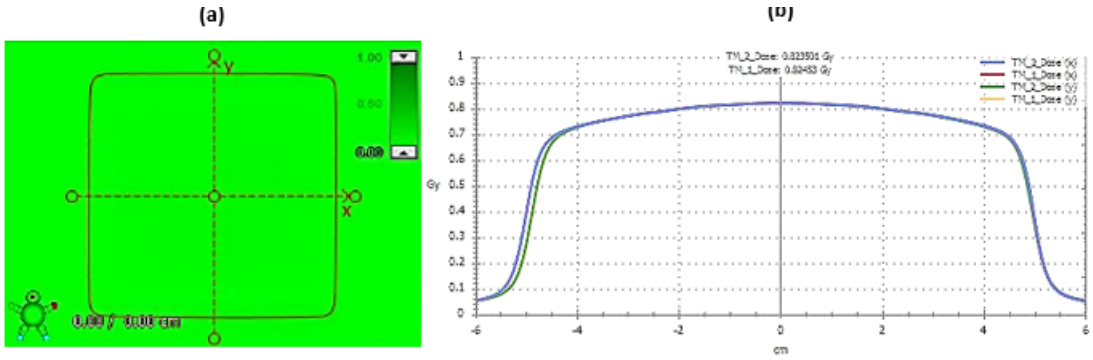

Figure 4.8: Results for Treatment Mode acquisition: (a) gamma analysis map obtained with a (3%, 3mm) criteria for the comparison between the portal dose images of the 10x10 cm^2 square fields, acquired with Treatment Mode and (b) comparison between the profiles of the square fields acquired with Treatment Mode. The x profile is represented with blue colour for the TM_2 portal dose image and with red colour for TM_1. In turn, the y profile with the green colour correspond to the TM_2 portal dose image and the one in yellow correspond to the TM_1. As is possible to see the dose profiles of both acquired portal dose images are perfectly aligned along the x and y axes, reason why it is only possible to see the TM_2 profiles. There is a slight difference between X and Y which could be explained by a need of MLC calibration.

For both analyses all the gamma values are lower than 0.1 and consequently the gamma mean value is very close to zero, 0.03 and 0.04 respectively. In relation to dose difference at the isocentre, the acquired portal dose images, TM_1 and TM_2, have a difference around

0.05% for a (3%, 3mm) and (2%, 2mm) criteria in gamma analysis, which is a negligible value. Besides that, it can be seen in Figure 4.8 (b) that the dose profiles of the acquired portal dose images are perfectly aligned for both axis (x and y) which confirms that there are no significant differences between the portal dose images TM_1 and TM_2.

In turn, for the portal dose images acquired with Developer Mode (DM_1 and DM_2) also all of the points pass the (3%, 3mm) criteria in gamma analysis as can be seen in Figure 4.9 (a), as well as in the gamma analysis with the (2%, 2mm) criteria. Once more, all the gamma values are lower than 0.1 for both analysis and the gamma mean value is very close to zero, 0.04 with the (3%, 3mm) criteria and 0.06 with (2%, 2mm). The acquired portal dose images, DM_1 and DM_2, have a dose difference at the isocentre around 0.2% for the (3%, 3mm) and (2%, 2mm) criteria in gamma analysis, where the DM_2 presents a slight underdose. However, when the dose difference map is analysed the mean value of dose difference is around 0.001 Gy which is a negligible value. As for the portal dose images TM_1 and TM_2, the dose profiles of acquired portal dose images with Developer Mode are thoroughly aligned in both axes as can be seen in Figure 4.9 (b).

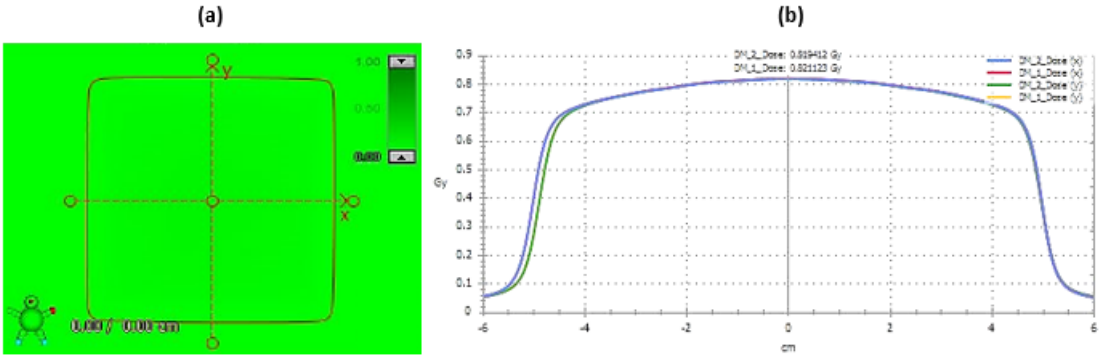

Figure 4.9: Results for Developer Mode acquisition: (a) gamma analysis map obtained with a (3%, 3mm) criteria for the comparison between the portal dose images of the 10x10 cm^2 square fields, acquired with Developer Mode and (b) comparison between the profiles of the square fields acquired wit Developer Mode. The x profile is represented with blue colour for the DM_2 portal dose image and with red colour for DM_1. In turn, the y profile with the green colour correspond to the DM_2 portal dose image and the one in yellow correspond to the DM_1. As is possible to see the dose profiles of both acquired portal dose images are perfectly aligned along the x and y axes, reason why it is only possible to see the DM_2 profiles.

Since the plans in this study are acquired in Developer Mode instead of in Treatment Mode, it is mandatory to verify if there are no significant differences between the portal dose images acquired with each one. Only then it is possible to conclude whether the results obtained with Developer Mode are reproducible with Treatment Mode. In Table 4.8 it is possible to see the gamma analysis values for all combinations, comparing each portal dose image acquired in Developer Mode (DM_1 and DM_2) with each one acquired in Treatment Mode (TM_1 and TM_2).

Table 4.8: Table with the results for Developer Mode validation. Four different comparisons were performed between portal dose images acquired with Treatment Mode and with Developer Mode, through a gamma analysis with (2%, 2mm) and (3%, 3mm) criteria.

	γ**(3%,3mm)**		γ**(2%,2mm)**	
	$\%\gamma < \mathbf{1}$	$\gamma_{\mathbf{mean}}$	$\%\gamma < \mathbf{1}$	$\gamma_{\mathbf{mean}}$
TM_1 vs DM_1	100	0.09	100	0.14
TM_1 vs DM_2	100	0.13	100	0.19
TM_2 vs DM_1	100	0.07	100	0.10
TM_1 vs DM_2	100	0.11	100	0.16

As is possible to see, for all cases the total of the points passed in the (3%, 3mm) and (2%, 2mm) gamma analysis which is indicated by a gamma passing rate value of 100%. Together with the gamma passing rate value, the mean gamma values around 0.1 are an indicative of a successful gamma analysis. Based on these results it is possible to conclude that there are no significant differences between the portal dose images acquired with Treatment Mode and Developer Mode, reason why all the results obtained with portal dose images acquired with Developer Mode can be applied to Treatment Mode.

4.2.3.2 Errors Validation

After the validation of the Developer Mode, it is important to verify if the MATLAB® program works as it is supposed to. So, before introducing errors through MATLAB® in clinical plans it is advisable to introduce the errors in a simple plan, as a square field of 10x10 cm^2. This way, it is easier to predict the results as well as detect some problem in the MATLAB® program.

In a first step, the acquired portal dose images in which a particular error was introduced, was compared with the original acquired portal dose image. The primary point was to verify if the introduced errors were detected, through gamma analysis and dose difference map, without interference from other possible sources of errors. Then the acquired portal dose images with an error was compared against the reference portal dose image calculated by Eclipse™ in order to determinate if the errors were detected with a clinical routine.

The gamma analysis with (2%, 2mm) and (3%, 3mm) gamma criteria as well as the dose difference maps were performed for all magnitudes of random and systematic errors, a dose threshold of 20% was also defined to perform both analysis, unless otherwise mentioned. Only the most relevant results are presented next.

4.2.3.2.1 Comparison with the Acquired Portal Dose Image

As mentioned in Material and Methods chapter, Section 3.5.1.1, several types of errors were introduced in the leaves were position of the MLC in order to evaluate the sensitivity of aS1200. Random (R), Systematic Close (SC), Systematic Open (SO), Systematic Shift in left (SL) or right (SR) direction with magnitudes ranging 0.5 mm to 1 cm were considered in this study.

When a Random (R) error is introduced the leaves open or close randomly and the field size changes according to each leaf position as is possible to see in Figure 4.10.

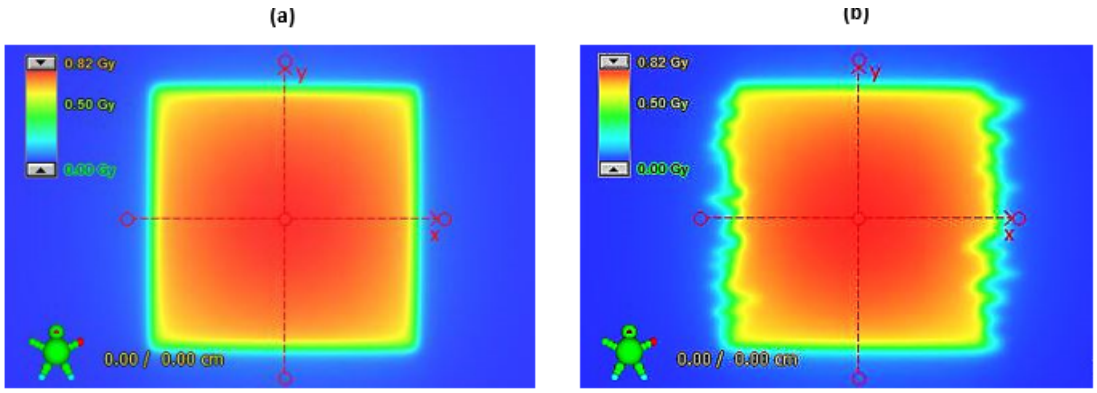

Figure 4.10: Portal dose images of 10x10 cm^2 square field, acquired in Developer Mode: (a) original square field 10x10 cm^2 and (b) the square field of 10x10 cm^2 with a random error of 5 mm introduced in the leaves positions of MLC.

Instead, in Table 4.9 are presented all the relevant results obtained with gamma analysis, comparing the dose distribution of original 10x10 cm^2 field acquired by EPID, without any error introduced, and the acquired portal dose image considering a specific error. So, only the errors types in which the error is first detected using a (3%, 3mm) or (2%, 2mm) were presented.

Table 4.9: Table with the relevant (2%, 2mm) and (3%, 3mm) gamma analysis results, comparing the original square field dose distribution acquired with EPID and acquired portal dose image in which a specific error was introduced: random (R), systematic close (SC), systematic open (SO), systematic left (SL) and systematic right (SR). A mean dose difference value is also presented for each relevant error type and magnitude.

Error (mm)	**γ(3%,3mm)**		**γ(2%,2mm)**		**Dose**
	$\%\gamma < 1$	**γ_{mean}**	**$\%\gamma < 1$**	**γ_{mean}**	**Difference (Gy)**
R 2	100	0.08	99.9	0.12	0.01
R 5	97.5	0.13	94.3	0.19	0.02
SC 2	100	0.20	96.3	0.30	0.02
SC 5	78.2	0.53	74.4	0.80	0.06
SO 2	100	0.14	94.3	0.21	0.02
SO 5	91.4	0.39	86.3	0.48	0.03
SL 2	100	0.15	91.7	0.23	0.04
SL 5	85	0.36	81.0	0.54	0.02
SR 2	100	0.18	92.9	0.27	0.02
SR 5	84.9	0.39	80.8	0.58	0.04

For R error of 0.5 mm and 1 mm, with means that the standard deviation is equal to 0.5 and 1 mm respectively, an excellent gamma analysis was obtained since all of the points passed in the (3%, 3mm) and (2%, 2mm) gamma analysis so that the gamma passing rate value was 100%, and the mean gamma value was under of 0.1. Considering a R error of 2 mm, a very close gamma passing rate value was obtained for (3%, 3mm) and (2%, 2mm)

criteria. In Figure 4.11 (a) is possible to see that for a R error of 5 mm a percentage of points fail the gamma analysis with the (3%, 3mm) criteria and the gamma passing rate value decreases significantly, as is possible to see in Table 4.9. The points that fail within the defined threshold area correspond to the leaves closing and the points that fail outside the threshold correspond to the leaves opening. As is possible to see the distribution of these points are completely random.

The DD map between the square field with R error of 5 mm and the original square field is shown in Figure 4.11 (b). In several regions within the square field area can be seen an underdose (in blue) while an overdose can be distinguished in the contour or in the outer region of the threshold. These results were expected after the evaluation of the results of the gamma analysis, since to the leaves closing is associated an underdose due the reduction of the field and, otherwise to the leaves opening is associated an increase of the square field and consequently an overdose. It is also possible to conclude that the introduction of random errors with a standard deviation of 5 can induce to a DD minimum around 0.4 Gy and maximum around 0.3 Gy.

As expected the gamma passing rate decreases when a (2%, 2 mm) criteria is defined for R error of 5 mm. In turn, with R errors of 1 cm a gamma passing rate values of 86.0% and 80.4 % were detected for the (3%, 3 mm) and (2%, 2mm) criteria, respectively.

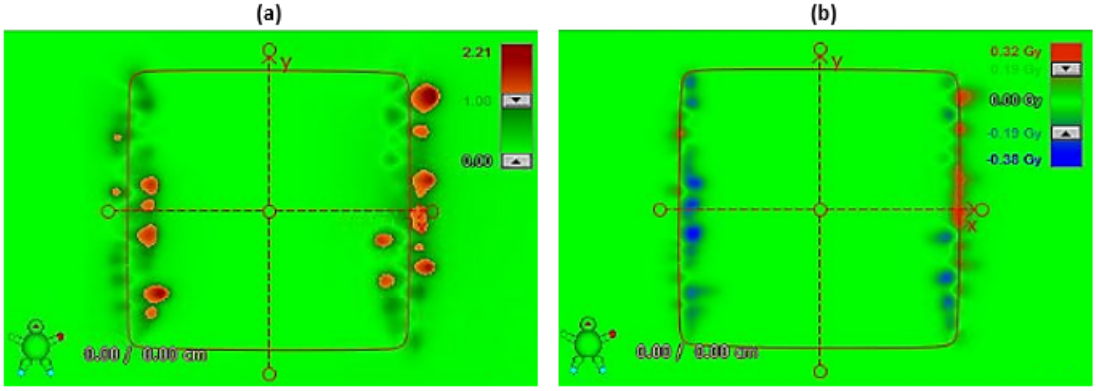

Figure 4.11: Dosimetric results for the comparison between the square field of 10x10 cm^2 and the square field of 10x10 cm^2 with a random error of 5 mm introduced in the leaves positions of MLC: (a) gamma analysis map obtained with a (3%, 3mm) criteria (b) dose difference map. A dose threshold of 20% was defined.

When a Systematic Close (SC) error is applied each leaf position closes and so the field size is reduced, Figure 4.12 (a). On the other hand, when Systematic Open (SO) error is introduced the error magnitude is added to each leaf position and consequently the field size is increased, 4.12 (b). So, as the error is introduced in the leaf position of the MLC, it is expected that at least errors higher than 2mm are revealed in the (2%, 2mm) gamma analysis and errors higher than 3mm are also detected in the (3%, 3mm) gamma analysis, which was verified by analysing the obtained results, Table 4.9. Errors lower than 2mm will only be detected if dose differences higher than 2% or 3%, depending of the gamma criteria defined, of the maximum dose were obtained.

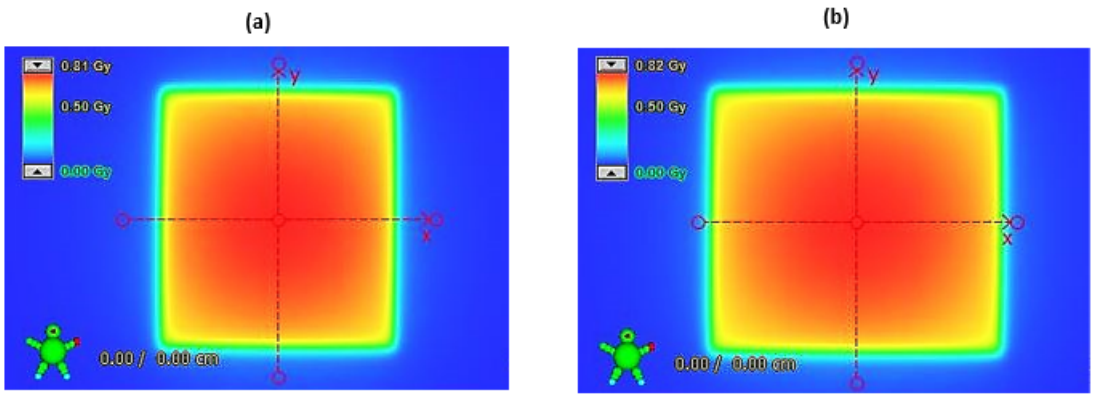

Figure 4.12: Portal dose images of 10x10 cm^2 square field, acquired in Developer Mode: (a) square field of 10x10 cm^2 with a systematic close error of 5 mm introduced in the leaves positions of MLC (b) square field of 10x10 cm^2 with a systematic open error of 5 mm introduced in the leaves positions of MLC.

For SC and SO errors of 0.5 mm and 1 mm all of the points passed in the (3%, 3mm) and (2%, 2mm) gamma analysis which was indicated by a gamma passing rate value of 100%. Also for all the mentioned cases, the mean gamma value was under of 0.1 which together with the gamma passing rate value is an indicative of an excellent gamma analysis. The results obtained for SC and SO of 2 mm considering a (3%, 3mm) and (2%, 2mm) criteria were expected since an error of 2mm in each side of the square field corresponds to 4% of the original square field area, so at least 4% of the points should fails de gamma analysis with (2%, 2mm) criteria due the distance to agreement. The remaining points that fail the gamma analysis when a SO of 2mm is applied should be related with the dose difference that for 2% of the points is higher than 2% of the maximum dose. As is possible to see in Figures 4.13 (a) and 4.14 (a), for both type of errors a percentage of points fail the gamma analysis in the contours of the square field along the y direction. For SC errors the points that fail the gamma analysis are located in the inner contours of the square field while for the SO errors these points are also in the outer contours. These are related with the reduction and increase of the square field, respectively. It is also important to notice that the maximum value of gamma, 1.01, is very low and close to 1, as is also possible to see in mentioned Figures.

In the DD map between the square field with a SC error of 2 mm and the original square field, Figure 4.13 (b), an underdose (in blue) can be seen in inner contour of both sides of the square field which means that reducing the field size by 2 mm induces to a DD around 0.2 Gy. On the other hand, in the DD map of the square field with a SO error of 2 mm against the original square field, Figure 4.14 (b), is possible to see an overdose (in red) in the inner contour but also in the outer contour which causes a DD in the order of 0.2 Gy. The reason why these overdose regions are not totally out of the contour is because the threshold area defined does not have exactly the area of the square field in order to consider all the relevant points. Considering that the magnitude of the error was the same for the SC and SC errors it was expected that the absolute dose difference value would be the same or at least very similar.

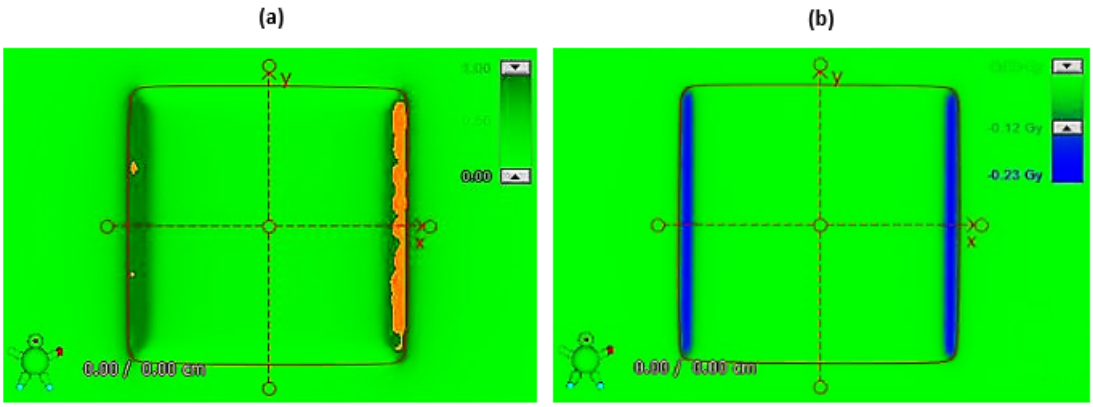

Figure 4.13: Dosimetric results for the comparison between the square field of 10x10 cm^2 and the square field of 10x10 cm^2 with a systematic close error of 2 mm introduced in the leaves positions of MLC: (a) gamma analysis map obtained with a (2%, 2mm) criteria (b) dose difference map. A dose threshold of 20% was defined.

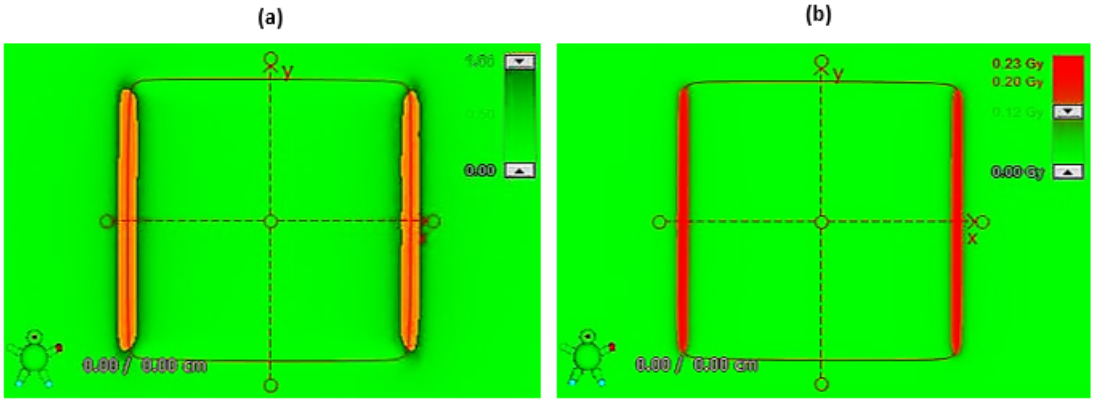

Figure 4.14: Dosimetric results for the comparison between the square field of 10x10 cm^2 and the square field of 10x10 cm^2 with a systematic open error of 2 mm introduced in the leaves positions of MLC: (a) gamma analysis map obtained with a (2%, 2mm) criteria (b) dose difference map. A dose threshold of 20% was defined.

The asymmetry observed in Figure 4.13 is only related with the automatic colour scale, since the green colour is defined for gamma index close to 1 and the orange is displayed for gamma indexes higher than one. So, for points with close gamma values, as 1.00 and 1.01 will present different colours which can induce to a wrong visual analysis. In fact, the points that fail the gamma analysis in the left side of square field have gamma values very close to the points in the right side.

Considering an error magnitude of 5 mm, for both type of errors the points that fail the (3%, 3mm) gamma analysis are in the contours of the square field along the y direction, as is possible to see in Figures 4.15 (a) and 4.16 (a). Since an error of 5mm was introduced in each side of the square field, which correspond to 10% of the original square field area, a gamma passing rate lower than 90% was expected. However, this value was only achieved when a SC error is applied, see Table 4.9. Contrary to what was observed for the (2%, 2mm) gamma analysis for error magnitude of 2 mm, there are significant difference between the gamma passing rate values and gamma mean values of the SC errors and SO errors, for (3%, 3mm) gamma analysis. These discrepancies are related to

the number of points that fail the gamma analysis in the area defined by the threshold of 20% for both cases. When large (> 2mm) SO errors are evaluated the majority of the points that fail the gamma analysis are out of the defined threshold, as is possible to see in Figure 4.16 (a), since most of the points in the increased area have a very low dose that does not correspond to 20% of the maximum dose. On the other hand, when a SC error is considered all the points that fail the gamma analysis are taken into account by the threshold since as the field was reduced in the x direction the points still have at least 20% of the maximum dose, see Figure 4.15 (a). So, for a SO error of 5 mm the number of points that fail the gamma analysis in the area defined by the threshold of 20% is lower than the ones considered for SC error of 5 mm and for that reason the gamma passing rate value is higher for the SO error and the gamma mean value is lower.

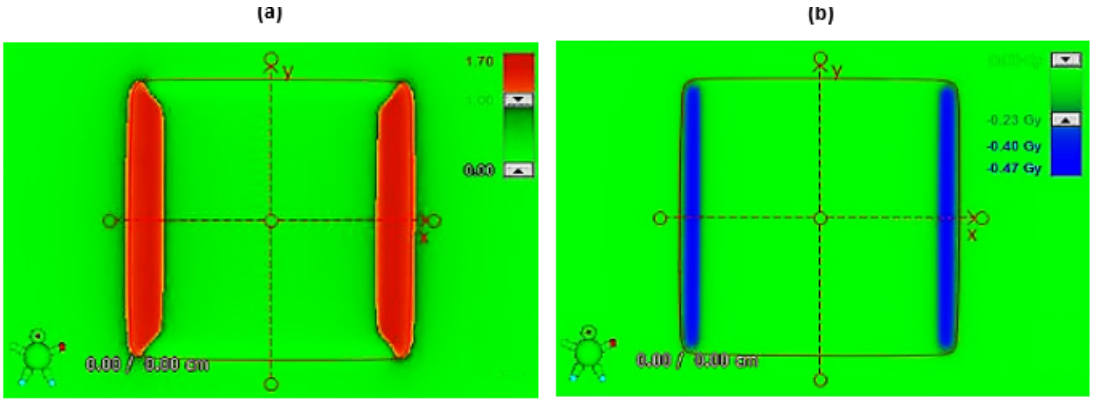

Figure 4.15: Dosimetric results for the comparison between the square field of 10x10 cm^2 and the square field of 10x10 cm^2 with a systematic close error of 5 mm introduced in the leaves positions of MLC: (a) gamma analysis map obtained with a (3%, 3mm) criteria (b) dose difference map. A dose threshold of 20% was defined.

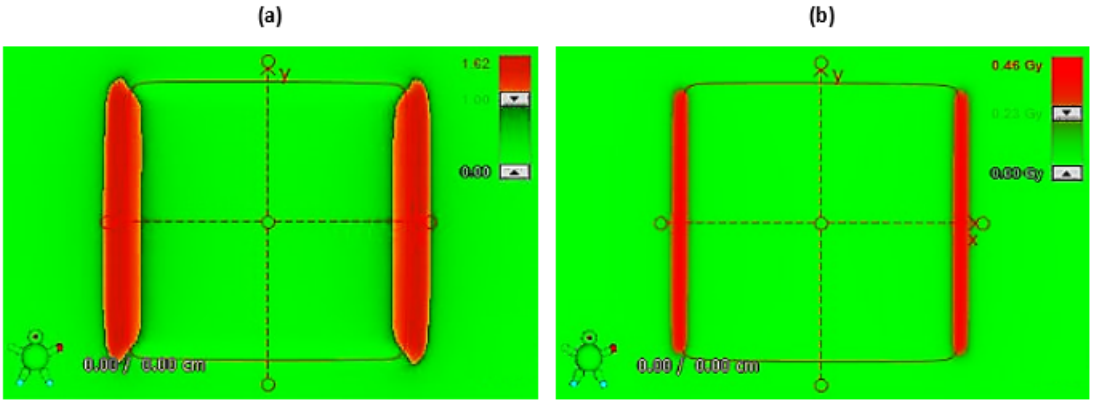

Figure 4.16: Dosimetric results for the comparison between the square field of 10x10 cm^2 and the square field of 10x10 cm^2 with a systematic open error of 5 mm introduced in the leaves positions of MLC: (a) gamma analysis map obtained with a (3%, 3mm) criteria (b) dose difference map. A dose threshold of 20% was defined.

In the Figure 4.15 (b), where the DD map between the square field with a SC error of 5 mm and the original square field is shown, an underdose (in blue) can be seen in the

inner contours as was expected by analysis of the results of the gamma analysis. So, it is possible to conclude that the field size by 5 mm induces to a DD between 0.2 and 0.5 Gy. In turn, in the DD map of the square field with a SO error of 5 mm against the original square field, 4.16 (b), it is possible to see an overdose (in red) mostly in the outer contour which means that increasing the field size by 5 mm causes a DD also between 0.2 and 0.5 Gy, as expected.

As is possible to see in Figure 4.17, where the threshold area is defined to be equal to the original square field area plus 1 cm, in order to cover the 5 mm that added in each side of the square field, a gamma passing rate value of 82.2 % was obtained. This is a more approximated value to the one obtained for a SC error of 5mm, 78.2%, proving the explanation given before for the discrepancies of the gamma passing rate values for SC and SO errors of 5 mm obtained with a threshold of 20%. Beside that the gamma value of 82.2% complies with the 10% of points that were expected to fail the gamma analysis.

The difference between the gamma passing rate values obtained for SC and SO errors of 2mm, with (2%, 2mm) criteria, were also explained by the dose threshold applied. As expected the gamma passing rate values decreases as the magnitude of the error increases, for each gamma analysis criteria. So, SC and SO errors of 1 cm were detected for the (3%, 3 mm) and (2%, 2mm) criteria, obtaining gamma passing rate values of 64.9% and 58.2 % for SC error and 86.7% and 79.7% for SO error, respectively. It is important to mention that large systematic errors with magnitudes higher than 1 cm are very unlikely to happen clinically.

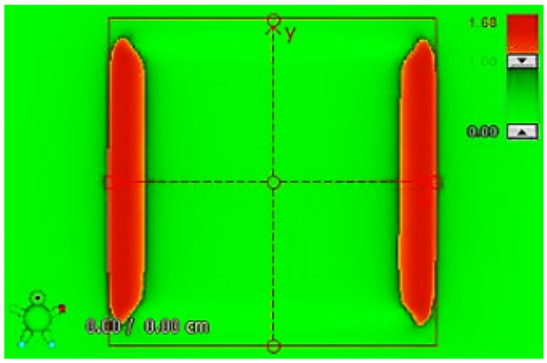

Figure 4.17: Gamma analysis map obtained with a (3%, 3mm) for the comparison between the square field of 10x10 cm^2 and the square field of 10x10 cm^2 with a systematic open error of 5 mm introduced in the leaves positions of MLC. A dose threshold equal to the original field size more 1 cm is defined.

Whenever a Systematic Shift is introduced the opposite leaves of the MLC moving in the same direction, without change the square field size. So, if a systematic left (SL) shift or a systematic right (SR) shift is applied the square field will be displaced to the left or right in relation to the original square field, see Figure 4.18. For that reason, as in the SC and SO error is expected that errors higher than 2mm are revealed in the (2%, 2mm) gamma analysis and errors higher than 3 mm are also detected in the (3%, 3mm) gamma analysis, in accordance with the obtained results.

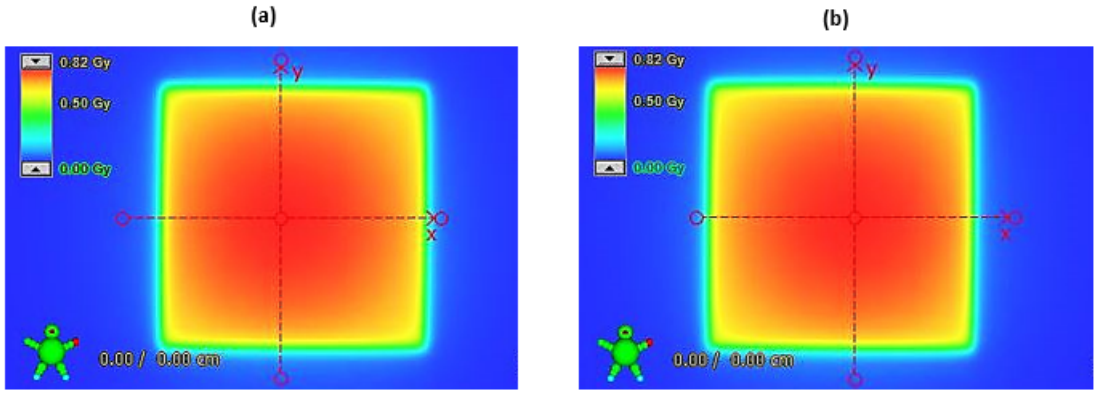

Figure 4.18: Portal dose images of 10x10 cm^2 square field, acquired in Developer Mode: (a) square field of 10x10 cm^2 with a systematic left shift error of 5 mm introduced in the leaves positions of MLC (b) square field of 10x10 cm^2 with a systematic right shift error of 5 mm introduced in the leaves positions of MLC.

For SL and SR errors of 0.5 mm and 1 mm the gamma passing rate value was 100% for the (3%, 3mm) and (2%, 2mm) gamma analysis. Also for both cases, the mean gamma value was around 0.1 which reinforces the point that there are no significant differences between the square fields with the SL or SR errors and the original square field.

As expected and as is shown in Table 4.9, for error magnitude of 2 mm the percentage of points that passes in (2%, 2mm) gamma analysis decreases to 92.9% for SL errors and to 91.7% for SR errors with are according with the values expected. In Figures 4.19 (a) and 4.20 (a) is possible to see that the points that fail the gamma analysis with the (2%, 2mm) criteria are mostly in the inner contour of the square field along the y direction.

As in the gamma analysis in the dose difference map the points with dose difference are also in the inner region of the contours of the square field. In the DD map between the square field with a SL error of 2 mm and the original square field, Figure 4.19 (b), an underdose (in blue) can be seen in the right contour of the square field (defined by the line y=x) while an overdose (in red) is obtained in the left region (along the line defined by y = -x).

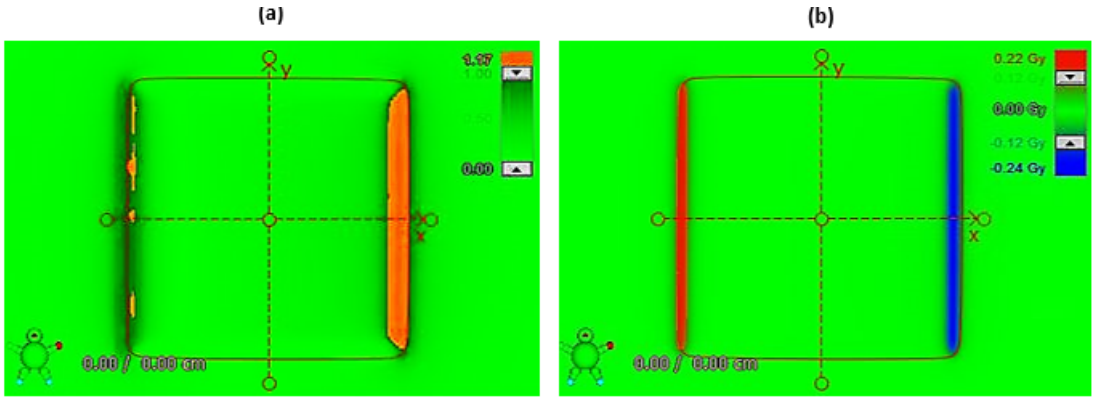

Figure 4.19: Dosimetric results for the comparison between the square field of 10x10 cm^2 and the square field of 10x10 cm^2 with a systematic left of 2 mm introduced in the leaves positions of MLC: (a) gamma analysis map obtained with a (2%, 2mm) criteria (b) dose difference map. A dose threshold of 20% was defined

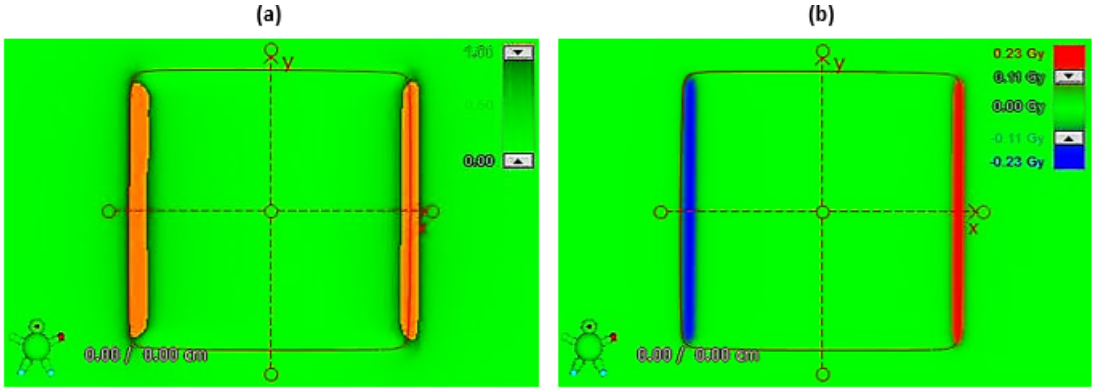

Figure 4.20: Dosimetric results for the comparison between the square field of 10x10 cm^2 and the square field of 10x10 cm^2 with a systematic right of 2 mm introduced in the leaves positions of MLC: (a) gamma analysis map obtained with a (2%, 2mm) criteria (b) dose difference map. A threshold of 20% was defined.

Analogous results were obtained for the DD map of the square field with a SR error of 2 mm against the original square field, Figure 4.20 (b). As it is possible to see an overdose (in red) is present in the right region of the square field and an underdose (in blue) is obtained in the left region of the field. According to the results a displacement of the field by 2 mm to the left as well as to the right induces to a DD around 0.2 Gy in the mentioned regions.

As expected for SL and SR errors with a magnitude of 5 mm a gamma passing rate under 100% was obtained in gamma analysis with the (3%, 3mm), see Table 4.9. Unlikely to what was observed for the (3%, 3mm) gamma analysis for the SC errors and SO errors, there are no significant differences between the gamma passing rate values as well as the mean gamma values for SL and SR of 5 mm. The reason why this happens is because the introduced errors only displace the square field to the left and right without modifying the square field area. So, in both cases a similar number of points that fail the gamma analysis are out of the region defined by the threshold of 20%. In the case of SL error, Figure 4.21 (a), these points are in the left side of the square field while for a SR error, Figure 4.22 (a), the points that fail the gamma analysis out of the area defined by the threshold of 20% are in the right region of the square field.

In Figure 4.21 (b), where the DD map between the square field with a SL error of 5 mm and the original square field is shown, an underdose (in blue) can be seen in the inner contour of the right side of the square field and an overdose (in red) mostly can be seen in the outer contour of the opposite side as was expected by analysis of the results of the gamma analysis. As for (2%, 2mm) gamma analysis, the results for the dose difference analysis between the square field with a SR error of 5 mm and the original square field were analogous to the SL error of 5 mm, Figure 4.22 (b). So, an overdose (in red) was obtained in the right region of the square field mostly in the outer contour and an underdose (in blue) was obtained in the left region of the field. Once more a relation between the SL and SR errors was found since the results show that the displacement of the field by 5 mm to the left induces to a DD around 0.5 Gy such as when the shift is to the right.

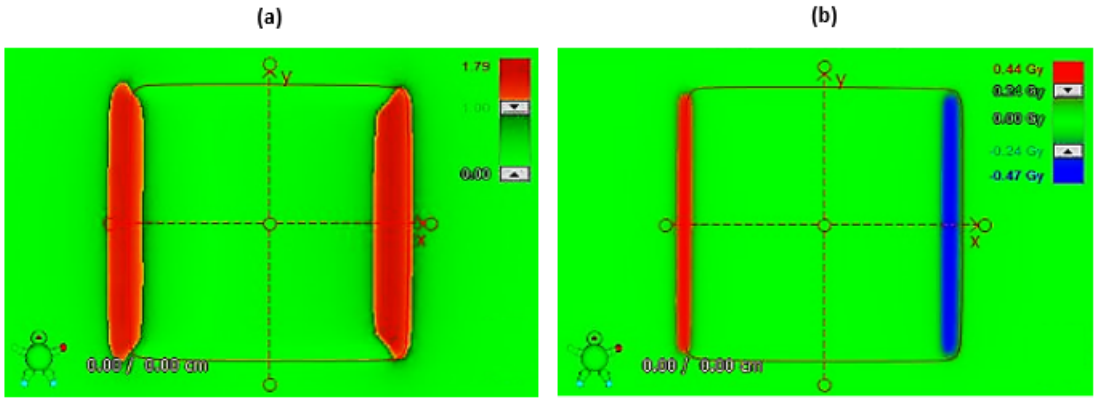

Figure 4.21: Dosimetric results for the comparison between the square field of 10x10 cm^2 and the square field of 10x10 cm^2 with a systematic left of 5 mm introduced in the leaves positions of MLC: (a) gamma analysis map obtained with a (3%, 3mm) criteria (b) dose difference map. A dose threshold of 20% was defined.

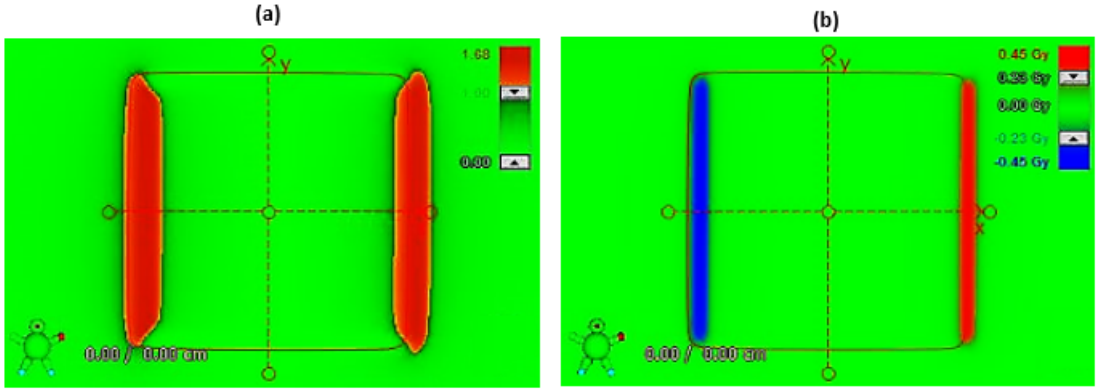

Figure 4.22: Dosimetric results for the comparison between the square field of 10x10 cm^2 and the square field of 10x10 cm^2 with a systematic right of 5 mm introduced in the leaves positions of MLC: (a) gamma analysis map obtained with a (3%, 3mm) criteria (b) dose difference map. A threshold of 20% was defined.

In Figure 4.23, the dose threshold is defined to be equal to the original square field area plus 1 cm in order to cover the 5 mm that were added on the left or the right side of the square field.A gamma passing rate value of 82.2 % was obtained for SL and SC. As expected, the same gamma passing rate values was obtained, which also verified when (2%, 2mm) criteria was set.

For errors of 1 cm were detected for the (3%, 3 mm) and (2%, 2mm) criteria, obtaining gamma passing rate values of 76.5% and 70.9 % for SL error and 76.6% and 71.2% for SL error, respectively.

The errors introduced through the developed MATLAB® routine were correctly detected by the Absolute Pre-Treatment Portal Dosimetry when other possible sources of errors are not considered. So, it is possible to conclude that the developed program is working as planned. Despite these results it is crucial to determinate if the errors were detected with a clinical routine.

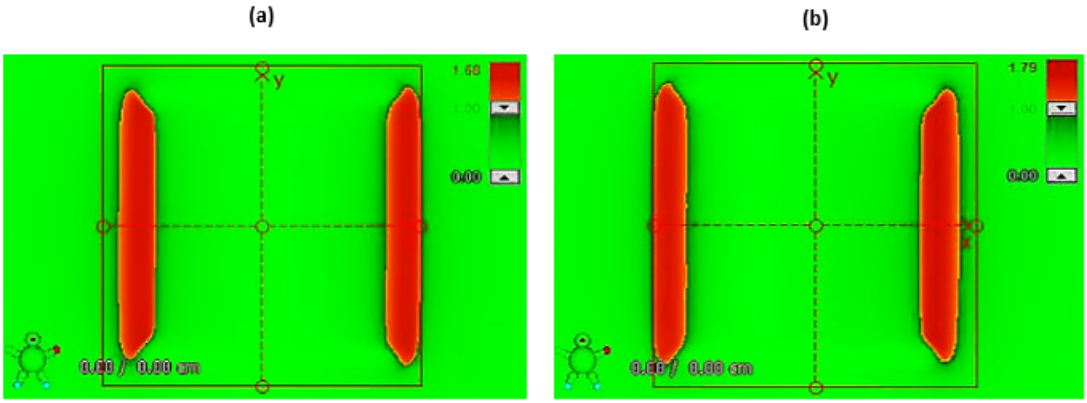

Figure 4.23: Gamma analysis map obtained with a (3%, 3mm) for the comparison between the square field of 10x10 cm^2 and the square field of 10x10 cm^2 with a systematic shift of 5 mm introduced in the leaves positions of MLC: (a) systematic left error and (b) systematic right error. A dose threshold equal to the original field size more 1 cm is defined.

4.2.3.2.2 Comparison with the Dose Distribution Calculated by Eclipse^{TM}

As mentioned in Section 3.4.1.2 the dose conversion factor of the Absolute Pre-Treatment Portal Dosimetry is defined in order to eliminate the discrepancy between the acquired portal dose image and the dose distribution calculated by the Eclipse^{TM} in the 10x10 cm^2 field. During the analysis of the verification plans, the dose conversion factor was set in 0.99 in order to match the isocentre values of both dose distributions, see Section 4.2.1.

To analyse the impact of each error type in a particular plan it is crucial have a reference situation where the dose distribution acquired by EPID without any error introduced is compared with the calculated dose distribution. For that reason a portal dose image of the original 10x10 cm^2 field was acquired with Developer Mode (DM_3).

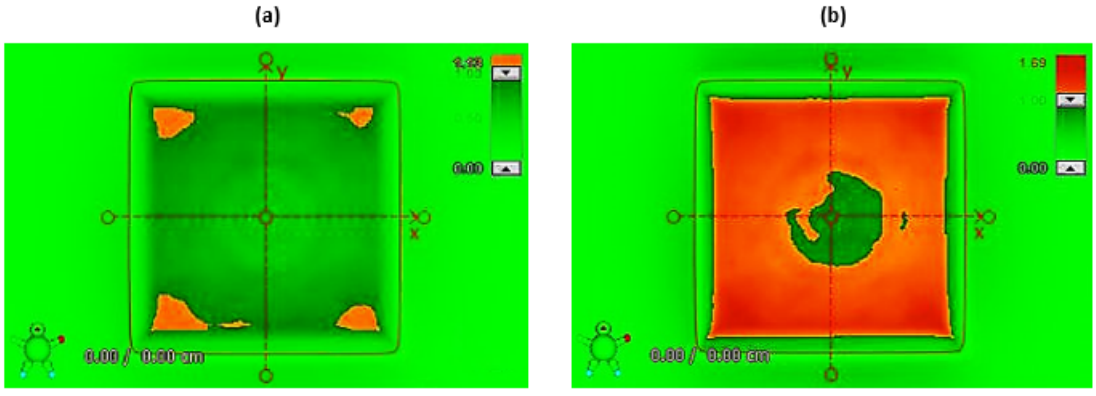

Figure 4.24: Dosimetric results for the comparison between the dose distribution of the 10x10 cm^2 field calculated by the Eclipse^{TM} and the dose distribution of the 10x10 cm^2 field acquired by EPID in Developer Mode: (a) gamma analysis map obtained with a (3%, 3mm) criteria (b) gamma analysis map obtained with a (2%, 2mm) criteria. A dose threshold of 20% was defined.

Comparing the acquired portal dose image DM_3, which was converted to dose considering the previous defined dose conversion factor, with the calculated dose distribution,

a gamma passing rate of 100% only was achieved for the (3%, 3mm) gamma analysis. On the other hand, with a (2%, 2mm) criteria the percentage of points that passes in gamma analysis drastically decreases to 32% as is possible to see in Figure 4.24. Also a high discrepancy is achieved for the gamma mean value which changed from 0.70 to 1.05.

To better understand the discrepancy of the results obtained in (2%, 2mm) gamma analysis, the portal dose image DM_3 was compared with the portal dose image acquired in Treatment Mode to verify the configuration of the Absolute Pre-Treatment Portal Dosimetry (TM_APDv) and with which the dose conversion factor was set, see Figure 4.5 which will be further mentioned as TM_APDv. For a (3%, 3mm) criteria all of the points passed in the gamma analysis while in a (2%, 2mm) gamma analysis only a gamma passing rate of 87.2% was achieved as is shown in Figure 4.25.

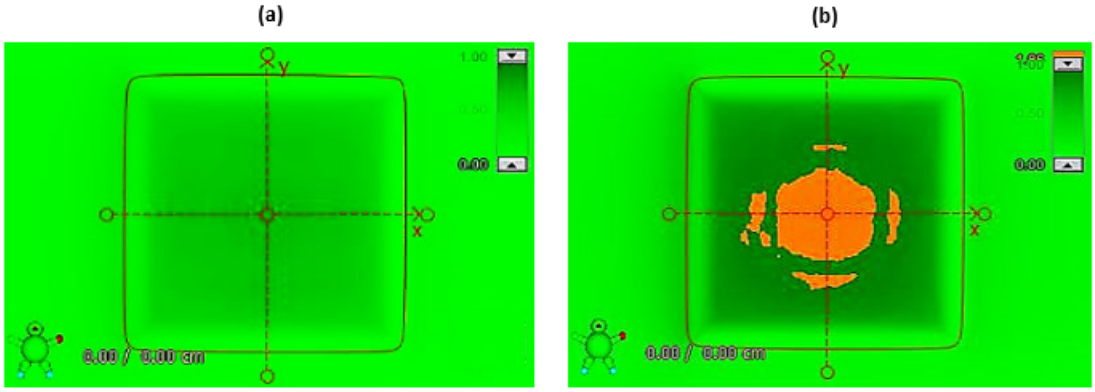

Figure 4.25: Dosimetric results for the comparison between the dose distribution of the 10x10 cm^2 field acquired in Treatment Mode and the dose distribution of the 10x10 cm^2 field acquired by EPID in Developer Mode: (a) gamma analysis map obtained with a (3%, 3mm) criteria (b) gamma analysis map obtained with a (2%, 2mm) criteria. A dose threshold of 20% was defined.

A significant difference between the dose profiles of the acquired portal dose images, DM_3 and TM_APDv, in both axes (x and y) can be seen in Figure 4.26. At the isocentre, the dose value of the acquired portal dose image in Treatment Mode is 0.846 Gy while the dose value of the portal dose image DM_3 is 0.829 Gy, which correspond to a dose difference of 2%.

These results can be explained by the variation of the output of the LINAC or by the need of recalibration of the EPID since the portal dose images were acquired with a time difference of 4 months. The output of the LINAC has small daily changes which affect the EPID results. Through the analysis of the graphic where are registered every output variation of the EDGE^{TM} for 6 MV energy with FFF beams, it was possible to see that the maximum difference between the output values registered in the days in which the portal dose images where acquired, June 5th and October 28th , is 1.2%. The remaining 0.5% can be justified with the need of calibration of the EPID which is recommended at each 3 months.

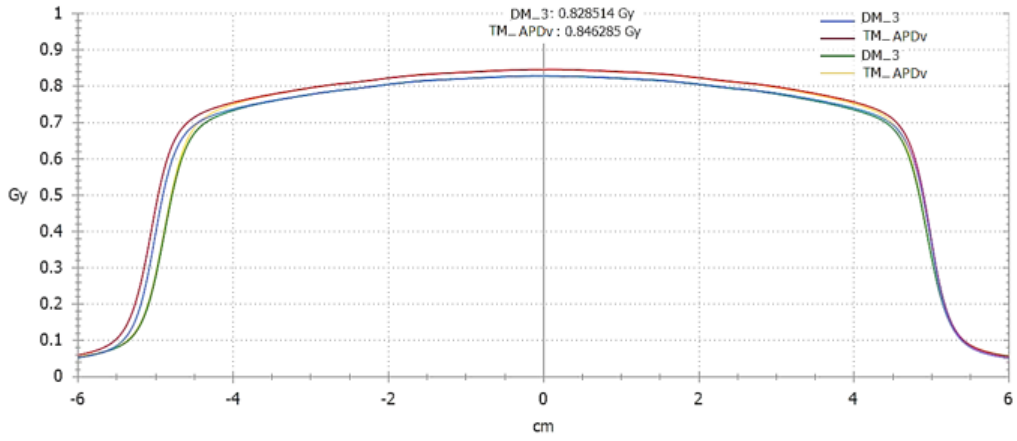

Figure 4.26: Comparison between the doses profiles of the square 10x10 cm^2 portal dose images, both converted to dose with a dose conversion equal to 0.99. The x profile is represented with blue colour for the DM_3 portal dose image and with red colour for TM_APDv. In turn, the y profile with the green colour correspond to the DM_3 portal dose image and the one in yellow correspond to the TM_APDv. As is possible to see the dose profiles are not aligned, especially in the central region of the profiles. So that, a dose difference of 2% is achieved at the isocentre.

In order to compensate the 2% of dose difference at the isocentre, the dose conversion factor was adjusted to 1.01 which corresponds to an increase of 2% of the previous value, 0.99. The acquired portal dose image DM_3, converted to dose considering the new value of the dose conversion factor, was, once again, compared with the portal dose image TM_APDv, converted to dose with the initial dose conversion factor. All of the points passed in the (3%, 3mm) and (2%, 2mm) gamma analysis so that the gamma passing rate value was 100%, and the mean gamma value was under of 0.1. Besides that, it can be seen in Figure 4.27 that the dose profiles of both acquired portal dose images, DM_3 and TM_APDv are perfectly aligned in the central region in x and y axes and there are no significant dose differences at the isocentre. However, in the x axis a little misalignment in the penumbra was observed. The penumbra region depends mainly of the collimation and considering that the two portal dose images were acquired with a difference time of 4 months, it is possible that a small correction of the MLC position are necessary since in this direction the field is defined by the MLC.

With these results, we conclude that a dose conversion factor of 1.01 should be applied in order to convert correctly the portal dose images acquired at this time.

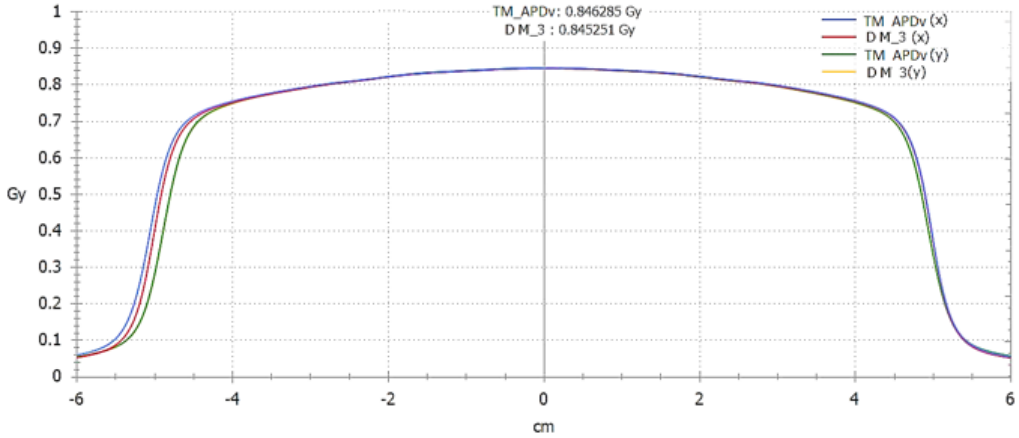

Figure 4.27: Comparison between the profiles of the square portal dose images, DM_3 and TM_APDv converted to dose with a dose conversion equal to 1.01 and 0.99 respectively. The x profile is represented with blue colour for the DM_3 portal dose image and with red colour for TM_APDv. In turn, the y profile with the green colour correspond to the DM_3 portal dose image and the one in yellow correspond to the TM_APDv. As is possible to see the dose profiles are perfectly aligned in the central region of the profiles.

The acquired portal dose image DM_3, converted to dose with a factor conversion equal to 1.01, was compared against the calculated dose distribution. The profiles are aligned in the central region in both axes and consequently there are no significant dose differences at the isocentre, 0.844Gy Gy and 0.845 Gy for the calculated dose distribution and DM_3 respectively, Figure 4.28 (a). A gamma passing rate of 100% was achieved for the (3%, 3mm) criteria while with a narrow criteria, (2%, 2 mm) the gamma passing rate value decreased to 97.9% which is a more reasonable value that the one obtained before adjust the dose conversion factor, see Figure 4.28 (b). The majority of the points that fail the gamma analysis are on the lower side of the square field.

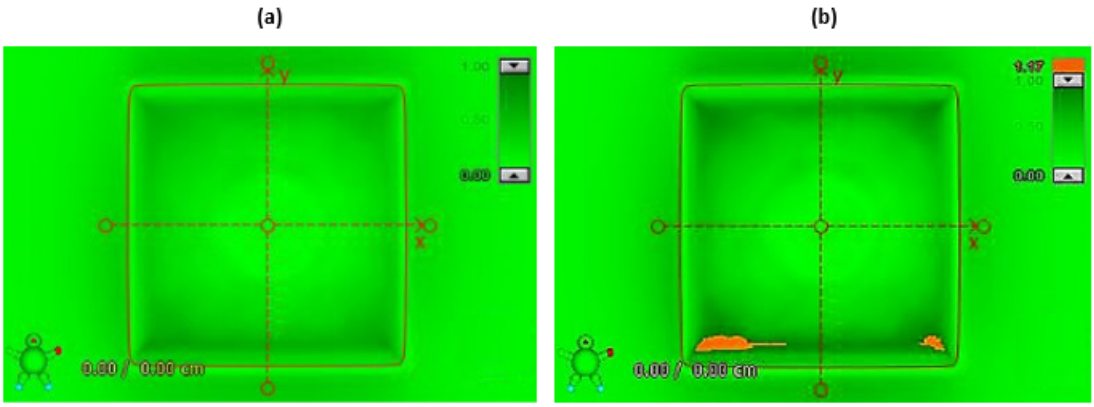

Figure 4.28: Dosimetric results for the comparison between the predicted dose distribution and the dose distribution of the 10x10 cm^2 field acquired by EPID in Developer Mode: (a) gamma analysis map obtained with a (3%, 3mm) criteria (b) gamma analysis map obtained with a (2%, 2mm) criteria. A dose threshold of 20% was defined.

In Figure 4.29, where the DD map of the dose distribution calculated by the Eclipse^{TM} and the dose distribution DM_3 is shown, an underdose (in blue) can be seen mainly near the field edge of the lower side and upper side of the square field as the results suggested by the gamma analysis with (2%, 2mm) criteria. A slight underdose can be also seen in the inner contour of the left and right side of the square field. Despite the excellent results obtained in the gamma analysis, the dose DD map results suggests that the measured square field is smaller than the calculated one as well as a misalignment between the two dose distributions. A smaller field size was previously suggested through the analysis of the profile in y direction for all measured portal dose images. The field in y direction was always smaller than in x direction, which can be explained by a MLC misalignment in this direction.

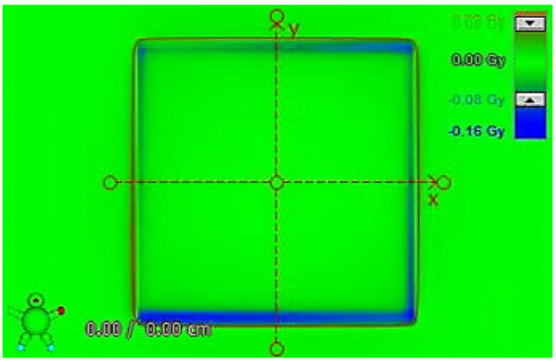

Figure 4.29: Dose difference map displayed for the comparison between the dose distribution of the 10x10 cm^2 field acquired in Treatment Mode and the dose distribution of the 10x10 cm^2 field acquired by EPID in Developer Mode. The maximum absolute value of dose difference is 0.08 Gy. A dose threshold of 20% was defined.

Since the errors were introduced in the leaves positions of the MLC, it is important to consider the discrepancies obtained in the x direction for the reference situation, where the dose distribution acquired by EPID in Developer Mode and without any error introduced, DM_3, is compared with the calculated dose distribution. As the profile has different behaviour in different regions is necessary to consider how the errors introduced will affect each one in order to analyse the results obtained by the gamma analysis, see Figure 4.30. The region (a) correspond to the area defined by the maximum dose to the line that correspond to the field size, in which the dose from the acquired portal dose image is almost the same to the dose of the predicted dose distribution. The theoretical field is defined at 50% of the maximum dose that in this particular case correspond to 0.42 Gy. The second one, region (b), corresponds to the area from the point that defines the field size to the threshold of 20%, from which the points are considered for the analysis gamma. However, it is important to note that the results in gamma analysis cannot be only justified by analysing the profile through the isocentre.

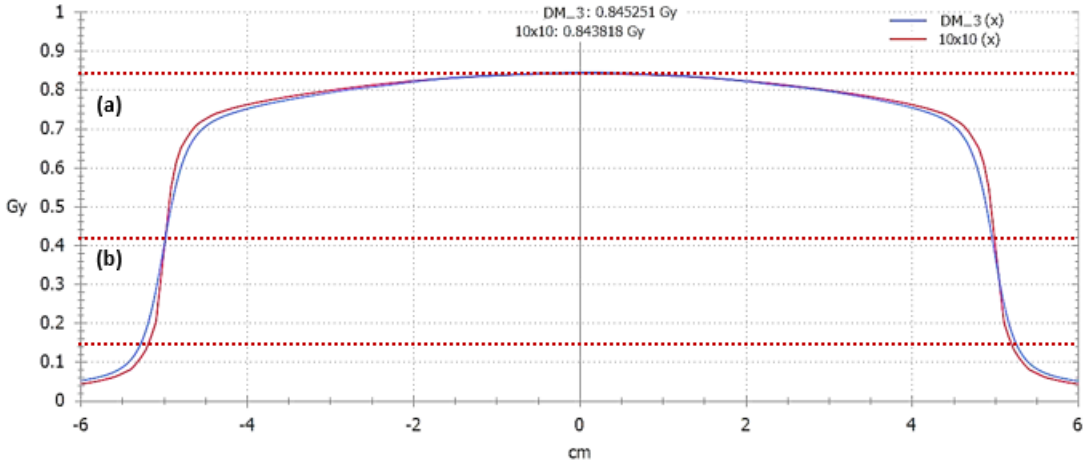

Figure 4.30: Comparison between the profiles of the square field portal dose images, DM_3 and TM_APDv converted to dose with a dose conversion equal to 1.01 and 0.99 respectively. The x profile is represented with blue colour for the DM_3 portal dose image and with red colour for TM_APDv. In turn, the y profile with the green colour correspond to the DM_3 portal dose image and the one in yellow correspond to the TM_APDv. As is possible to see the dose profiles are perfectly aligned in the central region of the profiles.

A priori, considering the results obtained for the reference situation, it is expected that the gamma passing rate value will decrease with the increment of the magnitude of SC errors. On the other hand, an increase in the gamma passing rate value until to a certain magnitude value of SO errors can be predicted and from that value the gamma passing rate will decrease.

For a magnitude of 0.5 mm for SC error a gamma passing rate of 100% was obtained in gamma analysis with the (3%, 3mm) while with a narrow criteria, (2%, 2mm), the percentage of points that passes in gamma analysis decreases to 96.9% as is shown in Table 4.9. The results suggest that at some point a misalignment around 1.5 mm is achieved between the two doses distributions on the reference situation. Considering the dose profile at isocentre as reference and take into account the difference between the dose profiles in the region (a), mainly in the penumbra region, it was expected that the number of points that fail the gamma analysis increase since the introduction of a SC error led to an increase in the discrepancy between the dose profiles of both dose distributions.

Similar results were obtained for SC errors of 1 mm. With the (3%, 3mm) criteria, a gamma passing rate value equal to 100% was achieved while for the (2%, 2mm) criteria, only 88.7% of the points passed in the gamma analysis. Taking in consideration the value previously achieved for the misalignment in the reference situation, 1.5 mm, it was expected that with a SC of 1mm a passing rate close to 100% was obtained for (3%, 3mm) gamma analysis, depending of the dose difference induced by the error.

When a SC error equal to 2 mm is introduced in the leaves position of the MLC, a gamma passing rate of 97.5% and 78.9% is obtained respectively for (3%, 3mm) and (2%, 2mm) criteria as was expected.

For SO errors, a gamma passing rate of 100% was obtained in gamma analysis with the (3%, 3mm) for magnitude errors range from 0.5 to 2 mm. In turn, the (2%, 2mm)

gamma analysis for the same magnitudes of the SO error revealed a gamma passing rate between 98.1% and 98.6%. Notice that the results of (2%, 2mm) gamma analysis that compare the dose distribution calculated by the Eclipse^{TM} with the dose distributions considering SO errors with magnitudes ranging from 0.5 to 2 mm are better than the gamma analysis values in the reference situation. Once again this can be mostly justified by the misalignment achieved between the calculated and measured dose distributions when errors are not considered, since the profile of the acquired portal dose image became closer to the profile of the calculated dose distribution when SO errors are introduced. The points that fail the gamma analysis with (2%, 2mm) criteria should be mainly in the left side of region (b). With a SO error of 5 mm the points that pass in gamma analysis decreases to 97.3% and 93.6% when the (3%, 3mm) and (2%, 2mm) criteria are respectively defined, which are worse results those obtained in reference situation.

Considering SL and SR errors with a magnitude of 0.5 mm and 1 mm, the total of the points pass in gamma analysis when a criteria of (3%, 3mm) is set. In turn, with a (2%, 2mm) criteria a gamma passing rate of 97.2% and 96.2% was obtained for SL and SR of 0.5 mm, respectively. With these results is possible to conclude that the dose distribution acquired with the EPID is more aligned with the calculated dose distribution in the right side than in the left side, since when the MLC is displaced 0.5 mm to the left side better results are achieved. Considering that all the profiles along the x axis have a similar behaviour when compared with the profile at the isocentre, the discrepancy of 1% may be related with the slight difference observed close to the central region, where the dose profile of the DM_3 is a little bit more misaligned in relation to the dose profile of the calculated dose distribution in the left side. So, when the SL error of 0.5 mm is introduced, and the leaves of MLC are displaced to the left, the dose profiles align in the referred region. For errors of 1 mm the gamma passing rate obtained with (2%, 2mm) criteria was 93% for SL and 92.9% for SR. In this case, the results are similar for SL and SR errors, which can be explained by the fact that the percentage of points that fails the (2%, 2mm) gamma analysis due the misalignment in region (b) on the left side and in region (a) on the right side, when a SL of 1mm is introduced, is similar to the percentage of points that fails the (2%, 2mm) gamma analysis due the misalignment in region (a) on the left side, when a SR of 1 mm is introduced.

When a shift of 2mm is introduced a gamma passing rate of 97.2% and 99.2%, with the (3%, 3mm) criteria was obtained for SL and SR, respectively. The discrepancy of the values of gamma passing rate is majority related with the alignment of the dose profiles in the defined region (b). As is possible to see in the reference situation, a greater discrepancy between the profiles is found on the left side than on the right one and so it is possible to predict and justify the results obtained.

In general, all the results are in agreement with what was expected since they can be predicted and justified considering the reference situation. Considering all the results, it is possible to conclude that the aS1200 and the absolute portal dose algorithm are able to detect several types of errors, which compromising the treatment plan. However, it is crucial evaluate the errors detection using clinical plans and considering the clinical

routine.

4.2.3.3 Clinical Results

Intentional errors were introduced in the clinical plans of two patients treated with VMAT, P and a B2, with a total of 8 treatment arcs.

A gamma analysis with (2%, 2mm) and (3%, 3mm) criteria was performed and dose difference maps were displayed in order to analyse the results obtained. As before, for the evaluation of PDPC package and Absolute Pre-Treatment Portal Dosimetry, a threshold of 10% was set to perform the gamma analysis as well as to analyse the dose difference maps.

In this Chapter acquired portal dose images with a particular error were only compared against to dose distribution calculated by Eclipse^{TM} in order to determinate if the errors were detected with a clinical routine. MLC errors with magnitudes ranging from 0.5 to 3 mm were introduced in all control points of each arc, which were individual measured and analysed. Then a composite portal dose image, taking into account the contributions of all arcs of the clinical plan, was created. It is important to refer that the collimator position in which each portal dose image was acquired is considered to determine the composite portal dose image. The focus in this Chapter are the results obtained for composite portal dose images.

Firstly, a portal dose image of the whole brain radiotherapy plan, B2, without any errors introduced was acquired through Developer Mode as reference, Figure 4.31 (b). A gamma passing rate of 100% and a gamma mean of 0.16 were obtained for the reference situation, using a (3%, 3mm) criteria. As shown in Figure 4.31 (c) the dose profiles through isocentre of dose distribution calculated by Eclipse® and acquired portal dose image are aligned along x and y directions, however a dose difference around 2% is obtained at CAX.

When the dose profile is analysed for each arc, a similar difference was achieved in the partial arc, with clock wise rotation, where a higher dose was delivered. These results were confirmed through a (2%, 2mm) gamma analysis, where a gamma passing rate of 99.7% was achieved for the composite portal dose image. Analysing each arc individually, the same partial arc as the one mentioned before, was the only one with a gamma passing rate under 100%, more precisely 99.4%.

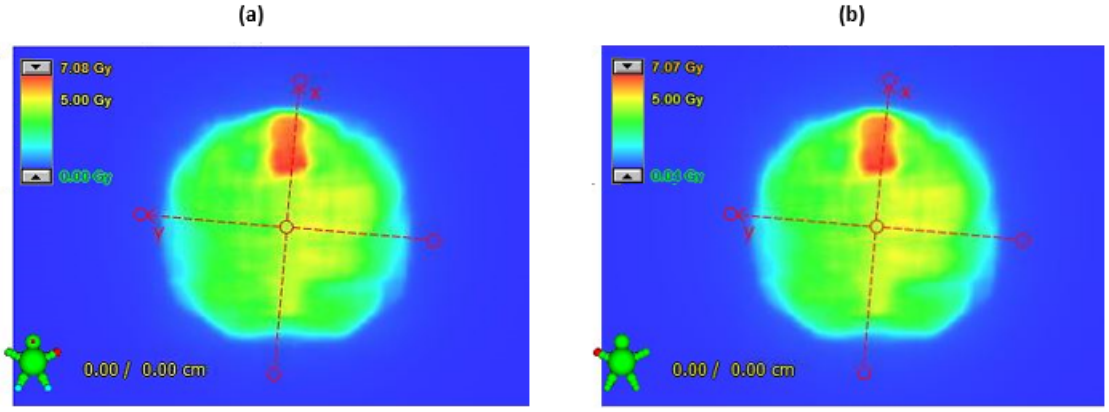

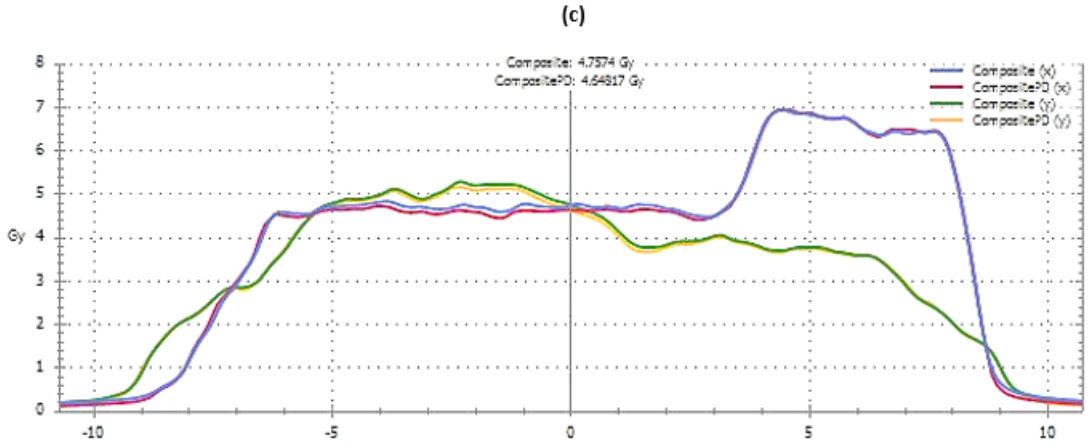

Figure 4.31: Reference portal dose image for VMAT plan B2: (a) dose distribution predicted considering the dose distribution calculated by Eclipse® for each individual arc, (b) dose distribution determined taking into account all the individual portal dose images, corresponding to each arc, acquired with the EPID and (c) comparison between the profiles of the predicted and measured composite portal dose image, Composite PD and Composite respectively. The x and y axes of profile correspond to the horizontal and vertical directions in portal dose images in (a) and (b).

To verify whether calculated and measured composite portal dose images are correctly determined when errors are considered, CAX values of each arc were added and the result was then compared with the isocenter value of the respective composite portal dose image. As is possible to see in Table 4.10, for both situations the sum of the isocentre value of each arc is exactly equal to the isocentre value of composite portal dose image. So, it is possible to conclude that each arc is correctly taken into account to determine composite portal dose image.

Table 4.10: Isocentre dose value for composite dose distribution, calculated based on each calculated arc by Eclipse®, and composite portal dose image, determined considering measured portal dose images of each individual arc. The VMAT plan B2 were composed by four partial arcs (180°), two of them with clock wise rotation (CW1 and CW2) and other two in counter clock wise rotation (CCW1 and CCW2). The isocentre values are presented in Gy.

Portal Dose Image	CAX dose value for Calculated Dose Distribution	CAX dose value for Acquired Portal Dose Image
CW1	2.306	2.363
CCW1	1.266	1.293
CW2	0.230	0.230
CCW2	0.846	0.871
Sum of Arcs	4.648	4.757
Composite	4.648	4.757

In Figure 4.32 is shown the gamma passing rate and gamma mean values for SC and SO errors. The SO errors seem to have more impact than SC errors in three individual portal dose images as well as composite portal dose image. Only for one of the individual arcs, the CW2, SC errors had more impact in gamma passing rate and gamma mean than SO errors. These results are easily explained analysing the reference situation. For CW1,

CCW1 and CCW2 a misalignment in calculated dose distribution and measured portal dose image was present and an overdose was obtained with respect to calculated dose distributions.

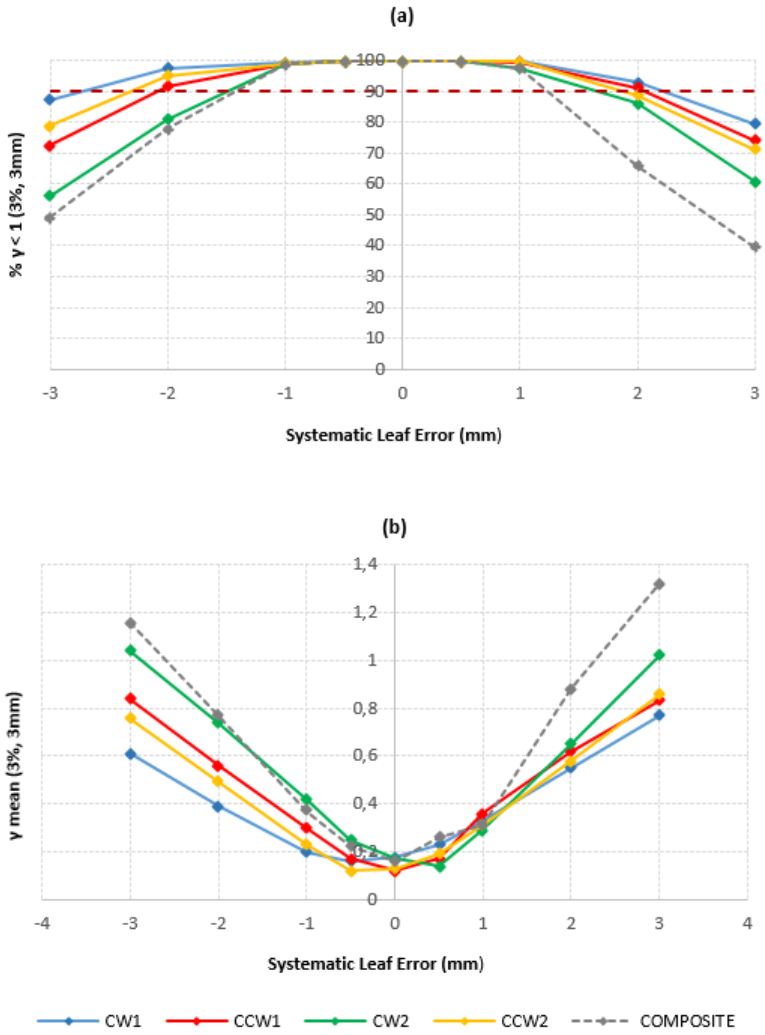

Figure 4.32: Gamma analysis results with (3%, 3mm) criteria, obtained considering SC and SO errors for VMAT plan B2: (a) gamma passing rate and (b) gamma mean values. The positive values in systematic leaf errors axis correspond to SO and the negative ones correspond to SC errors.

Considering that SC errors are associated to underdoses and SO errors induce overdoses, when SC errors where introduced the dose difference previously detected was attenuated and when SO errors were introduced the dose difference was accentuated. Therefore the gamma passing rate was lower for SC errors than SO errors. In turn, for arc CW2, both profiles (x and y) of calculated dose distribution and acquired portal dose image match perfectly through isocentre, which can signify that introduced errors were correctly taken into account. This can also be the reason why for this particular arc the gamma passing rate is lower for all considered magnitudes. Another reason for these results is related with the size of segments. So, probably the CW2 had more small segments and for that reason the introduced errors are more expressive. In general, the results are according to

what is expected since the gamma passing rate decreases and the gamma mean increases with the introduction of higher errors magnitudes.

With SC and SO errors of 0.5 mm the gamma passing rate is higher than the defined acceptance level (90%) for all individual and composite portal doses images and the same also happens, for three individual portal dose images, when a SC of 1 mm is introduced. This is one more evidence that the gamma passing rate acceptance level should be adapted, maybe be establish at 95%, when a (3%, 3mm) gamma analysis is performed to evaluate pre-treatment patient-specific QA with EPID, see Section 4.2.2.

A gamma passing rate of 98.7% and 77.7% was obtained introducing a SC error 1 and 2 mm, respectively. The gamma passing rate value obtained for the composite portal dose image, considering a SC error of 2 mm, was not expected since when the arcs are individually evaluated, only values between 81% and 97.3% are obtained. For SO of 2 mm also similar results were obtained, so all individual portal dose images were gamma passing rate values ranging from 86% to 92.8% and for the composite portal dose image a gamma passing rate of 65.8% was achieved. These results can be explained by the influence of each arc errors in the composite portal dose image.

In the present case, each arc is delivered with a different collimator position (185°, 175°, 85° and 95°). Although the portal dose images of each arc have been acquired at different positions, as the SC or SO errors were introduced in leaves position, which have for each arc the same movement relative direction, and with the same magnitude, it is expected that the gamma passing rate obtained for each arc are close to each other. Contrary, when a composite portal dose image is analysed, the errors introduced in each arc are taken into account. So, the errors were considered in different directions relative to the central axis of the composite portal dose image, affecting both directions of composite portal dose image profiles. In regions where the contribution of two or more arcs is considered the errors obtained for composite portal dose image may exceed the magnitude introduced in each arc and therefore fail the (3%, 3mm) gamma analysis due to distance agreement. For that reason the gamma passing rate achieved for composite portal dose image is lower than the mean value of gamma passing rate of all arcs.

As explained in Figure 4.33 and Figure 4.34, it is possible to see that SC and SO errors of 2mm are revealed in x and y profile, as consequence of the each arc contribution.

In the Figures 4.33 (a) and 4.34 (a) the DD map between calculated dose distribution and composite portal dose image, with a SC or SO error of 2 mm respectively, is shown. As expected an underdose was achieved when SC error was considered and an overdose was obtained for SO error. Differently to what happened for square fields, the dose difference, as well as the points that fail the gamma analysis, are mainly found inside the field, since the VMAT fields are covered by multiple segments and so the errors are mainly introduced inside the field. It is important to refer that when a narrow gamma analysis criteria is applied a gamma passing rate under 100% is obtained for SC and SO errors with magnitude of 0.5 mm, which is a very positive result since the error is detected. The results obtained when SL and SR errors were considering for radiotherapy plan B2 were summarized in Table 4.11.

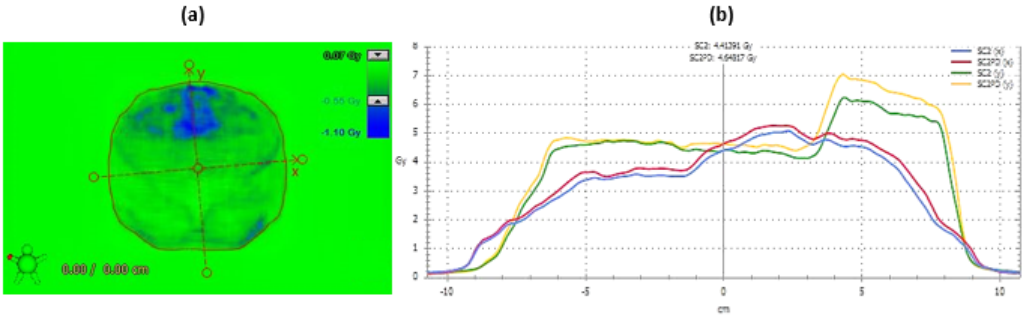

Figure 4.33: Results obtained for SC errors of 2 mm in composite portal dose image: (a) dose difference map, in which the maximum value of dose difference was 1.10, (b) comparison between the profiles of the calculated dose distribution and acquired composite portal dose image, SC2PD and SC2 respectively. The x and y directions of profile correspond to the ones identified in portal dose image (a), which correspond to a different direction of the reference situation.

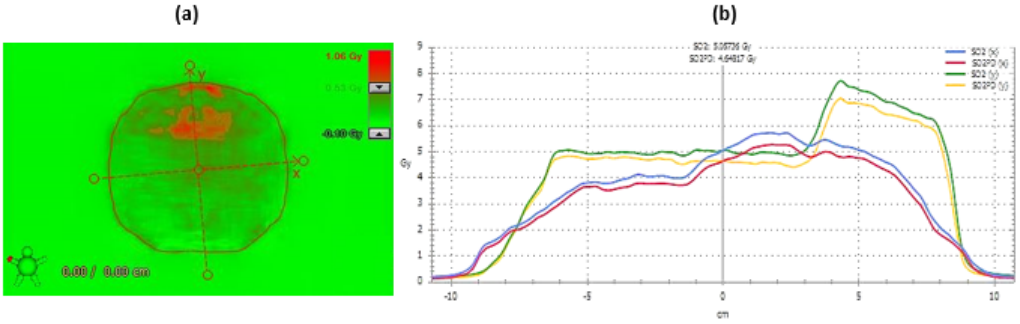

Figure 4.34: Results obtained for SO errors of 2 mm in composite portal dose image: (a) dose difference map, in which the maximum value of dose difference was 1.06, (b) comparison between the profiles of the calculated dose distribution, without considering any error, and acquired composite portal dose image, SO2PD and SO2 respectively. The x and y directions of profile correspond to the ones identified in portal dose image (a), which correspond to a different direction of the reference situation.

For both error types, SL and SR, a gamma passing rate significantly under 100% only was obtained with a magnitude of 3 mm. These results were expected since the introduced errors only displace the portal dose image to the left and right without modifying the area. In reference situation it is possible to see that the profiles are perfectly aligned, with exception of the slight dose in the central region, so it is expected that the gamma analysis fails when an error magnitude covered by the analysis criteria, (3%, 3mm), is applied. Considering random errors of 1mm, a gamma passing rate of 100% was also obtained for all individual portal dose images as well as for composite portal dose image. It would be important apply random errors with other magnitudes to better understand the sensitivity of aS1000.

The obtained results suggested that aS1200 EPID and the absolute portal dosimetry system are able to correctly detect SC, SO, SR and SL errors, however in order to detect errors with smaller magnitudes that can also affect the treatment, it is important perform a gamma analysis with a narrow criteria, like (2%, 2mm). In this way is possible to evaluate with more precision any significant error that may arise during the pre-treatment

Table 4.11: Table with the relevant (2%, 2mm) and (3%, 3mm) gamma analysis results, comparing the original square field dose distribution acquired with EPID and acquired portal dose image in which a specific error was introduced: random (R), systematic close (SC), systematic open (SO), systematic left (SL) and systematic right (SR). A mean dose difference value is also presented for each relevant error type and magnitude.

Error (mm)	**γ(3%,3mm)**				
	CW1	**CCW1**	**CW2**	**CCW2**	**Composite**
SL 0.5	100	100	100	100	100
SL 1	100	100	100	100	100
SL 2	100	100	100	100	99.6
SL 3	99.8	99.6	99.5	99.8	95.9
SR 0.5	100	100	100	100	100
SR 1	100	100	100	100	100
SR 2	100	100	100	100	100
SR 3	99.9	98.9	92.6	99.5	96.6

patient-specific QA with EPID and therefore avoid that a determinant error occur in the first radiotherapy session.

In order to confirm the results previously obtained, errors were introduced in the paravertebral radiotherapy plan, P. However, in this study only SC and SO errors where introduced since these are the most relevant, Figure 4.35. In contrast to what happened to plan B2, for SC and SO with 0.5 mm of magnitude a gamma passing rate of 93.8 and 95.3 respectively were obtained when a gamma criteria of (3%, 3mm) was set. The reason behind these results can once again be related with the size and number of segments. In fact, the plan P had more segments than B2, since it is a more demanding plan, with a single shot scheme and a delivered dose of 24 Gy.

Although the general behaviour of gamma results for SC and SO errors are according to what was obtained for plan B2, since the gamma passing rate decreases and the gamma mean increases with the introduction of higher errors magnitudes, Figure 4.35(b), the values obtained are more expressive which is expected considering the number of segments of each plan.

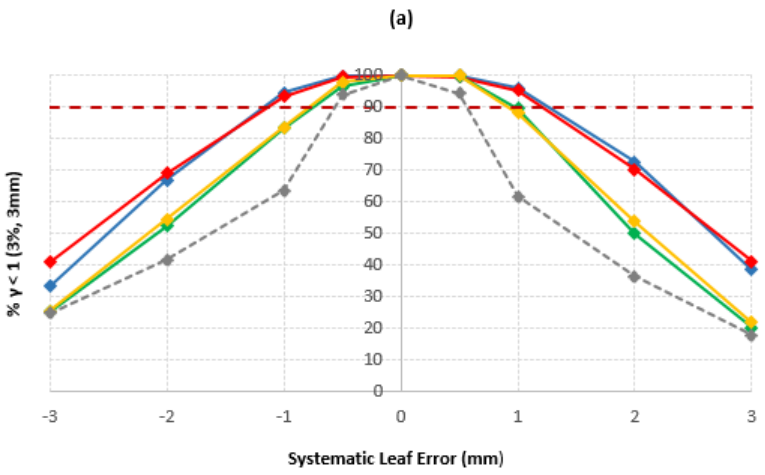

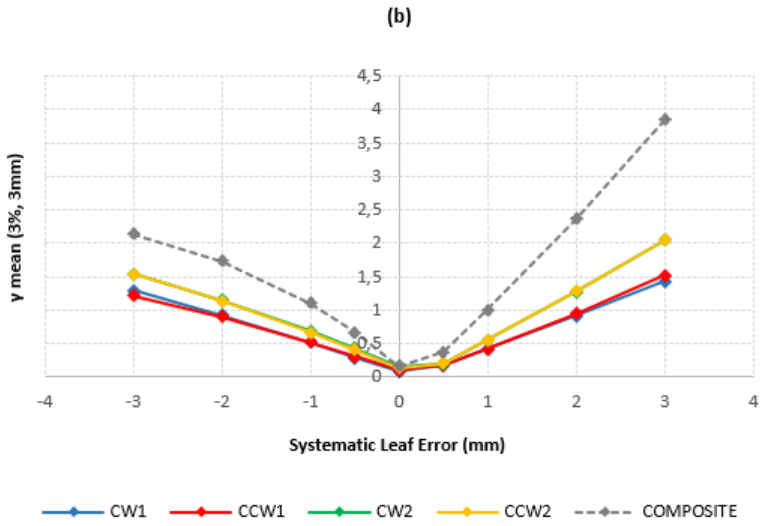

Figure 4.35: Gamma analysis results with (3%, 3mm) criteria, obtained considering SC and SO errors for VMAT plan P: (a) gamma passing rate and (b) gamma mean values. The positive values in systematic leaf errors axis correspond to SO and the negative ones correspond to SC errors.

SC and SO errors introduced in plan were also evaluated with ArcCHECK®. In order to use the calculations previously done to perform the clinical pre-treatment patient-specific QA with ArcCHECK®, for each error the whole plan was measured in one time, so some differences could be expected, since with EPID each arc was acquired individually and the a composite portal dose image was determined. Looking at Figure 4.36, it is possible to see that both dosimetric systems present symmetric results for SC and SO errors, which was expected. For both errors types and all considered magnitudes, with exception of errors with 3 mm of magnitude, the errors effects are more expressive when measured with EPID. Note that, for errors with standard deviation of 0.5 mm the gamma passing rate decreased more from reference situation for portal dosimetry, which means that the error of 0.5 have more impact when measured with EPID and analysed with Absolute Portal Dosimetry solution. In fact, considering the sensitivity of both devices it was expected that errors with the smallest magnitude were easily detected with aS1200.

The results obtained regarding errors magnitudes of 1 mm were the most discrepant between dosimetric devices, which also can be explained by the sensitivity of ArcCHECK® since 1 mm is also close to pixel sensitivity. As expected, for higher magnitudes, the systems behaviour is similar and the gamma passing rate achieved for errors of 2 and 3 mm are very close.

In order to evaluate better the results, it would be important redo the analysis for each arc and therefore compare the results obtained with Absolute Portal Dosimetry and ArcCHECK®. The errors should be also introduced in more plans, considering several treatment sites and with different fractionation schemes, to verify the obtained results. It is important keep in mind that perform EPID dosimetry with FFF beams is a new aspect with only few studies reported and so, the obtained results are very promising and encourages the continuation of the study for implementation of pre-treatment patient-specific QA with EPID, for FFF beams.

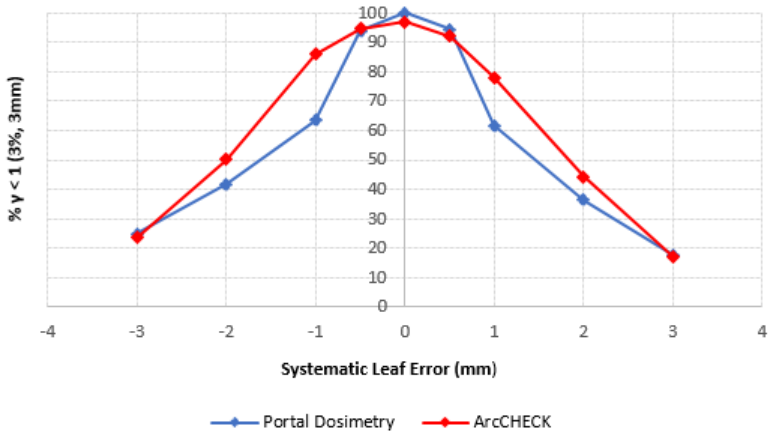

Figure 4.36: Gamma passing rate results, with (3%, 3mm) criteria, obtained with EPID and ArcCHECK® considering SC and SO errors for plan P. The positive values in systematic leaf errors axis correspond to SO and the negative ones correspond to SC errors.

Chapter 5

Conclusion and Future Work

With the introduction of advanced irradiation techniques (IMRT and VMAT) in clinical practice, as well as with the prescription of more demanding fractionated schemes, where less irradiation fractions with higher doses per fraction are considered, the accuracy and feasibility of pre-treatment patient-specific QA procedures gains a higher importance. Thus, it is possible to detect, before the patient treatment session starts, human or mechanical errors that could compromise the entire radiotherapy treatment and result in serious injuries.

The potential of EPIDs to perform patient-specific QA has been largely explored due its high resolution and automated acquisition of portal images. In this study we performed initial tests for the implementation of pre-treatment patient-specific QA with EPID, for the Varian LINACs (Varian Medical Systems, Palo Alto, CA, USA) available in the Radiotherapy Department of the Foundation Champalimaud, the TrueBeam^{TM} and EDGE^{TM} systems.

On the TrueBeam^{TM} System was tested an improved method, called Portal Dosimetry Pre-Configuration (PDPC) package, to calibrate the aS1000 and to configure the PDIP algorithm that allow to obtain a predicted portal dose image at the EPID level, with which the portal dose image acquired by the EPID is compared. A 2D beam profile correction matrix, which includes an improved backscatter correction for fields from 5x5 cm^2 to 15x15 cm^2, is used during aS1000 calibration in order to recover the beam profile removed by flood-field correction, instead of the diagonal beam profile of a 40x40 cm^2 field used in standard configuration of Portal Dosimetry. The pre-configured PDIP algorithm assumes that the scatter behaviour of different EPIDs of the same type can be modelled by identical scatter kernels and so no extra measurements are needed.

A set of verification measurements were analysed in order to verify the correct installation of PDPC package. The central axis (CAX) dose value of predicted and acquired portal dose image of different square fields sizes, ranging from 3x3 cm^2 and 22x22 cm^2 were compared, as well as the crossline and inline profiles. The obtained results indicated that the output factors used in the PDIP algorithm to predict the portal dose image match with the actual output factors of the EPID, since the difference between the CAX dose value of predicted and acquired portal dose images was lower than 1% for all square fields sizes. The profiles analyses proved that the 2D beam profile matrix, used in aS1000 cali-

bration, allows to obtain very good results for the most relevant square fields, which are in accordance with the ones predicted by the PDIP algorithm. Furthermore, the backscatter correction is effective for square fields from 5x5 cm^2 to 15x15 cm^2. The excellent gamma analysis results obtained comparing the predicted and acquired portal dose images of the AIDA field, which is used to determine the EPID scatter kernels in the standard configuration of Portal Dosimetry, consequently confirmed the assumption that the scatter behaviour of different EPIDs of the same type can be modelled by the same scatter kernels.

For 3 IMRT plans from breast cancer patients, a total 17 individual fields, the gamma analysis results were better with PDPC package configuration, with gamma passing rates higher than 99.5% for all fields, than with standard configuration of the Portal Dosimetry. Once again, the results suggest that the 2D beam profile matrix is a better approach to recover the beam profile instead of the diagonal profile used in standard configuration of Portal Dosimetry, as well as the effectiveness of backscatter correction. Comparing the PDPC package with the currently patient-specific QA device (ArcCHECK®) for 11 IMRT plans and 22 VMAT plans, a total of 71 and 86 fields respectively, better results were achieved using Portal Dosimetry. These results can be explained by the higher EPID resolution when compared with ArcCHECK® and also with the geometry of EPID. Although all the presented results conclude that the PDPC package is valuable approach to simplify the configuration of Portal Dosimetry solution and the clinical study suggest that the EPID is better than ArcCHECK®, it is important to carry out further studies in order to determine if all possible human and mechanic errors that can occur before the first treatment session are correctly detected through Portal Dosimetry before replacing the ArcCHECK®.

On the EDGE™ System we performed the installation and evaluation of an even more advanced Portal Dosimetry solution, the so-called the Absolute Pre-Treatment Portal Dosimetry package that also allowed us to evaluate pre-treatment patient-specific QA of IMRT and VMAT plans with FFF beams, which is a new aspect in EPID dosimetry. The Absolute Pre-Treatment Portal Dosimetry solution allows converting a portal dose image CU to a portal dose image in Gy. A PSM, allow to correct the portal image for pixel sensitivities regardless of the position of the EPID at the calibration time, is used to recover the beam profile instead the flood-field image.

Since the version of ARIA® installed in the Radiotherapy Department does not support the Portal Dosimetry solution for FFF beams, acquiring portal dose images cannot be done automatically. A workaround to acquire portal dose images was adopted, and so each plan was calculated in a phantom structure. Ten cancer patient plans treated with VMAT, a total of 40 arcs, were analysed to evaluate the clinical performance of Absolute Pre-treatment Portal Dosimetry. Considering that all tested plans were VMAT treatments, delivered with FFF beams and planned with hypofractionated or single shot schemes, very positive and promising results were obtained. For all but one patient, gamma passing rate values higher than 98% were achieved.

One of the main advantage associated to Absolute Pre-Treatment Portal Dosimetry is that the dose distribution, with which the portal dose dosimetry acquired by EPID is

compared, is calculated by the same algorithm that is used to calculate the clinical plans. However, it is important to measure more patient plans to evaluate more efficiently the clinical performance of Absolute Pre-Treatment Portal Dosimetry, particularly the impact of composite portal dose images creation.

Before considering the adoption of the Absolute Pre-Treatment Portal Dosimetry, it is important to ensure that this solution detects all significant errors that may arise during the pre-treatment patient-specific QA. Therefore, the sensitivity of the aS1200 EPID during pre-treatment patient-specific QA was studied in order to understand whether this solution is able to detect some particular and common errors. An entire routine to introduce errors in patient plans, without interfere in Champalimaud clinical routine, was developed. As the native language of EDGE^{TM} System is XML, the DICOM-RT plan was converted to a XML, through a software called Veritas. Since Veritas is a research software and since there is little information about it available, several studies were performed before obtaining a correct conversion. Among other things, we noticed that some parameters of DICOM-RT plan are not correctly converted by Veritas and for that reason it was still necessary to manually correct the XML file.

Subsequently, a MATLAB® program was completely developed to introduce errors in the XML patient plan which was then directly load on the Vision Workstation of EDGE^{TM} System, in Developer Mode. A special attention to MLC movement and its mechanical limitations were required to develop the MATLAB® program. An intensive study of Developer Mode was essential to learn how load XML files, how to start the radiation delivery, how import the acquired portal dose images and so on.

Considering that the present study was carried out in Developer Mode but the clinical plans were delivered in Treatment Mode, portal dose images acquired in Developer Mode and Treatment Mode were compared. Based on the obtained dosimetric results it was possible to conclude that there are no significant differences between the portal dose images acquired with Treatment Mode and Developer Mode, and for that reason all the results obtained with portal dose images acquired with Developer Mode can be applied to Treatment Mode.

For, square fields of 10x10 cm^2, acquired portal dose images in which a particular error was introduced through the MATLAB® program, were compared with the original acquired portal dose image. Random and Systematic errors, from 2mm, were successfully detected by (2%, 2mm) gamma analysis and dose difference maps which means that the MATLAB® program works as was supposed when no other possible sources of errors are considered. When acquired portal dose images with an error were compared with the reference portal dose image calculated by Eclipse^{TM}, random and systematic errors were also successfully detected, even considering the reference situation in which some differences were already seen. However, the introduction of some errors SO, where leaves are systematically opened, lead to better gamma results than the ones obtained for the reference situation. So, in this particular case, the errors would not be detected with a clinical routine.

The same errors types with similar magnitudes were introduced in clinical plans of

two patients treated with VMAT, a total of 8 treatment arcs. As expected the gamma passing rate decreases and the gamma mean increases with the introduction of errors with higher magnitudes. The dosimetric results obtained for both composite portal dose images, in which all arcs of a particular plan are added together, were more expressive that the ones obtained for each individual arc. The impact of each particular error had on each individual arc will depend on the number and size of segments constituting each one. Also, the collimator rotation in which each arc is delivered can might influence decisively the effect of each arc errors in composite portal dose images. Further study to explain the increased sensitivity of composite portal dose images is required. A (2%, 2mm) gamma analysis might be performed to analyse with more accuracy the effect of each particular error.

For one of the plans, the gamma results obtained for composite portal dose image were compared with the ArcCHECK® results. Errors of 0.5 and 1 mm are more easily detected when measured with EPID and analysed with Absolute Portal Dosimetry solution which was expected considering the sensitivity of both devices. In order to better evaluate the results, it would be important compare the results obtained with EPID and ArcCHECK® for each individual arc and perform a gamma analysis with a tighter criteria.

Considering the diversity of treatment site and fractionation schemes of the plans delivered in EDGE™ System, it is crucial to include more patient plans in the studied. Only this way it is possible to conclude whether EPID is really better than ArcCHECK®. However, knowing that EPID dosimetry with FFF beams is a new aspect with only few studies reported, the obtained results are very encouraging. In a close future, a new version of Absolute Pre-Treatment Portal Dosimetry, in which a MLC correction is added will be available to test, so it would be interesting compare the results with the ones presented here.

Future Work

This work should be continued to implement portal dosimetry based patient pre-treatment QA in the clinic and replace the cumbersome and low-resolution ArcCHECK® solution that is currently used. The methods enabling absolute dosimetry in Gy are to be preferred over the CU-based methods. The developed sensitivity-testing procedures should be simplified and improved so that all remaining bugs that require manual corrections (from e.g. Veritas) are resolved. Introduce errors directly in DICOM RT plans could be a good option. Furthermore the introduced errors which up to now mainly consisted of MLC errors should be extended with different errors like collimator and gantry angles and monitor unit errors. In this way many clinical cases can be studied rapidly and accurately with both portal dosimetry and ArcCHECK®. If portal dosimetry then still performs equal to or better than ArcCHECK®, we can safely start using portal dosimetry clinically.

The developed routine, with in-house MATLAB® program and Developer Mode, is also a good start point to explore the possibility of use developer mode for automation of routine pre-treatment patient-specific QA procedures.

Finally, although the pre-treatment patient-specific QA enables the detection of specific

errors priori to first patient session, it is also fundamental implement in vivo procedures with which is possible detect errors during each treatment session. Hence, it is possible to monitor and ensure the accuracy of the actual radiotherapy treatment. Some back-projection algorithms were developed in order to correlate the dose at the EPID level to the dose inside the patient, and in this way it is possible to reconstruct the 3D dose within the patient volume. So, in order to get a complete picture of the treatment accuracy, studies to implement in vivo dosimetry with the EPID in the Radiotherapy Department should be performed as well.

References

[1] World Health Organization. Cancer - Key Facts, 2016.

[2] World Health Organization.Risk Factors for Cancers. prevention and control, 2016.

[3] International Atomic Energy Agency. Investigation of an Accidental Exposure of Radiotherapy Patients in Panama: Technical Report of a Team of Experts.

[4] M. Gantchew, "Radiotherapy Risk Profile," Rentgenologiya i Radiologiya, vol. 49, no. 4. World Cancer Report Press, pp. 14–21, 2010.

[5] American Cancer Society. Goals of Radiotherapy, 2015.

[6] E. Podgorsak. Review of Radiation Oncology Physics: A Handbook for Teachers and Students. International Atomic Energy Agency, Vienna, AT, 2005.

[7] C. F. Dunne-Daly, "Principles of radiotherapy and radiobiology.," Semin. Oncol. Nurs., vol. 15, no. 4, pp. 250–259, 1999.

[8] J. M. Brown, D. J. Carlson, and D. J. Brenner, "The tumor radiobiology of SRS and SBRT: Are more than the 5 Rs involved?," Int. J. Radiat. Oncol. Biol. Phys., vol. 88, no. 2, pp. 254–262, 2014.

[9] International Commission on Radiation Units and Measurements (ICRU), Prescribing, Recording, and Reporting Photon-Beam Intensity-Modulated Radiation Therapy (IMRT), Report 83, 2010.

[10] C. W. Song, H. Park, R. J. Griffin, and S. H. Levitt, "Radiobiology of Stereotactic Radiosurgery and Stereotactic Body Radiation Therapy," 2012.

[11] N. Suntharalingam, E. B. Podgorsak, and J. H. Hendry, "Basic Radiobiology," Rev. Radiat. Oncol. Phys. A Handb. Teach. Students, pp. 397–412, 1993.

[12] E. B. Podgorsak, P. Metcalfe and J. V. Dyk, " The Modern Technology of Radiation Oncology", chap. 11, 349–435 (MedicalPhysics Publishing, 1999).

[13] S. J. Blake, “On the development of a novel detector for simultaneous imaging and dosimetry in radiotherapy,” . PhD Degree, University of Sydney,2014.

[14] J. M. D. Roberts, “A Portal Imager-Based Patient Dosimetry System”, Master Degree, University of Victoria, 2013.

[15] M. Teoh, C. H. Clark, K. Wood, S. Whitaker, and a Nisbet, “Volumetric modulated arc therapy: a review of current literature and clinical use in practice.,” Br. J. Radiol., vol. 84, no. 1007, pp. 967–96, Nov. 2011.

[16] D. a Palma, W. F. a R. Verbakel, K. Otto, and S. Senan, “New developments in arc radiation therapy: a review.,” Cancer Treat. Rev., vol. 36, no. 5, pp. 393–9, Aug. 2010.

[17] A. Taylor and M. E. B. Powell, “Intensity-modulated radiotherapy-What is it?,” Cancer Imaging, vol. 4, no. 2, pp. 68–73, Jan. 2004.

[18] M. M. Matuszak, D. Yan, I. Grills, and A. Martinez, “Clinical applications of volumetric modulated arc therapy.,” Int. J. Radiat. Oncol. Biol. Phys., vol. 77, no. 2, pp. 608–16, Jun. 2010.

[19] R. A. Kinhikar, A. B. Pawar, U. Mahantshetty, V. Murthy, D. D. Dheshpande, and S. K. Shrivastava, “Rapid Arc, helical tomotherapy, sliding window intensity modulated radiotherapy and three dimensional conformal radiation for localized prostate cancer: a dosimetric comparison.,” J. Cancer Res. Ther., vol. 10, no. 3, pp. 575–82.

[20] M. Olloni, ”Commissioning of 6 MV FFF Photon Beam for SBRT”, Master Degree, 2013.

[21] M. Wendling, R. Louwe, L. McDermott, J. J. Sonke, M. van Herk, and B. Mijnheer. Accurate two-dimensional IMRT verification using a back-projection EPID dosimetry method. Medical physics, 33:259-273, 2006.

[22] W. van Elmpt, L. McDermott, S. Nijsten, M. Wendling, P. Lambin, and B. Mijnheer, “A literature review of electronic portal imaging for radiotherapy dosimetry.,” Radiother. Oncol., vol. 88, no. 3, pp. 289–309, 2008.

[23] M. van Herk, “Physical aspects of a liquid-filled ionization chamber with pulsed polarizing voltage.,” Med. Phys., vol. 18, no. 4, pp. 692–702, 1991.

[24] J. Chang, G. S. Mageras, and C. C. Ling, “Evaluation of rapid dose map acquisition of a scanning liquid-filled ionization chamber electronic portal imaging device,” Int.

J. Radiat. Oncol., vol. 55, no. 5, pp. 1432–1445, 2003.

[25] M. Mohammadi, E. Bezak, and P. Reich, "The use of extended dose range film for dosimetric calibration of a scanning liquid-filled ionization chamber electronic portal imaging device," vol. 8, no. 1, pp. 69–84, 2007.

[26] L. E. Antonuk, Y. El-Mohri, W. Huang, K. W. Jee, J. H. Siewerdsen, M. Maolinbay, V. E. Scarpine, H. Sandler, and J. Yorkston, "Initial performance evaluation of an indirect-detection, active matrix flat-panel imager (AMFPI) prototype for megavoltage imaging," Int. J. Radiat. Oncol. Biol. Phys., vol. 42, no. 2, pp. 437–454, 1998.

[27] L. E. Antonuk, J. Yorkston, W. Huang, H. Sandler, J. H. Siewerdsen, and Y. El-Mohri, "Megavoltage imaging with a large-area, flat-panel, amorphous silicon imager," Int. J. Radiat. Oncol. Biol. Phys., vol. 36, no. 3, pp. 661–672, 1996.

[28] A. Van Esch, T. Depuydt, and D. P. Huyskens, "The use of an aSi-based EPID for routine absolute dosimetric pre-treatment verification of dynamic IMRT fields," Radiother. Oncol., vol. 71, no. 2, pp. 223–234, 2004.

[29] P. B. Greer and C. C. Popescu, "Dosimetric properties of an amorphous silicon electronic portal imaging device for verification of dynamic intensity modulated radiation therapy.," Med. Phys., vol. 30, no. 7, pp. 1618–1627, 2003.

[30] P. B. Greer, "Correction of pixel sensitivity variation and off-axis response for amorphous silicon EPID dosimetry.," Med. Phys., vol. 32, no. 12, pp. 3558–3568, 2005.

[31] L. Parent, J. Seco, P. M. Evans, A. Fielding, and D. R. Dance, "Monte Carlo modelling of a-Si EPID response: the effect of spectral variations with field size and position.," Med. Phys., vol. 33, no. 12, pp. 4527–40, Dec. 2006.

[32] J. V Siebers, J. O. Kim, L. Ko, P. J. Keall, and R. Mohan, "Monte Carlo computation of dosimetric amorphous silicon electronic portal images.", Med. Phys., vol. 31, no. 7, pp. 2135–46, Jul. 2004.

[33] W. J. C. van Elmpt, S. M. J. J. G. Nijsten, R. F. H. Schiffeleers, A. L. a J. Dekker, B. J. Mijnheer, P. Lambin, and A. W. H. Minken, "A Monte Carlo based three-dimensional dose reconstruction method derived from portal dose images.," Med. Phys., vol. 33, no. 7, pp. 2426–2434, 2006.

[34] S. Nijsten, "Porta Dosimetry in Radiotherapy," Radiother. Oncol., vol. 92, p. S50, 2009.

[35] L. N. McDermott, R. J. W. Louwe, J. J. Sonke, M. B. van Herk, and B. J. Mijnheer,

"Dose-response and ghosting effects of an amorphous silicon electronic portal imaging device.," Med. Phys., vol. 31, no. 2, pp. 285–95, 2004.

[36] Y. El-Mohri, L. E. Antonuk, J. Yorkston, K. W. Jee, M. Maolinbay, K. L. Lam, and J. H. Siewerdsen, "Relative dosimetry using active matrix flat-panel imager (AMFPI) technology.," Med. Phys., vol. 26, no. 8, pp. 1530–41, 1999.

[37] B. M. C. McCurdy, "Dosimetry in radiotherapy using a-Si EPIDs: Systems, methods, and applications focusing on 3D patient dose estimation," J. Phys. Conf. Ser., vol. 444, p. 012002, 2013.

[38] B. M. McCurdy, K. Luchka, and S. Pistorius, "Dosimetric investigation and portal dose image prediction using an amorphous silicon electronic portal imaging device.," Med. Phys., vol. 28, no. 6, pp. 911–24, 2001.

[39] C. Kirkby and R. Sloboda, "Consequences of the spectral response of an a-Si EPID and implications for dosimetric calibration.," Med. Phys., vol. 32, no. 8, pp. 2649–58, 2005.

[40] A. Van Esch, B. Vanstraelen, J. Verstraete, G. Kutcher, and D. Huyskens, "Pretreatment dosimetric verification by means of a liquid-filled electronic portal imaging device during dynamic delivery of intensity modulated treatment fields," Radiother. Oncol., vol. 60, no. 2, pp. 181–190, 2001.

[41] S. M. J. J. G. Nijsten, A. W. H. Minken, P. Lambin, and I. A. D. Bruinvis, "Verification of treatment parameter transfer by means of electronic portal dosimetry.," Med. Phys., vol. 31, no. 2, pp. 341–7, 2004.

[42] B. Warkentin, S. Steciw, S. Rathee, and B. G. Fallone, "Dosimetric IMRT verification with a flat-panel EPID," Med. Phys., vol. 30, no. 12, p. 3143, 2003.

[43] S. Steciw, B. Warkentin, S. Rathee, and B. G. Fallone, "Three- dimensional IMRT verification with a flat-panel EPID," Med. Phys. 32, 600–612 , 2005.

[44] S. B. Jiang, G. C. Sharp, T. Neicu, R. I. Berbeco, S. Flampouri, and T. Bortfeld, "On dose distribution comparison.," Phys. Med. Biol., vol. 51, no. 4, pp. 759–776, 2006.

[45] D. A. Low and J. F. Dempsey, "Evaluation of the gamma dose distribution comparison method.," Med. Phys., vol. 30, no. 9, pp. 2455–2464, 2003.

[46] D. a Low, W. B. Harms, S. Mutic, and J. a Purdy, "A technique for the quantitative evaluation of dose distributions.," Med. Phys., vol. 25, no. 5, pp. 656–661, 1998.

[47] D. A. Low, "Gamma Dose Distribution Evaluation Tool," Journal of Physics: Conference Series, vol. 250. p. 012071, 2010.

[48] Varian Medical Systems Inc. PortalVision aS1000: The state of the art in electronic portal imaging, 2006.

[49] P. Storchi and E. Woudstra, "Calculation of the absorbed dose distribution due to irregularly shaped photon beams using pencil beam kernels derived from basic beam data," Phys. Med. Biol., vol. 41, no. 4, pp. 637–656, 1996.

[50] B. W. King, D. Morf, and P. B. Greer, "Development and testing of an improved dosimetry system using a backscatter shielded electronic portal imaging device," Med. Phys., vol. 39, no. 5, p. 2839, 2012.

[51] C. Kirkby and R. Sloboda, "Comprehensive Monte Carlo calculation of the point spread function for a commercial a-Si EPID," Med. Phys., vol. 32, no. 4, p. 1115, 2005.